

# Multi-task Learning for Heterogeneous Data via Integrating Shared and Task-Specific Encodings

Yang Sui<sup>1</sup>, Qi Xu<sup>2</sup>, Yang Bai<sup>1</sup>, and Annie Qu<sup>3\*</sup>

<sup>1</sup>*School of Statistics and Data Science,*

*Shanghai University of Finance and Economics*

<sup>2</sup>*Department of Statistics and Data Science, Carnegie Mellon University*

<sup>3</sup>*Department of Statistics, University of California, Irvine*

## Abstract

Multi-task learning (MTL) has become an essential machine learning tool for addressing multiple learning tasks simultaneously and has been effectively applied across fields such as healthcare, marketing, and biomedical research. However, to enable efficient information sharing across tasks, it is crucial to leverage both shared and heterogeneous information. Despite extensive research on MTL, various forms of heterogeneity, including distribution and posterior heterogeneity, present significant challenges. Existing methods often fail to address these forms of heterogeneity within a unified framework. In this paper, we propose a dual-encoder framework to construct a heterogeneous latent factor space for each task, incorporating a task-shared encoder to capture common information across tasks and a task-specific encoder to preserve unique task characteristics. Additionally, we explore the intrinsic similarity structure of the coefficients corresponding to learned latent factors, allowing for adaptive integration across tasks to manage posterior heterogeneity. We introduce a unified algorithm that alternately learns the task-specific and task-shared encoders and coefficients. In theory, we investigate the excess risk bound for the proposed MTL method using local Rademacher complexity and apply it to a new but related task. Through simulation studies, we demonstrate that the proposed method outperforms existing data integration methods across various settings. Furthermore, the proposed method achieves superior predictive performance for time to tumor doubling across five distinct cancer types in PDX data.

*Keywords:* Adaptivity, Data integration, Disentangled encodings, Distribution shift, Posterior shift

---

\*Corresponding author: aqu2@uci.edu.

# 1 Introduction

Datasets for specific scientific tasks could lack sufficient samples to train accurate machine learning models. In recent decades, multi-task learning (MTL) has been successfully applied across fields such as biomedical applications (Wang et al., 2019), computer vision (Gao et al., 2019), and natural language processing (Sanh et al., 2019). MTL is a training paradigm in which machine learning models are trained on data from multiple tasks simultaneously, allowing them to borrow information across tasks to improve overall predictive performance. This approach can increase data efficiency and potentially lead to faster convergence and more accurate predictions for related or downstream tasks (Crawshaw, 2020). However, achieving these benefits in MTL can be difficult, especially when tasks exhibit unknown or elusive heterogeneity from various sources. MTL presents the following major challenges:

1. **Distribution heterogeneity.** The distributions of the same input features can differ across tasks, a phenomenon known as distribution heterogeneity, or covariate shift (Nair et al., 2019). This issue is particularly prevalent in biomedical datasets. For instance, RNA-sequencing distributions vary substantially across tumor types in cancer studies (Polyak et al., 2011). If not properly addressed, these differences may obscure biological signals and lead to misleading conclusions, especially when dealing with limited sample size for each tumor type.
2. **Posterior heterogeneity.** The associations between input features and responses may vary across tasks due to distinct scientific goals, a phenomenon we refer to as posterior heterogeneity, or posterior drift (Maity et al., 2024; Qin et al., 2024). In the context of cancer studies, for instance, the relationship between gene expression profiles and tumor growth rates can differ significantly across cancer types. Ignoring posterior heterogeneity could undermine the effectiveness of integrating different datasets.
3. **Complex patterns.** The latent relationship between input features and responses

is often more complex than linear relations in many real-world applications. For instance, in cancer studies, the association between genomic data and clinical outcomes frequently involves complex, high-order interactions that require advanced learning models to capture. Similarly, in biomedical imaging analysis, the association between voxel intensities and clinical outcomes often involves intricate spatial correlations and patterns that require more complicated models to capture higher-order interactions (Litjens et al., 2017). Overlooking such complex patterns, including nonlinear relationships, significantly restricts the learning capacity of MTL.

Various existing data integration methods address one of the aforementioned challenges. For distribution heterogeneity, importance-weighting estimators and their variants have been proposed to mitigate shift problems (Shimodaira, 2000; Ma et al., 2023). To tackle posterior heterogeneity, numerous studies employ parameter space constraints, such as fused penalties, to estimate regression coefficients that capture subgroup structures (Tang and Song, 2016; Tang et al., 2021; Duan and Wang, 2023). For example, Tang and Song (2016) introduced a regularized fusion method to identify and merge inter-task homogeneous parameter clusters in regression analysis. Tang et al. (2021) developed a separation penalty with multi-directional shrinkages, enabling the selection of different relevant variables for distinct individuals. Another approach is transfer learning, which borrows information from source data to target data in the field of statistics (Li et al., 2022; Tian and Feng, 2023; Zhang et al., 2024). While these existing multi-group data integration methods effectively address individual types of heterogeneity, they are generally limited to one specific type of heterogeneity. Furthermore, these methods often rely on structured model assumptions, such as linearity, which constrain their ability to capture complex relationships.

Besides statistical data integration methods, there is a growing literature on MTL using deep learning methods, such as deep neural networks. These methods can be broadly classified into four categories: The first category involves balancing individual loss functions

for different tasks, a common approach to ease multi-task optimization (Du et al., 2018; Liu et al., 2019a; Hang et al., 2023). However, these methods rely on weighting strategies, risking instability or suboptimal performance if not well-tuned (Kendall et al., 2018). The second category focuses on network architecture design, including hard parameter sharing (Subramanian et al., 2018; Bai et al., 2022), which shares layers across tasks, and soft parameter sharing (Yang and Hospedales, 2016), which maintains task-specific parameters with regularization. Hard parameter sharing struggles to capture task-specific details (Han et al., 2024), while soft parameter sharing increases computational costs and risks overfitting with limited data. The third category addresses negative transfer by using gradient modulation to mitigate conflicts in task dynamics (Yu et al., 2020; Abdollahzadeh et al., 2021), but managing gradients across tasks can destabilize training (Wang and Tsvetkov, 2021). The fourth category employs knowledge distillation to transfer knowledge from single-task to multi-task networks (Liu et al., 2019b; Clark et al., 2019), but its effectiveness is limited when tasks are too diverse, as the distilled knowledge may fail to generalize (Xu et al., 2020). Although the above approaches can integrate data from multiple tasks, it often incurs substantial computational costs and lacks interpretability.

Our primary objective is to develop a unified framework for MTL which addresses the above challenges. To tackle distribution heterogeneity, we employ task-specific and task-shared encoders to construct a heterogeneous latent factor space for each task, where the task-shared encoder retains the common information across different tasks, and the task-specific encoders preserve the heterogeneous characteristics for each task. The proposed dual-encoder framework is capable of capturing more complex data structures compared to traditional linear factor models (Bing et al., 2020; Fan and Gu, 2023). Simultaneously, we uncover the intrinsic similarity structure of the coefficients corresponding to task-specific and task-shared latent factors, adaptively integrating data from multiple tasks to handle posterior heterogeneity. The proposed framework can be regarded as a general extension of

composite structures in MTL (Tripuraneni et al., 2020; He et al., 2024; Watkins et al., 2024). Compared to these, our framework incorporates additional task-specific encoders to retain more heterogeneous information. Specifically, our contributions are summarized as follows:

1. **Methodologically**, we disentangle the latent factor space into task-specific and task-shared components and capture the similarity structure of the corresponding coefficients, aiming to tackle distribution and posterior heterogeneity, respectively.
2. **Theoretically**, we establish the excess risk bound for the proposed MTL method using local Rademacher complexity, analyzing the impacts of different parameters, including sample sizes and network architecture, on the excess risk. Building on the rate of convergence, we also examine the performance of a new but related task under the task heterogeneity assumption.
3. **Computationally**, we propose a unified algorithm which learns task-specific and task-shared encoders and coefficients alternately, transforming the constraint minimization problem into a penalized minimization problem to effectively address computational challenges in MTL.
4. **Numerically**, the proposed MTL method demonstrates superior performance over existing methods in various simulation studies especially when sample sizes of tasks are relatively small. Additionally, we analyze real-world data and show our method achieves more accurate predictions from five heterogeneous cancer types in Patient-Derived Xenograft data.

We introduce the proposed MTL method in Section 2. In Section 4, we present algorithms for estimating the encoders and coefficients. Section 3 derives the theoretical properties of the proposed MTL method, including the excess risk bound and its extension to a new but related task. Section 5 illustrates the empirical performance of the proposed MTL method through various simulation studies. In Section 6, we apply the proposed method

to Patient-Derived Xenograft data. Finally, we provide discussion and concluding remarks in Section 7. Additional theoretical and numerical results, along with detailed technical proofs, are provided in Appendices.

## 2 Methodology

**Notations.** We use the convention that  $[r] = [1, \dots, r]$  represents the list of contiguous integers from 1 to  $r$ . The  $\ell_2$  norm of a vector is represented by  $\|\cdot\|$ , and the Frobenius norm of a matrix is represented by  $\|\cdot\|_F$ . Moreover, we use  $X_r$  to represent random variables, and  $X_{ri}$  to denote a specific realization of  $X_r$ .

**Problem Description.** Let  $\mathcal{X} \subseteq \mathbb{R}^d$  and  $\mathcal{Y} \subseteq \mathbb{R}$  denote the input feature space and output space, respectively. Suppose we have  $R$  heterogeneous tasks with probability distributions  $\{(X_r, Y_r) \sim P_r\}_{r=1}^R$ , supported over  $\mathcal{X} \times \mathcal{Y}$ . Each distribution  $P_r(X, Y)$  can be decomposed as  $P_X(X_r)P_{Y|X}(Y_r|X_r)$  for  $r \in [R]$ . We consider that both distribution and posterior heterogeneity exist simultaneously across the  $R$  tasks: the former refers to  $P(X_r)$  differing across tasks, while the latter indicates variation in  $P_{Y|X}(Y_r|X_r)$  across different  $r$ . These two forms of heterogeneity are commonly encountered in MTL applications involving genetic and biomedical data (Fagny et al., 2017; Li et al., 2024). Ignoring either one can significantly undermine the empirical performance of MTL.

In this work, we propose a unified latent factor model to incorporate both types of heterogeneity. First, we project input features into a latent space using encoders and disentangle them into one task-shared encoder and one task-specific encoder, where the task-specific encoder accounts for the distribution heterogeneity. Second, task-specific coefficients are employed on top of the two encoders to address the task heterogeneity. Formally, we consider the following model for the  $r$ -th task:

$$\mathbb{E}_r[Y_r] = \alpha_r^\top S_r(X_r) + \beta_r^\top C(X_r), \quad (1)$$

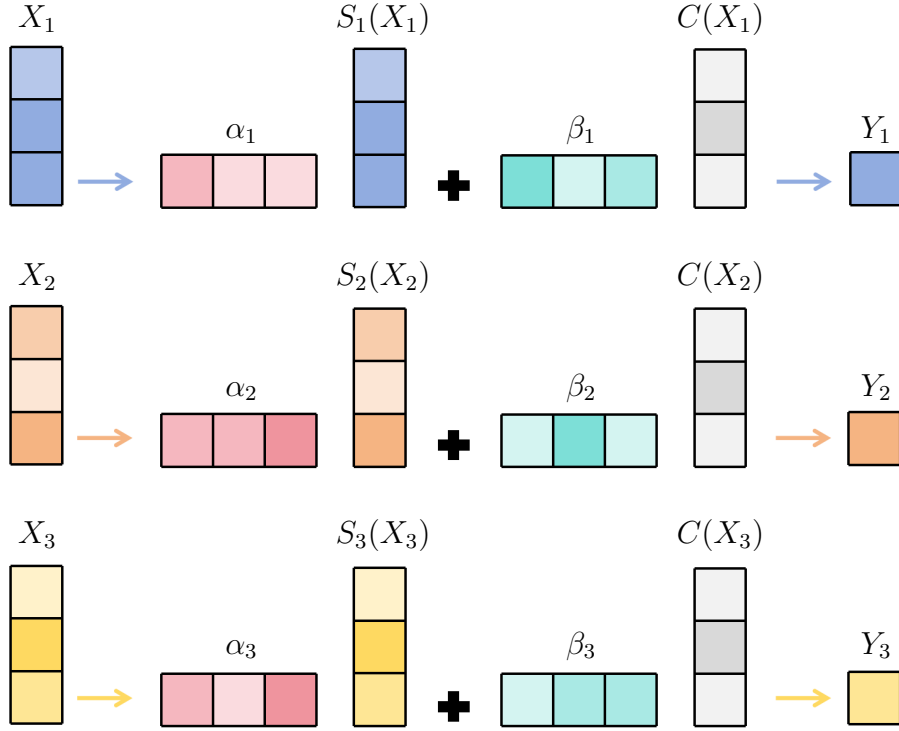


Figure 1: Diagram of the proposed MTL framework for heterogeneous data: A dual-encoder framework to address distribution heterogeneity and explore coefficient similarity structures across tasks.

where  $\mathbb{E}_r$  denotes the expectation over the distribution  $P_r$ . In Figure 1, we present a flowchart illustrating the MTL process for three tasks. In (1),  $S_r(\cdot) \in \mathcal{S}$  is the task-specific encoder for the  $r$ -th task, designed to learn latent factors specific to this task, with  $\mathcal{S}$  being the function class of task-specific neural networks mapping from  $\mathbb{R}^d$  to  $\mathbb{R}^q$ , and  $S_r(X_r)$  captures task-specific heterogeneity, such as certain RNA-sequencing distributions or mutation patterns that vary significantly across different tumor types. Similarly,  $C(\cdot) \in \mathcal{C}$  is the task-shared encoder for all  $R$  tasks, designed to learn shared latent factors across tasks, with  $\mathcal{C}$  representing the function class of task-shared neural networks mapping from  $\mathbb{R}^d$  to  $\mathbb{R}^p$ , and  $C(X_r)$  represents information shared across all tumor types, such as general genomic features or biomarkers broadly associated with cancer progression and treatment response.

The coefficients  $\alpha_r \in \mathbb{R}^q$  and  $\beta_r \in \mathbb{R}^p$  correspond to the task-specific and task-shared latent factors, respectively. The task-specific and task-shared encoders  $\{S_r(\cdot), C(\cdot)\}$  can be

interpreted as a set of basis functions, with  $\{\alpha_r, \beta_r\}$  acting as the corresponding weights. Note that the model in (1) is primarily designed for regression tasks but can be extended to accommodate classification tasks or other tasks.

We briefly introduce the task-specific and task-shared encoders  $\{\{S_r(\cdot)\}_{r=1}^R, C(\cdot)\}$  here, with detailed descriptions provided in the Supplementary Material S.4. First, for different tasks, the task-specific encoders  $\{S_r(\cdot)\}_{r=1}^R$  can include different network architectures. However, to reduce computational costs and simplify theoretical analysis, we assume that  $\{S_r(\cdot)\}_{r=1}^R$  for all tasks come from the same feed-forward neural network architecture  $\mathcal{S} = \mathcal{NN}(W_S, D_S, B_S)$ , where  $W_S$  and  $D_S$  represent the width and depth of the neural network, respectively. The weight matrices together with the bias vectors contain  $E_S = \sum_{i=1}^{D_S} p_{i+1,S}(p_{i,S} + 1)$  entries in total, and the parameters are bounded by a constant  $B_S$ . The numerical results in simulation and real data analyses demonstrate that assuming an identical neural network architecture across different tasks is reasonable. Similarly, for the task-shared encoder  $C(\cdot)$ , we approximate it by a feed-forward neural network  $\mathcal{C} = \mathcal{NN}(W_C, D_C, B_C)$ , where  $W_C$  and  $D_C$  are the width and depth of the neural network, respectively. The weight matrices together with the bias vectors contain  $E_C = \sum_{i=1}^{D_C} p_{i+1,C}(p_{i,C} + 1)$  entries in total, and the parameters are bounded by a constant  $B_C$ .

To extract the latent factor space for each task, we employ two latent encoders to represent task-specific and shared factors. This design ensures that the unique characteristics of each task are effectively captured while also learning shared information across tasks. Several existing works, such as Bing et al. (2020); Fan and Gu (2023), utilize linear factor models by assuming  $X = BF + u$ , where  $F$  represents latent factors,  $B$  is the loading matrix, and  $u$  denotes noise. However, these models often struggle to capture the complex factors inherent in datasets, particularly in genetic and biomedical data, where nonlinear relationships play a critical role. Instead, our dual-encoder framework is designed to capture more intricate structures. For single-task learning, the linear factor model becomes a simplified special



case of our framework with only one linear encoder.

Another related direction is the  $\beta_r^\top C(X_r)$  composite structure in (1), which aligns with multi-task representation learning suggested by Tripuraneni et al. (2020); He et al. (2024); Watkins et al. (2024) and hard parameter sharing networks (Liu et al., 2019c; Bai et al., 2022). However, these works only consider the scenario where different tasks share the same encoder, neglecting distribution heterogeneity across multiple datasets. Our model addresses this issue by incorporating  $\alpha_r^\top S_r(X_r)$ , which accounts for the task-specific information in the  $r$ -th task, thereby capturing the latent factor space more comprehensively. Moreover, these methods ignore the potential similarity in mappings from the latent factors to responses. However, the similarity between mappings can facilitate the integration of diverse datasets. Our aim is to explore the intrinsic similarity structure of the coefficients  $\{\alpha_r\}_{r=1}^R$  and  $\{\beta_r\}_{r=1}^R$ , which correspond to the task-specific and task-shared latent factors across all tasks. Specifically, we impose the following assumption on  $\{\alpha_r\}_{r=1}^R$  and  $\{\beta_r\}_{r=1}^R$ :

**Assumption 1.** For any  $r \in [R]$ ,  $\alpha_r \in \mathcal{A}_r$ , where  $\mathcal{A}_r = \{\alpha_r \in \mathbb{R}^q : \|\alpha_r - \bar{\alpha}\| \leq B_r^s\}$  and  $\beta_r \in \mathcal{B}_r$ , where  $\mathcal{B}_r = \{\beta_r \in \mathbb{R}^p : \|\beta_r - \bar{\beta}\| \leq B_r^c\}$ .

For the shared latent factors  $\{C(X_r)\}_{r=1}^R$ , it is natural to impose a similarity structure on their corresponding coefficients  $\{\beta_r\}_{r=1}^R$ , as explored in Duan and Wang (2023). Additionally, we examine the similarity structure of the coefficients  $\{\alpha_r\}_{r=1}^R$  corresponding to the task-specific latent factors  $\{S_r(X_r)\}_{r=1}^R$ . This approach aligns with the soft parameter sharing framework, which enforces similarity across different networks through regularization (Yang and Hospedales, 2016). In particular,  $\bar{\alpha}$  and  $\bar{\beta}$  represent the centers of the coefficients  $\{\alpha_r\}_{r=1}^R$  and  $\{\beta_r\}_{r=1}^R$ , respectively. The sets  $\{B_r^s\}_{r=1}^R$  and  $\{B_r^c\}_{r=1}^R$  denote the distances of the coefficients  $\{\alpha_r\}_{r=1}^R$  and  $\{\beta_r\}_{r=1}^R$  from the centers  $\bar{\alpha}$  and  $\bar{\beta}$  for all tasks. When the coefficients  $\alpha_r$  of two tasks are sufficiently similar and close to  $\bar{\alpha}$ , their corresponding  $B_r^s$  values will be particularly small. Conversely, if the coefficient  $\alpha_r$  of a task differs significantly from those of other tasks, it will be far from  $\bar{\alpha}$ , resulting in a large corresponding  $B_r^s$ . By

imposing these constraints on the coefficients  $\{\alpha_r\}_{r=1}^R$  and  $\{\beta_r\}_{r=1}^R$ , our model adaptively searches the intrinsic similarity structure of these coefficients during the optimization process. Notably, we do not require  $\{\{\alpha_r\}_{r=1}^R, \bar{\alpha}\}$  and  $\{\{\beta_r\}_{r=1}^R, \bar{\beta}\}$  to be identifiable, as our focus is on the predictive capacity for response  $Y_r$ . We only require the trained  $\{\{\alpha_r\}_{r=1}^R, \bar{\alpha}\}$  and  $\{\{\beta_r\}_{r=1}^R, \bar{\beta}\}$  to satisfy the relationship in Assumption 1.

Suppose that for the  $r$ -th task, we observe  $n_r$  *i.i.d.* samples  $\{X_{ri}, Y_{ri}\}_{i \in [n_r]}$  from the probability distribution  $P_r$ . Following Assumption 1, we focus on the following empirical risk minimization problem:

$$\begin{aligned}
& \{\{\hat{\alpha}_r, \hat{\beta}_r, \hat{S}_r(\cdot)\}_{r=1}^R, \hat{\alpha}, \hat{\beta}, \hat{C}(\cdot)\} \\
= & \arg \min_{\{\{\alpha_r, \beta_r, S_r(\cdot)\}_{r=1}^R, \bar{\alpha}, \bar{\beta}, C(\cdot)\}} \frac{1}{R} \sum_{r=1}^R \frac{1}{n_r} \sum_{i=1}^{n_r} (Y_{ri} - \alpha_r^\top S_r(X_{ri}) - \beta_r^\top C(X_{ri}))^2 + \sum_{r=1}^R \lambda^o \|\bar{S}_r^\top \bar{C}_r\|_F^2, \\
& \text{s.t. } S_r(\cdot) \in \mathcal{S}, \|\alpha_r - \bar{\alpha}\| \leq B_r^s, \|\beta_r - \bar{\beta}\| \leq B_r^c, \text{ for } r \in [R], C(\cdot) \in \mathcal{C},
\end{aligned} \tag{2}$$

where  $\bar{S}_r \in \mathbb{R}^{n_r \times q}$  and  $\bar{C}_r \in \mathbb{R}^{n_r \times p}$  are the matrices whose rows are the task-specific latent factors  $S_r(X_{ri})$  and task-shared latent factors  $C(X_{ri})$  for the  $r$ -th task in (3). The penalty term  $\|\bar{S}_r^\top \bar{C}_r\|_F^2$  is imposed to discourage redundancy and ensure that  $S_r(X_{ri})$  and  $C(X_{ri})$  encode different information from the input features  $X_{ri}$ . We use the same regularization parameter  $\lambda^o$  for all  $R$  tasks. Such a strategy is commonly used in domain adaptation (Bousmalis et al., 2016; Bica and van der Schaar, 2022). Note that the minimization problem (2) is difficult to solve due to the complex constraints imposed on the coefficients  $\{\{\alpha_r, \beta_r\}_{r=1}^R, \bar{\alpha}, \bar{\beta}\}$ . Instead, we transform (2) into an equivalent minimization problem

without constraints as follows:

$$\begin{aligned}
& \{\{\widehat{\alpha}_r, \widehat{\beta}_r, \widehat{S}_r(\cdot)\}_{r=1}^R, \widehat{\bar{\alpha}}, \widehat{\bar{\beta}}, \widehat{C}(\cdot)\} \\
= & \arg \min_{\{\{\alpha_r, \beta_r, S_r(\cdot)\}_{r=1}^R, \bar{\alpha}, \bar{\beta}, C(\cdot)\}} \frac{1}{R} \sum_{r=1}^R \frac{1}{n_r} \sum_{i=1}^{n_r} (Y_{ri} - \alpha_r^\top S_r(X_{ri}) - \beta_r^\top C(X_{ri}))^2 \\
& + \sum_{r=1}^R (\lambda_r^s \|\alpha_r - \bar{\alpha}\| + \lambda_r^c \|\beta_r - \bar{\beta}\| + \lambda^o \|\bar{S}_r^\top \bar{C}_r\|_F^2). \tag{3}
\end{aligned}$$

In the minimization problem (3),  $\{\lambda_r^s, \lambda_r^c\}_{r=1}^R$  are regularization parameters for the coefficients  $\{\alpha_r, \beta_r\}_{r=1}^R$ . By properly tuning the regularization parameters  $\{\lambda_r^s, \lambda_r^c\}_{r=1}^R$ , the minimization problem (3) can handle different levels of posterior heterogeneity. Similar discussions are also provided in in (Duan and Wang, 2023). Recall from Assumption 1 that if the coefficient  $\alpha_r$  for the  $r$ -th task is very close to the center  $\bar{\alpha}$ , then the corresponding distance  $B_r^s$  will be small. In this case, the regularization parameter  $\lambda_r^s$  in (3) will be large, and vice versa. It is worth noting that for a single task, the regularization parameters  $\lambda_r^s$  and  $\lambda_r^c$  for the coefficients  $\alpha_r$  and  $\beta_r$  may differ. This allows the intrinsic similarity structures for  $\{\alpha_r\}_{r=1}^R$  and  $\{\beta_r\}_{r=1}^R$  to vary. We provide a detailed discussion of the constraint minimization problem (2) and the penalized minimization problem (3) in the Supplementary Material S.5, along with their relationships. We demonstrate that the constraint minimization problem (2) and the penalized minimization problem (3) yield consistent estimates when employing common algorithms, such as the alternating update algorithm.

### 3 Theoretical Guarantees

In this section, we establish our excess risk bound for the proposed MTL framework via local Rademacher complexity and the learning ability for a new but related task. In particular, we investigate the bound on the local Rademacher complexity of the composite function class, including task-specific and task-shared parts, and the application of this bound to

MTL. Next, conditional on the theoretical results above, we provide the excess risk of a new task based on the heterogeneity assumption.

For ease of notation, let  $X = \{\{X_{ri}\}_{i \in [n_r]}\}_{r \in [R]}$  denote all observed samples in  $R$  tasks and rewrite  $S_r(\cdot), C(\cdot)$  as  $S_r, C$ . We consider the minimizers of the population risk

$$\{\{\alpha_{*r}, \beta_{*r}, S_{*r}\}_{r=1}^R, C_*\} = \arg \min_{\{\{\alpha_r, \beta_r, S_r\}_{r=1}^R, C\}} \frac{1}{R} \sum_{r=1}^R \mathbb{E}_r [Y_r - \alpha_r^\top S_r(X_r) - \beta_r^\top C(X_r)]^2,$$

where  $S_r \in \mathcal{S}$  for  $r \in [R]$ ,  $C \in \mathcal{C}$  and  $\{\alpha_r, \beta_r\}_{r=1}^R$  satisfy Assumption 1 with distance sets  $\{B_s^c, B_r^c\}_{r=1}^R$ . We define the MTL risk for any estimate  $\{(\hat{\alpha}_r, \hat{\beta}_r, \hat{S}_r)_{r=1}^R, \hat{C}\}$  as,

$$R_{MTL}(\{\hat{\alpha}_r, \hat{\beta}_r, \hat{S}_r\}_{r=1}^R, \hat{C}) = \frac{1}{R} \sum_{r=1}^R \mathbb{E}_r [Y_r - \hat{\alpha}_r^\top \hat{S}_r(X_r) - \hat{\beta}_r^\top \hat{C}(X_r)]^2.$$

To investigate theoretical properties of  $R_{MTL}$ , we require the following key assumptions:

**Assumption 2.** *The  $\ell_2$  loss is  $b$ -bounded, i.e..  $0 \leq (y' - y)^2 \leq b \leq \infty$  for all  $y', y \in \mathcal{Y}$ .*

**Assumption 3.** (a) *Given Assumption 1 holds, there exist constants  $B_\alpha$  and  $B_\beta$  such that  $\|\bar{\alpha}\| \leq B_\alpha$  and  $\|\bar{\beta}\| \leq B_\beta$ . (b) *The input features  $X \in \mathcal{X} \subseteq \mathbb{R}^d$  satisfy that  $\|X\| \leq B_X$ . (c) *The task-specific encoder  $S_r(\cdot) \in \mathcal{S}$ , where  $\mathcal{S} = \mathcal{NN}(W_S, D_S, B_S)$ , satisfies  $\|S_r(X)\| \leq B_s$  for any  $X \in \mathcal{X}$  and  $r \in [R]$ , the task-shared encoder  $C(\cdot) \in \mathcal{C}$ , where  $\mathcal{C} = \mathcal{NN}(W_C, D_C, B_C)$ , satisfies  $\|C(X)\| \leq B_c$  for any  $X \in \mathcal{X}$ .***

Assumption 2 constrains the upper bound of the  $\ell_2$  loss, a condition that is standard and easily achievable in MTL (Tripuraneni et al., 2020; Watkins et al., 2024), such as when  $y$  is upper-bounded. Assumption 3 is standard in regression problems (Jiao et al., 2023; He et al., 2024). In contrast to He et al. (2024), who directly constrain the upper bounds of all  $\{\alpha_r\}_{r=1}^R$  and  $\{\beta_r\}_{r=1}^R$ , Assumption 3 only requires constraining the upper bounds of the two centers  $\bar{\alpha}$  and  $\bar{\beta}$ . By combining this with the distances between the corresponding coefficients and the centers in Assumption 1, we can capture the intrinsic similarity structure among  $\{\alpha_r\}_{r=1}^R$  and  $\{\beta_r\}_{r=1}^R$ .

In addition to the above assumptions, we introduce several useful definitions, including local Rademacher complexity and the sub-root function. Specifically, let  $u, R, \{n_r\}_{r=1}^R \in \mathbb{N}$ , denote  $\mathcal{Z}$  as an input space,  $\mathcal{Q}$  as a class of vector-valued functions such that  $\mathcal{Q} : \mathcal{Z} \rightarrow \mathbb{R}^u$ , and a dataset  $Z = \{\{z_{ri}\}_{i \in [n_r]}\}_{r \in [R]}$ , where  $z_{ri} \in \mathcal{Z}$ . We denote  $\widehat{\mathcal{R}}_Z(\mathcal{Q}^{\otimes R})$  as the data-dependent Rademacher complexity and  $\widehat{\mathcal{R}}_Z(\mathcal{Q}^{\otimes R}, r) = \widehat{\mathcal{R}}_Z(\{\tilde{q} \in \mathcal{Q}^{\otimes R} : V(\tilde{q}) \leq r\})$  as the local Rademacher complexity, where  $V(\cdot) : \mathcal{Q}^{\otimes R} \rightarrow \mathbb{R}$ . In our applications, we consider any  $V(\cdot)$  satisfying  $V(\tilde{q}) \leq \frac{b}{R} \sum_{r=1}^R \frac{1}{n_r} \sum_{i=1}^{n_r} \sum_{k=1}^u (q_r(z_{ri}))_k$ , as in Watkins et al. (2024), where  $b$  is the uniform bound on the range of  $q$  in the  $\ell_2$  norm. Additionally, we use  $\psi(r)$  to denote the sub-root function. Detailed definitions can be found in the Supplementary Material S.6.

We are mostly interested in the local Rademacher complexity of the  $\ell_2$  loss applied to the function class. Specifically, if we define such a class as  $\ell_2 \circ (\mathcal{A}(\mathcal{S})^{\otimes R} + \mathcal{B}^{\otimes R}(\mathcal{C})) = \{(\ell_2 \circ (\alpha_1^\top S_1 + \beta_1^\top C), \dots, \ell_2 \circ (\alpha_R^\top S_R + \beta_R^\top C)) | \alpha_r \in \mathcal{A}_r, \beta_r \in \mathcal{B}_r, S_r \in \mathcal{S} \text{ for } r \in [R], C \in \mathcal{C}\}$ , then we seek to bound  $\widehat{\mathcal{R}}_Z(\ell_2 \circ (\mathcal{A}(\mathcal{S})^{\otimes R} + \mathcal{B}^{\otimes R}(\mathcal{C})), r)$ . Based on the above assumptions and definitions, we establish the following local Rademacher result for MTL.

**Theorem 1.** *Let  $\{\{\widehat{\alpha}_r, \widehat{\beta}_r, \widehat{S}_r\}_{r=1}^R, \widehat{C}\}$  be an empirical risk minimizer as given in (2) and  $N = \sum_{r=1}^R n_r$ . Let  $\psi(r) \geq b\mathbb{E}[\widehat{\mathcal{R}}_X(\ell_2 \circ (\mathcal{A}(\mathcal{S})^{\otimes R} + \mathcal{B}^{\otimes R}(\mathcal{C})), r)]$  with  $r^*$  being the fixed point of  $\psi(r)$ . Then, under Assumption 2, with probability at least  $1 - 2e^{-\delta}$ , it holds that*

$$\begin{aligned} & R_{MTL}(\{\widehat{\alpha}_r, \widehat{\beta}_r, \widehat{S}_r\}_{r=1}^R, \widehat{C}) - R_{MTL}(\{\alpha_{*r}, \beta_{*r}, S_{*r}\}_{r=1}^R, C_*) \\ & \leq c \left( \sqrt{R_{MTL}(\{\alpha_{*r}, \beta_{*r}, S_{*r}\}_{r=1}^R, C_*)} \left( \sqrt{\frac{b\delta}{N}} + \sqrt{\frac{r^*}{b}} \right) + \frac{b\delta}{N} + \frac{r^*}{b} \right), \end{aligned} \quad (4)$$

where  $c$  is a absolute constant.

In Theorem 1, the inequality (4) bounds the excess risk in terms of local Rademacher complexity parameters, the fixed points  $r^*$ , and the minimum population risk for MTL across all  $R$  tasks,  $R_{MTL}(\{\alpha_{*r}, \beta_{*r}, S_{*r}\}_{r=1}^R, C_*)$ . This bound is considered optimistic, as it interpolates between  $\sqrt{r^*}$  and  $r^*$ , depending on  $R_{MTL}(\{\alpha_{*r}, \beta_{*r}, S_{*r}\}_{r=1}^R, C_*)$ . The fixed

point  $r^*$  is a function of  $\mathcal{A}(\mathcal{S})^{\otimes R} + \mathcal{B}^{\otimes R}(\mathcal{C})$ , representing complexity with respect to the total number of samples across  $R$  tasks. This also highlights the advantage of integrating samples from different tasks. Dependence on the minimum population risk is useful in various contexts. For instance, when  $R_{MTL}(\{\alpha_{*r}, \beta_{*r}, S_{*r}\}_{r=1}^R, C_*) = 0$ , we achieve a bound of  $r^*$ .

In the following, we establish the theoretical result providing an upper bound for the fixed point  $r^*$  under regularity assumptions.

**Theorem 2.** *Under the setting of Theorem 1 and Assumptions 1 and 3, with probability at least  $1 - 3e^{-\delta}$ , the fixed point  $r^*$  of  $\psi(r)$  is bounded by*

$$r^* \leq cb \left( \left( \widehat{\mathcal{F}}_X(\mathcal{A}(\mathcal{S})^{\otimes R} + \mathcal{B}^{\otimes R}(\mathcal{C})) \right)^2 (\log \sqrt{N})^4 + \frac{D_X^2 (\log \sqrt{N})^2 + b(1 + \delta)}{N} \right),$$

where  $c$  is an absolute constant. Define  $B_{max}^s = \max_r B_r^s$ ,  $B_{max}^c = \max_r B_r^c$ ,  $\bar{n} = \max_r n_r$ , and  $\underline{n} = \min_r n_r$ , then,

$$\begin{aligned} \widehat{\mathcal{F}}_X(\mathcal{A}(\mathcal{S})^{\otimes R} + \mathcal{B}^{\otimes R}(\mathcal{C})) = & \left( 4(B_\alpha + B_{max}^s) L_S q \sqrt{\frac{R \log \bar{n}}{N}} + (B_\alpha + B_{max}^s) \sqrt{\frac{Rq}{N}} \right. \\ & \left. + 4(B_\beta + B_{max}^c) L_C p \sqrt{\frac{\log N}{N}} + (B_\beta + B_{max}^c) \sqrt{\frac{Rp}{N}} \right), \end{aligned}$$

with  $L_S = B_X(B_S)^{D_S} \sqrt{D_S + 1 + \log d}$  and  $L_C = B_X(B_C)^{D_C} \sqrt{D_C + 1 + \log d}$ . For  $D_X$ ,

$$\begin{aligned} D_X \leq & O((B_\alpha + B_{max}^s)^2) + O((B_\alpha + B_{max}^s) \underline{n}^{-1/2}) + O \left( (B_\alpha + B_{max}^s) \sqrt{\frac{p \log((B_\alpha + B_{max}^s) \bar{n})}{\underline{n}}} \right) \\ & + O \left( (B_\alpha + B_{max}^s) \sqrt{\frac{E_S \log((B_\alpha + B_{max}^s)^2 Q_S \bar{n})}{\underline{n}}} \right) \\ & + O((B_\beta + B_{max}^c)^2) + O((B_\beta + B_{max}^c) \underline{n}^{-1/2}) + O \left( (B_\beta + B_{max}^c) \sqrt{\frac{p \log((B_\beta + B_{max}^c) \bar{n})}{\underline{n}}} \right) \\ & + O \left( (B_\beta + B_{max}^c) \sqrt{\frac{E_C \log((B_\beta + B_{max}^c)^2 Q_C \bar{n})}{\underline{n}}} \right), \end{aligned}$$

with  $Q_S = D_S(2B_S)^{D_S+1}(\prod_{j=1}^{D_S} p_{j,S})(\prod_{j=2}^{D_S} p_{j,S}!)^{-1/E_S}$ , and  $Q_C = D_C(2B_C)^{D_C+1}(\prod_{j=1}^{D_C} p_{j,C})(\prod_{j=2}^{D_C} p_{j,C}!)^{-1/E_C}$ .

Note that the fixed point  $r^*$  controls the order of the rate in Theorem 1. Therefore, Theorem 2 interpolates between a rate of  $1/\sqrt{N}$  and  $1/N$ , where the fast rate can be achieved in some realizable settings. Next, we discuss the impact of various parameters on the MTL excess risk rate based on Theorem 2. First, the sample sizes across different tasks, the terms  $O(R^{1/2}N^{-1/2})$ ,  $O(R^{1/2}(\log \bar{n})^{1/2}N^{-1/2})$ ,  $O((\log N)^{1/2}N^{-1/2})$  in  $\widehat{\mathcal{F}}_X(\mathcal{A}(\mathcal{S})^{\otimes R} + \mathcal{B}^{\otimes R}(\mathcal{C}))$ , and the term  $O((\log \bar{n})^{1/2}\underline{n}^{-1/2})$  in  $D_X$ , indicate that a larger total sample size  $N$  and a larger average sample size per task  $N/R$  lead to smaller generalization error. However, when sample sizes across tasks are highly imbalanced (e.g., when the largest sample size  $\bar{n}$  is significantly greater than the smallest  $\underline{n}$ ), this imbalance can weaken the convergence rate. Similar findings have also been observed in He et al. (2024). Second, we observe that the high divergence of the input dimension  $d$  and the output dimensions  $q$  and  $p$  of the task-specific and task-shared encoders weakens the convergence rate. Third, the parameters  $B_{max}^s$  and  $B_{max}^c$ , which correspond to the similarity structure of the coefficients in Assumption 1, also impact the convergence rate of excess risk. This suggests that the farthest distance from the centers  $\bar{\alpha}$  and  $\bar{\beta}$  across all  $R$  tasks diminishes the effectiveness of MTL. Fourth, the network architecture parameters of the task-specific and task-shared encoders also play a role, such as  $L_S = B_X(B_S)^{D_S}\sqrt{D_S + 1 + \log d}$  and  $L_C = B_X(B_C)^{D_C}\sqrt{D_C + 1 + \log d}$  in  $\widehat{\mathcal{F}}_X(\mathcal{A}(\mathcal{S})^{\otimes R} + \mathcal{B}^{\otimes R}(\mathcal{C}))$ . When  $D_S$  and  $D_C$  are large, the encoders  $S_r(X_r)$  and  $C(X_r)$  can approximate a larger function space but result in a less tighter upper bound on the generalization error. Similar findings regarding the network architecture parameters are also reflected in  $Q_S$  and  $Q_C$  in  $D_X$ . We provide detailed derivations and explanations of  $\widehat{\mathcal{F}}_X(\mathcal{A}(\mathcal{S})^{\otimes R} + \mathcal{B}^{\otimes R}(\mathcal{C}))$  and  $D_X$  in the Supplementary Material S.9.

Additionally, based on the above theoretical results for the proposed MTL method, we consider a new but related task  $(X_0, Y_0)$  given  $R$  existing tasks and investigate the excess

risk of this new task while sharing the same latent factor extractor  $C(\cdot)$ . We consider the following minimization problem over  $n_0$  samples  $\{X_{0i}, Y_{0i}\}_{i \in [n_0]}$  :

$$\{\hat{\alpha}_0, \hat{\beta}_0, \hat{S}_0\} = \arg \min_{\{\alpha_0, \beta_0, S_0\}} \frac{1}{n_0} \sum_{i=1}^{n_0} (Y_{0i} - \alpha_0^\top S_0(X_{0i}) - \beta_0^\top \hat{C}(X_{0i}))^2,$$

where  $\hat{C}$  is the minimizer of (2). We propose a heterogeneity assumption to characterize the differences between the new task and the existing  $R$  tasks, and prove theoretical results that interpolate between a rate of  $1/\sqrt{n_0} + 1/\sqrt{N}$  and  $1/n_0 + 1/N$ . Detailed analyses can be found in the Supplementary Material S.6.

## 4 Estimation and Implementation

In this section, we introduce the estimation and hyperparameter tuning procedures of the proposed MTL framework for  $R$  heterogeneous datasets. Specifically, for the minimization (3), there are two parts of parameters to be estimated. The first part includes the task-specific and task-shared encoders, and the second part is the corresponding coefficients. We divide (3) into the following steps and alternately update several components of parameters.

Step 1: Given estimated  $\{\{\hat{\alpha}_r\}_{r=1}^R, \hat{\alpha}\}$  and  $\{\{\hat{\beta}_r\}_{r=1}^R, \hat{\beta}\}$ , we can estimate  $\{S_r(\cdot)\}_{r=1}^R$  and  $C(\cdot)$  through

$$\{\{\hat{S}_r(\cdot)\}_{r=1}^R, \hat{C}(\cdot)\} = \arg \min_{\{\{S_r(\cdot)\}_{r=1}^R, C(\cdot)\}} \frac{1}{R} \sum_{r=1}^R \frac{1}{n_r} \sum_{i=1}^{n_r} (Y_{ri} - \hat{\alpha}_r^\top S_r(X_{ri}) - \hat{\beta}_r^\top C(X_{ri}))^2 + \sum_{r=1}^R \lambda^o \|\bar{S}_r^\top \bar{C}_r\|_F^2,$$

where  $S_r(\cdot) \in \mathcal{S}$  for  $r \in [R]$ , and  $C(\cdot) \in \mathcal{C}$ . Specifically, we employ the Adam optimizer (Kingma and Ba, 2014) for optimizing  $\{\{S_r(\cdot)\}_{r=1}^R, C(\cdot)\}$ .

Step 2: Given estimated  $\{\hat{S}_r(\cdot)\}_{r=1}^R, \hat{C}(\cdot)$  and  $\{\hat{\alpha}_r\}_{r=1}^R$ , we can estimate  $\{\beta_r\}_{r=1}^R$  and  $\bar{\beta}$



through the following optimization:

$$\{\{\widehat{\beta}_r\}_{r=1}^R, \widehat{\bar{\beta}}\} = \arg \min_{\{\{\beta_r\}_{r=1}^R, \bar{\beta}\}} \frac{1}{R} \sum_{r=1}^R \frac{1}{n_r} \sum_{i=1}^{n_r} (Y_{ri} - \widehat{\alpha}_r^\top \widehat{S}_r(X_{ri}) - \beta_r^\top \widehat{C}(X_{ri}))^2 + \sum_{r=1}^R \lambda_r^c \|\beta_r - \bar{\beta}\|. \quad (5)$$

Note that given  $\{\widehat{S}_r(\cdot)\}_{r=1}^R$ ,  $\widehat{C}(\cdot)$  and  $\{\widehat{\alpha}_r\}_{r=1}^R$ , (5) is a convex optimization problem. For efficient implementation of (5), we define  $v_r = \beta_r - \bar{\beta}$  for  $r \in [R]$  and transform (5) to a more simplified form,

$$\{\{\widehat{v}_r\}_{r=1}^R, \widehat{\bar{\beta}}\} = \arg \min_{\{\{v_r\}_{r=1}^R, \bar{\beta}\}} \frac{1}{R} \sum_{r=1}^R \frac{1}{n_r} \sum_{i=1}^{n_r} (Y_{ri} - \widehat{\alpha}_r^\top \widehat{S}_r(X_{ri}) - (v_r + \bar{\beta})^\top \widehat{C}(X_{ri}))^2 + \sum_{r=1}^R \lambda_r^c \|v_r\|.$$

We will optimize the two blocks of variables  $\{v_r\}_{r=1}^R$  and  $\bar{\beta}$  iteratively. If  $\bar{\beta}$  is fixed, we optimize  $R$  independent minimization problems,

$$\widehat{v}_r = \arg \min_{v_r} \frac{1}{R} \frac{1}{n_r} \sum_{i=1}^{n_r} (Y_{ri} - \widehat{\alpha}_r^\top \widehat{S}_r(X_{ri}) - (v_r + \bar{\beta})^\top \widehat{C}(X_{ri}))^2 + \lambda_r^c \|v_r\|, \quad r \in [R]. \quad (6)$$

A natural algorithm for handling nonsmooth convex regularizers such as  $\|\cdot\|$  is to employ proximal gradient descent. The iteration for solving (6) is

$$v_r^{t+1} = \text{prox}_{\eta \lambda_r^c} \left( v_r^t - \eta \frac{2}{R n_r} \left( \sum_{i=1}^{n_r} \widehat{C}(X_{ri}) \right) (\widehat{\alpha}_r^\top \widehat{S}_r(X_{ri}) + (v_r + \bar{\beta})^\top \widehat{C}(X_{ri}) - Y_{ri}) \right), \quad r \in [R],$$

where  $\text{prox}_a(v) = (1 - c/\|v\|)_+ v$  and  $\eta$  is the learning rate. If  $\{\widehat{v}_r\}_{r=1}^R$  is fixed, we can estimate  $\bar{\beta}$  through

$$\widehat{\bar{\beta}} = \arg \min_{\bar{\beta}} \frac{1}{R} \sum_{r=1}^R \frac{1}{n_r} \sum_{i=1}^{n_r} (Y_{ri} - \widehat{\alpha}_r^\top \widehat{S}_r(X_{ri}) - (\widehat{v}_r + \bar{\beta})^\top \widehat{C}(X_{ri}))^2,$$

Step 3: We obtain the estimates of  $\{\alpha_r\}_{r=1}^R$  and  $\bar{\alpha}$  when  $\{\widehat{S}_r(\cdot)\}_{r=1}^R$ ,  $\widehat{C}(\cdot)$ , and  $\{\widehat{\beta}_r\}_{r=1}^R$  are fixed, following a similar approach to Step 2. The details are omitted here for brevity.

For simplicity, we use the same learning rate in all steps. To stabilize the optimization during the iterations, we utilize the exponential scheduler (Patterson and Gibson, 2017), which decays the learning rate by a constant per epoch. In all of our numerical tasks, we use 0.95 as a decaying constant for the exponential scheduler. For hyperparameter tuning, the proposed MTL method includes multiple hyperparameters: network structure-related hyperparameters (e.g., network depth, network width, and encoder output dimensions) and optimization-related hyperparameters (e.g., regularization parameters  $\{\lambda_r^s, \lambda_r^c\}_{r=1}^R$ , orthogonality penalty parameter  $\lambda^o$ , mini-batch size, learning rate). These hyperparameters induce an extremely large search space, making the grid search method (Yu and Zhu, 2020) practically infeasible. Instead, we randomly sample 50 hyperparameter settings in each experiment over the pre-specified search space (detailed specifications of the hyperparameter space are provided in the Supplementary Material S.3), and the best hyperparameter setting is selected if it attains the smallest loss on an independent validation set. We repeat Steps 1–3 until convergence and obtain the estimators  $\{\{\hat{\alpha}_r, \hat{\beta}_r, \hat{S}_r(\cdot)\}_{r=1}^R, \hat{C}(\cdot)\}$ . The detailed training algorithm is listed in Algorithm 1.

---

**Algorithm 1** The proposed MTL method training algorithm

---

**Input:**  $R$  training datasets  $\{\{X_{ri}, Y_{ri}\}_{i \in [n_r]}\}_{r \in [R]}$ , hyper-parameters including network structure-related hyper-parameters (e.g., network depths  $D_S, D_C$ , network widths  $W_S, W_C$ , encoder output dimensions  $q$  and  $p$ ), optimization-related hyper-parameters (e.g., regularization parameters for the similarity structure  $\{\lambda_r^s, \lambda_r^c\}_{r=1}^R$ , regularization parameter for discouraging redundancy  $\lambda^o$ , mini-batch sizes  $\{B_r\}_{r=1}^R$  for  $R$  datasets, learning rate  $\eta$ , and training epochs  $E$ ).

**Initialization:** Initialize parameters in  $\{\{\hat{\alpha}_r^{(0)}, \hat{\beta}_r^{(0)}, \hat{S}_r^{(0)}(\cdot)\}_{r=1}^R, \hat{C}^{(0)}(\cdot)\}$ .

**Training:**

**for**  $e$  in  $1 : E$  **do**

**for** Mini-batches sampled from  $\{\{X_{ri}, Y_{ri}\}_{i \in [n_r]}\}_{r \in [R]}$  **do**

$$\{\{\hat{S}_r^{(e)}(\cdot)\}_{r=1}^R, \hat{C}^{(e)}(\cdot)\} = \arg \min_{\{\{S_r(\cdot)\}_{r=1}^R, C(\cdot)\}} \frac{1}{R} \sum_{r=1}^R \frac{1}{B_r} \sum_{i=1}^{B_r} (Y_{ri} - \hat{\alpha}_r^{(e-1)\top} S_r(X_{ri}) - \hat{\beta}_r^{(e-1)\top} C(X_{ri}))^2 + \sum_{r=1}^R \lambda^o \|\bar{S}_r^\top \bar{C}_r\|_F^2$$

$$\{\{\hat{\beta}_r^{(e)}\}_{r=1}^R, \hat{\beta}^{(e)}\} = \arg \min_{\{\{\beta_r\}_{r=1}^R, \bar{\beta}\}} \frac{1}{R} \sum_{r=1}^R \frac{1}{B_r} \sum_{i=1}^{B_r} (Y_{ri} - \hat{\alpha}_r^{(e-1)\top} \hat{S}_r^{(e)}(X_{ri}) - \beta_r^\top \hat{C}^{(e)}(X_{ri}))^2 + \sum_{r=1}^R \lambda_r^c \|\beta_r - \bar{\beta}\|$$

$$\{\{\hat{\alpha}_r^{(e)}\}_{r=1}^R, \hat{\alpha}^{(e)}\} = \arg \min_{\{\{\alpha_r\}_{r=1}^R, \bar{\alpha}\}} \frac{1}{R} \sum_{r=1}^R \frac{1}{B_r} \sum_{i=1}^{B_r} (Y_{ri} - \alpha_r^\top \hat{S}_r^{(e)}(X_{ri}) - \hat{\beta}_r^{(e-1)\top} \hat{C}^{(e)}(X_{ri}))^2 + \sum_{r=1}^R \lambda_r^c \|\alpha_r - \bar{\alpha}\|$$

**end for**

**end for**

---

## 5 Simulation

In this section, we evaluate the finite-sample performance of the proposed MTL framework using simulated data. We generate data under various designs and compare our method with existing approaches. Specifically, we generate the simulated data using the following latent factor models:

$$X_r = F_r B_r + E_r, \quad (7)$$

$$Y_r = (F_r \odot F_r)^\top (\gamma_c + \gamma_r)/d + \varepsilon_r, \quad \text{for any } r \in [R]. \quad (8)$$

In (7) and (8), the latent factor space for the  $r$ -th dataset is denoted as  $F_r$ . We impose a partially shared structure for  $\{F_r\}_{r=1}^R$  as  $F_r = F V_r$  for  $r \in [R]$ , where the entries of  $F$  are drawn from standard normal distributions, and  $\{V_r\}_{r=1}^R$  are derived from the  $V$  matrix of a random matrix SVD decomposition. Here,  $\{V_r\}_{r=1}^R$  share  $d_c$  common columns and differ in  $d - d_c$  columns to ensure the presence of  $d$  task-shared latent factors and  $d - d_c$  task-specific latent factors for each dataset. In (7),  $\{B_r\}_{r=1}^R$  are orthogonal matrices obtained from the QR decomposition of random matrices with elements from standard normal distributions to ensure that the latent factors from the two parts do not depend on each other. For simplicity, we set  $B_1 = \dots = B_R$ . Additionally,  $\{E_r\}_{r=1}^R$  are noises with entries sampled from  $N(0, \sigma_e^2)$  in (7). In (8),  $\odot$  denotes the Hadamard product,  $\gamma_c$  represents the shared mapping from latent factors to responses, and  $\{\gamma_r\}_{r=1}^R$  are the task-specific components. Each element in  $\gamma_c$  is drawn from  $N(0, \sigma_c^2)$ , while the elements in  $\{\gamma_r\}_{r=1}^R$  are drawn from  $N(0, \sigma_r^2)$  for  $r \in [R]$ . Also,  $\{\varepsilon_r\}_{r=1}^R$  are noises sampled from  $N(0, \sigma_e^2)$  in (8).

For all tasks, we generate  $3n_r$  samples for each task, splitting them equally into training, validation, and testing sets. We train the model on the training set, perform a grid search for hyperparameter tuning, and apply early stopping based on performance on the validation set. For evaluation, we calculate the root-mean-square error (RMSE) for each task on the

testing data, given by:  $\sqrt{n_r^{-1} \sum_{i=1}^{n_r} (\hat{Y}_{ri} - Y_{ri})^2}$ . We repeat the numerical studies 100 times and calculate the means and standard deviations of the RMSEs. By default, we consider  $n_r = 200$  for  $r \in [R]$ ,  $d = 20$ ,  $d_c = 10$ ,  $\sigma_e = 0.05$ ,  $\sigma_c = 10$ ,  $\sigma_r = \bar{\sigma}$  for  $r \in [R]$ , where  $\bar{\sigma} = 1$ .

Based on the data generation process (DGP), we generate samples  $\{\{X_{ri}, Y_{ri}\}_{i \in [3n_r]}\}_{r \in [R]}$  for all tasks. These samples reflect both distribution heterogeneity, as  $d - d_c$  latent factors in  $\{V_r\}_{r=1}^R$  vary across tasks, and posterior heterogeneity, as the coefficients  $\{\gamma_r\}_{r=1}^R$  differ among tasks. Moreover, the DGP incorporates nonlinear relationships through the element-wise square of latent factors to add the complexity to the MTL framework.

We compare the proposed MTL method with the following competing methods: (a) The meta-analysis (Meta) method (Maity et al., 2022), which assumes that the coefficients from different datasets consist of a shared component and a unique component, estimated through a modified regression framework. (b) The adaptive and robust multi-task learning (ARMUL) method (Duan and Wang, 2023), which applies adaptive algorithms to leverage possible similarities among tasks while accommodating their differences. The code provided in their paper (<https://github.com/kw2934/ARMUL>) was used with default parameter settings, and tuning parameters were selected using cross-validation. (c) The fused lasso approach in regression coefficients clustering (FLARCC) method (Tang and Song, 2016), which applies a fusion penalty to identify and merge inter-task homogeneous parameter clusters in regression analysis. This method was implemented using the R package metafuse (<https://CRAN.R-project.org/package=metafuse>), and the penalty parameter was tuned based on the EBIC as described in their paper. (d) The single-task learning (STL) method, which trains a neural network on each dataset independently. For Meta, ARMUL, and FLARCC, the nonparametric component is formulated as a linear combination of cubic spline basis functions, following He et al. (2024). Since Meta, ARMUL, and FLARCC are primarily designed for linear settings, datasets with linear relationships between latent factors and responses are also generated for a fair comparison, as detailed in the Supplementary Material

S.2.

## 5.1 Different Heterogeneity Scenarios

In this subsection, we investigate the empirical performance of the proposed MTL method and the competing methods under different heterogeneity scenarios. Specifically, we set  $R = 2$ , i.e., two datasets, and consider the following three scenarios of heterogeneity.

- Setting 1 (Distribution heterogeneity):  $V_1$  and  $V_2$  share  $d_c$  common columns and differ in  $d - d_c$  columns to have  $F_1$  and  $F_2$  with partially shared latent factors while retaining distinct ones. We choose  $d_c = \{5, 10, 15, 20\}$ . We set  $\bar{\sigma} = 0$  to maintain homogeneous mappings for all tasks.
- Setting 2 (Posterior heterogeneity): We use the same  $V_1$  and  $V_2$  to preserve homogeneous latent feature spaces, while  $\bar{\sigma}$  takes values from 1 to 5 to capture heterogeneity in posterior mappings from  $F_r$  to  $Y_r$  for  $r \in [R]$ .
- Setting 3 (Both distribution and posterior heterogeneity): We combine both types of heterogeneity. Specifically,  $V_1$  and  $V_2$  share  $d_c = 10$  common columns and differ in  $d - d_c$  columns. Additionally, we set  $\bar{\sigma}$  from 1 to 5.

The means and standard deviations of RMSE for three settings are provided in Table 1. In setting 1, a larger  $d_c$  indicates less significant distribution heterogeneity between the two datasets, and the marginal distributions of the two datasets are homogeneous when  $d_c = 20$ . Our method consistently outperforms other competing methods under varying  $d_c$ s, achieving approximately 22% improvement compared to the best of the competing methods. Compared to STL, our method effectively integrates shared information across datasets. On the other hand, the other three methods do not perform well under the nonlinear relationships and distribution heterogeneity settings, and perform worse than STL. In setting 2, as  $\bar{\sigma}$  increases, the posterior heterogeneity between the two datasets becomes

more pronounced, in which STL is expected to perform well, and integrative methods may gain less improvement. Even so, the proposed method consistently demonstrates the best performance for varying  $\bar{\sigma}$ . Its advantage over STL gradually decreases as  $\bar{\sigma}$  increases, which is expected because there is less shared information to integrate when  $\bar{\sigma}$  is large. Although the other three methods can handle posterior heterogeneity to some extent, they are not able to capture the nonlinear relationships well. Setting 3 considers both distribution and posterior heterogeneity. First, our proposed method remains the best, effectively addressing both types of heterogeneity. When  $\bar{\sigma} = 1$ , it achieves an improvement of over 22.18% compared to STL. However, as  $\bar{\sigma}$  increases, the improvement gradually decreases, similar to the trend observed in Setting 2. Second, note that the prediction errors in setting 3 are higher due to the presence of distribution heterogeneity, making setting 3 more challenging than setting 2. Third, none of the other three methods can compete well with the STL under this complex scenario.

## 5.2 Impact of Different Parameters

In this subsection, we examine the effect of different sample sizes and heterogeneity parameters with a larger number of datasets. We set  $R = 3$ , i.e., three datasets, and consider the following three settings, with the DGP similar to that in Subsection 5.1:

- Setting 4: All other parameters are set as in the default setting, with  $n_1 = n_2 = n_3$  varying from  $\{200, 400, 600\}$ .
- Setting 5: All other parameters are set as in the default setting, with  $n_1 = n_2 = 200$  and  $n_3 = 400$ .
- Setting 6: All other parameters are set as in the default setting, with  $\sigma_1 = \sigma_2 = 1$  and  $\sigma_3 = 5$ .

The means and standard deviations of RMSE for settings 4-6 are provided in Table 2. For

Setting 1						
$d_c$	Dataset	MTL	Meta	FLARCC	ARUML	STL
5	Dataset 1	<b>1.797 (0.323)</b>	3.182 (0.539)	3.442 (0.586)	3.074 (0.535)	2.352 (0.422)
	Dataset 2	<b>1.806 (0.355)</b>	3.190 (0.521)	3.482 (0.615)	3.084 (0.524)	2.348 (0.421)
10	Dataset 1	<b>1.781 (0.325)</b>	3.182 (0.542)	3.401 (0.572)	3.074 (0.543)	2.358 (0.399)
	Dataset 2	<b>1.798 (0.348)</b>	3.210 (0.529)	3.423 (0.559)	3.121 (0.550)	2.382 (0.449)
15	Dataset 1	<b>1.781 (0.322)</b>	3.185 (0.554)	3.414 (0.565)	3.074 (0.539)	2.350 (0.414)
	Dataset 2	<b>1.785 (0.329)</b>	3.227 (0.514)	3.455 (0.587)	3.111 (0.519)	2.362 (0.412)
20	Dataset 1	<b>1.770 (0.328)</b>	3.182 (0.538)	3.392 (0.563)	3.071 (0.526)	2.335 (0.409)
	Dataset 2	<b>1.771 (0.335)</b>	3.204 (0.522)	3.462 (0.587)	3.136 (0.526)	2.359 (0.414)
Setting 2						
$\bar{\sigma}$	Dataset	MTL	Meta	FLARCC	ARUML	STL
1	Dataset 1	<b>1.807 (0.313)</b>	3.206 (0.561)	3.432 (0.540)	3.090 (0.549)	2.358 (0.432)
	Dataset 2	<b>1.835 (0.323)</b>	3.218 (0.528)	3.456 (0.601)	3.155 (0.534)	2.358 (0.407)
2	Dataset 1	<b>1.923 (0.313)</b>	3.261 (0.585)	3.493 (0.539)	3.140 (0.570)	2.410 (0.451)
	Dataset 2	<b>1.922 (0.339)</b>	3.261 (0.544)	3.507 (0.603)	3.204 (0.547)	2.401 (0.441)
3	Dataset 1	<b>2.114 (0.361)</b>	3.347 (0.609)	3.586 (0.550)	3.221 (0.590)	2.449 (0.469)
	Dataset 2	<b>2.129 (0.377)</b>	3.334 (0.568)	3.595 (0.595)	3.282 (0.566)	2.455 (0.431)
4	Dataset 1	<b>2.270 (0.344)</b>	3.461 (0.632)	3.710 (0.565)	3.331 (0.609)	2.524 (0.492)
	Dataset 2	<b>2.246 (0.378)</b>	3.433 (0.598)	3.713 (0.603)	3.388 (0.589)	2.511 (0.476)
5	Dataset 1	<b>2.421 (0.370)</b>	3.600 (0.656)	3.864 (0.577)	3.466 (0.627)	2.624 (0.478)
	Dataset 2	<b>2.417 (0.412)</b>	3.556 (0.633)	3.852 (0.606)	3.518 (0.617)	2.590 (0.468)
Setting 3						
$\bar{\sigma}$	Dataset	MTL	Meta	FLARCC	ARUML	STL
1	Dataset 1	<b>1.834 (0.335)</b>	3.204 (0.567)	3.433 (0.569)	3.091 (0.566)	2.362 (0.425)
	Dataset 2	<b>1.838 (0.382)</b>	3.221 (0.541)	3.448 (0.555)	3.139 (0.555)	2.406 (0.455)
2	Dataset 1	<b>1.941 (0.335)</b>	3.258 (0.592)	3.489 (0.572)	3.221 (0.608)	2.393 (0.440)
	Dataset 2	<b>1.958 (0.368)</b>	3.263 (0.559)	3.498 (0.554)	3.262 (0.580)	2.435 (0.462)
3	Dataset 1	<b>2.117 (0.351)</b>	3.342 (0.618)	3.584 (0.575)	3.330 (0.626)	2.464 (0.455)
	Dataset 2	<b>2.119 (0.392)</b>	3.334 (0.584)	3.582 (0.560)	3.365 (0.611)	2.486 (0.467)
4	Dataset 1	<b>2.313 (0.392)</b>	3.455 (0.643)	3.710 (0.589)	3.480 (0.601)	2.533 (0.463)
	Dataset 2	<b>2.295 (0.415)</b>	3.469 (0.594)	3.695 (0.573)	3.388 (0.589)	2.522 (0.475)
5	Dataset 1	<b>2.445 (0.374)</b>	3.593 (0.669)	3.869 (0.603)	3.466 (0.644)	2.618 (0.496)
	Dataset 2	<b>2.439 (0.416)</b>	3.555 (0.633)	3.842 (0.591)	3.518 (0.620)	2.625 (0.508)

Table 1: Prediction losses on testing data using different methods under Settings 1-3.

setting 4, we investigate the impact of sample size on the proposed MTL method. As the sample size increases, both MTL and STL show significant improvements, while the other three methods exhibit less noticeable gains due to nonlinear relationships and distribution heterogeneity. Compared to STL, when  $n_1 = n_2 = n_3 = 200$ , the average improvement of the proposed MTL method across the three datasets reaches 35.80%. However, as  $n$  increases to 400, the average improvement drops to 23.51%, suggesting that our method is particularly

advantageous in smaller sample settings. In setting 5, the third dataset has a larger sample size. The prediction results indicate that the proposed MTL method achieves a lower RMSE for dataset 3, and the overall prediction performance across all three datasets is notably better compared to the case where  $n_1 = n_2 = n_3 = 200$ . In setting 6, we examine varying levels of posterior heterogeneity across the datasets. Since  $\sigma_3 = 5$  for the third dataset indicates stronger posterior heterogeneity, the performance of the proposed MTL method is weaker compared to setting 4 with  $n_1 = n_2 = n_3 = 200$ . Nonetheless, the proposed method still outperforms other competing methods, followed by the STL. The competing methods Meta, FLARCC, and ARUML perform worse than STL in this scenario.

Setting 4						
$n$	Dataset	MTL	Meta	FLARCC	ARUML	STL
200	Dataset 1	<b>1.518 (0.260)</b>	3.123 (0.546)	3.353 (0.543)	3.034 (0.577)	2.350 (0.415)
	Dataset 2	<b>1.515 (0.279)</b>	3.127 (0.506)	3.310 (0.572)	3.017 (0.491)	2.374 (0.416)
	Dataset 3	<b>1.515 (0.254)</b>	3.157 (0.512)	3.333 (0.574)	3.054 (0.529)	2.360 (0.430)
400	Dataset 1	<b>1.120 (0.306)</b>	3.147 (0.523)	3.174 (0.620)	2.987 (0.501)	1.650 (0.292)
	Dataset 2	<b>1.110 (0.307)</b>	3.156 (0.497)	3.182 (0.631)	2.989 (0.508)	1.626 (0.264)
	Dataset 3	<b>1.126 (0.309)</b>	3.151 (0.502)	3.181 (0.620)	2.983 (0.504)	1.640 (0.277)
600	Dataset 1	<b>0.972 (0.156)</b>	3.133 (0.499)	3.089 (0.480)	2.964 (0.502)	1.259 (0.218)
	Dataset 2	<b>0.967 (0.152)</b>	3.153 (0.493)	3.126 (0.486)	2.976 (0.499)	1.273 (0.232)
	Dataset 3	<b>0.976 (0.148)</b>	3.148 (0.487)	3.116 (0.512)	2.992 (0.493)	1.279 (0.200)
Setting 5						
	Dataset	MTL	Meta	FLARCC	ARUML	STL
	Dataset 1	<b>1.353 (0.238)</b>	3.152 (0.525)	3.390 (0.523)	3.030 (0.512)	2.347 (0.434)
	Dataset 2	<b>1.339 (0.223)</b>	3.149 (0.554)	3.398 (0.568)	3.038 (0.525)	2.366 (0.425)
	Dataset 3	<b>1.317 (0.211)</b>	3.181 (0.492)	3.379 (0.521)	3.019 (0.510)	1.637 (0.272)
Setting 6						
	Dataset	MTL	Meta	FLARCC	ARUML	STL
	Dataset 1	<b>1.713 (0.276)</b>	3.127 (0.547)	3.393 (0.542)	3.052 (0.578)	2.350 (0.415)
	Dataset 2	<b>1.717 (0.276)</b>	3.129 (0.505)	3.350 (0.568)	3.031 (0.492)	2.374 (0.416)
	Dataset 3	<b>2.053 (0.300)</b>	3.543 (0.565)	3.753 (0.594)	3.436 (0.580)	2.631 (0.440)

Table 2: Prediction losses using different methods under settings 4-6.

Furthermore, we explore the performance of our proposed MTL method in scenarios with a larger number of datasets. Specifically, we set  $R = 4$  and  $R = 5$ , representing four and five datasets, respectively, with all other parameters set to their default values. The prediction results are provided in Table 3. Based on the previous two- and three-dataset settings, it



is evident that as the number of datasets increases, more information can be integrated, and the proposed MTL method achieves better predictions with greater improvements compared to STL. The other competing methods such as Meta, FLARCC, and ARUML also show similar improvements. For instance, in ARUML, the prediction loss for dataset 1 with  $R = 5$  is lower than with  $R = 4$ . However, the competing methods do not address distribution heterogeneity and complex relationships between response and predictors, and therefore, their overall improvements remain limited.

4 datasets					
Dataset	MTL	Meta	FLARCC	ARUML	STL
Dataset 1	<b>1.320 (0.228)</b>	3.200 (0.577)	3.360 (0.520)	3.008 (0.516)	2.351 (0.421)
Dataset 2	<b>1.328 (0.226)</b>	3.128 (0.505)	3.382 (0.543)	3.013 (0.518)	2.366 (0.425)
Dataset 3	<b>1.330 (0.202)</b>	3.158 (0.525)	3.386 (0.541)	3.030 (0.499)	2.346 (0.411)
Dataset 4	<b>1.316 (0.210)</b>	3.155 (0.529)	3.389 (0.517)	3.023 (0.530)	2.348 (0.388)
5 datasets					
Dataset	MTL	Meta	FLARCC	ARUML	STL
Dataset 1	<b>1.243 (0.220)</b>	3.148 (0.565)	3.274 (0.506)	2.956 (0.517)	2.340 (0.433)
Dataset 2	<b>1.234 (0.204)</b>	3.121 (0.516)	3.274 (0.523)	2.996 (0.518)	2.332 (0.397)
Dataset 3	<b>1.248 (0.201)</b>	3.186 (0.526)	3.305 (0.518)	3.040 (0.533)	2.362 (0.380)
Dataset 4	<b>1.244 (0.204)</b>	3.185 (0.507)	3.286 (0.534)	3.020 (0.542)	2.374 (0.405)
Dataset 5	<b>1.244 (0.218)</b>	3.136 (0.538)	3.267 (0.505)	3.040 (0.527)	2.366 (0.416)

Table 3: Prediction losses using different methods for 4 datasets and 5 datasets.

## 6 Application to Patient-derived Xenograft Studies

In this section, we analyze patient-derived xenograft data using the proposed MTL method and compare ours with various competing methods. The challenge of this data is the heterogeneity of human cancer is reflected in the molecular and phenotypic diversity of tumors in patients (Polyak et al., 2011). For instance, RNA-sequencing distributions vary across different tumor types, as do their associations with target variables. These differences pose significant challenges for MTL when applied to limited cancer data.

PDX studies conduct large-scale screenings in mice, evaluating a wide range of FDA-approved and preclinical cancer therapies (Gao et al., 2015). Specifically, PDX studies are

established by directly transplanting primary tumors from patients into immunodeficient mice (Siolas and Hannon, 2013). Tumor fragments are collected from patients through surgery or biopsy (Hidalgo et al., 2014) and implanted into mice to form PDX lines, allowing for longitudinal measurements of tumor size and growth rates. Once tumors reach sufficient size, they can be passaged to other mice, enabling multiple therapeutic tests. Additionally, high-throughput genomic analyses, such as RNA-sequencing and DNA-sequencing, can be performed on the original patient tumors. Importantly, the characteristics of the primary tumors are preserved throughout the expansion process (Hidalgo et al., 2014).

The original data comes from the Novartis PDX studies (Gao et al., 2015), and we follow the filtering and preprocessing steps outlined by Rashid et al. (2020) to obtain genomic data and tumor measurements. Specifically, we select PDX lines which had not undergone any treatment to avoid the confounding effects of treatment. In total, 173 PDX lines are collected across five tumor types: Breast Cancer (BRCA) with 38 PDX lines, Cutaneous Melanoma (CM) with 32 PDX lines, Colorectal Cancer (CRC) with 43 PDX lines, Non-Small Cell Lung Cancer (NSCLC) with 25 PDX lines, and Pancreatic Ductal Adenocarcinoma (PDAC) with 35 PDX lines. The limited number of PDX lines for each tumor type highlights the necessity of MTL. For each PDX line, the pre-treatment covariates, consistent with Rashid et al. (2020), include RNA-sequencing data, copy number data, and mutation data, covering a total of 32,504 variables. Our outcome of interest is time to tumor doubling (TTD), defined as the number of days from baseline for the tumor to double in size. Due to the skewness in the TTD distribution, we apply the natural logarithm transformation for the analysis.

To reduce dimensionality, we perform PCA on the original pre-treatment covariates for all five tumor types together, resulting in 122-dimensional input features. These principal components account for 95% of the cumulative variance. The left panel of Figure 2 visualizes the t-SNE (Van der Maaten and Hinton, 2008) results of the input features for the five tumor types. The t-SNE plot indicates some separation among tumor types, with CRC and

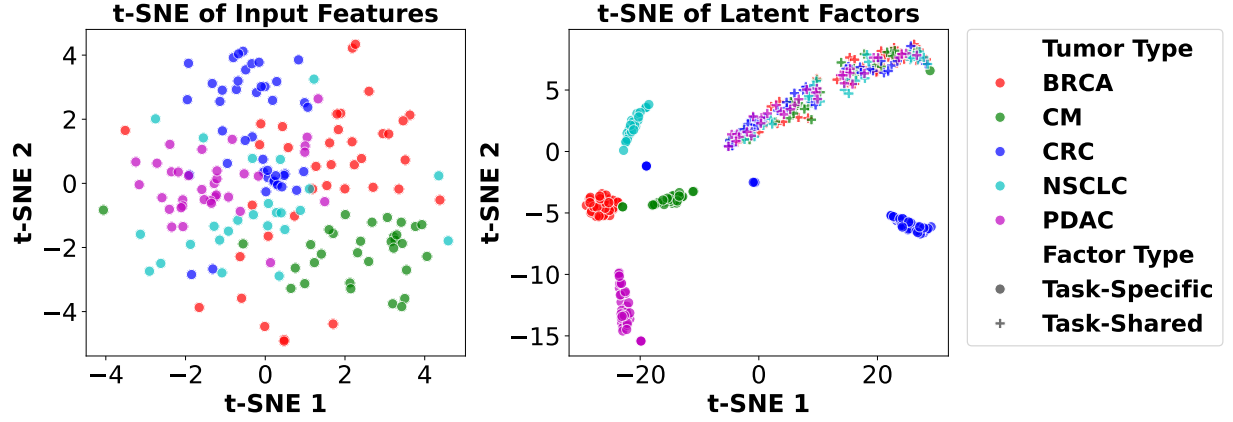


Figure 2: The left panel shows the t-SNE visualization of the input features after PCA processing, while the right panel presents the t-SNE visualization of the learned task-specific and task-shared latent factors using our proposed method.

CM exhibiting the most distinct distributions, suggesting notable distribution heterogeneity in the input features. For the competing method FLARCC, fewer features are used to avoid singularity. For each tumor type, the PDX lines are approximately split into three equal parts: training, validation, and testing sets. For MTL and STL, models are trained on the training set, with early stopping and tuning performed on the validation set. For the other three methods, the training and validation sets are combined for model training.

We repeat the experiment 100 times and calculate the RMSEs for each method on the testing set. The prediction results are summarized in Table 4. As shown in Table 4, the proposed MTL method achieves the best prediction losses across all five tumor types. Compared to STL, the improvements for the five tumor types are 6.77%, 8.32%, 5.99%, 10.82%, and 10.22%, respectively. For Meta, which assumes a specific structure for the posterior mapping, this assumption may not hold for the PDX data, resulting in the worst predictive performance. Both FLARCC and ARUML are limited by their ability to only capture linear relationships and their insufficiency to address distribution heterogeneity, resulting in inferior performance compared to STL. The right panel of Figure 2 shows the t-SNE visualization of the latent factors obtained from a single training session, where our method effectively captures both shared and task-specific latent factors. Notably, the

task-specific latent factors of the five tumor types exhibit significant differences in their distributions.

Tumor Type	MTL	Meta	FLARCC	ARUML	STL
BRCA	<b>0.937 (0.203)</b>	2.014 (0.404)	1.706 (0.284)	1.181 (0.173)	1.005 (0.191)
CM	<b>0.760 (0.170)</b>	1.543 (0.368)	0.921 (0.173)	1.215 (0.226)	0.829 (0.184)
CRC	<b>1.021 (0.203)</b>	2.208 (0.590)	1.536 (0.351)	1.274 (0.132)	1.086 (0.221)
NSCLC	<b>1.021 (0.207)</b>	2.031 (0.418)	1.793 (0.381)	1.289 (0.271)	1.145 (0.209)
PDAC	<b>0.879 (0.193)</b>	1.267 (0.343)	1.569 (0.368)	1.077 (0.173)	0.979 (0.191)

Table 4: Prediction losses across different methods for 5 tumor types.

We also compute the relative distances  $\{\|\hat{\alpha}_r - \hat{\alpha}\|/\|\hat{\alpha}\|, \|\hat{\beta}_r - \hat{\beta}\|/\|\hat{\beta}\|\}_{r=1}^5$  in each training session and calculate their averages. The results are shown in Table 5. We observe that the averages of  $\|\hat{\alpha}_r - \hat{\alpha}\|/\|\hat{\alpha}\|$  are smaller when  $r = 5, 4, 2$  for the task-specific latent factors, while the averages of  $\|\hat{\beta}_r - \hat{\beta}\|/\|\hat{\beta}\|$  are smaller when  $r = 2, 4, 1$  for the task-shared latent factors. This indicates that the mappings of task-specific latent factors are more similar for PDAC, NSCLC, and CM, whereas the mappings of task-shared latent factors are more similar for CM, NSCLC, and BRCA. We visualize the estimates of  $\{\{\hat{\alpha}_r\}_{r=1}^5, \hat{\alpha}\}$  and  $\{\{\hat{\beta}_r\}_{r=1}^5, \hat{\beta}\}$  from a single training session in Figure 3. It is evident that, for the task-specific latent factors, the coefficients for PDAC, NSCLC, and CM closely resemble  $\hat{\alpha}$ , while those for BRCA and CRC show noticeable differences. For the task-shared latent factors, the coefficients for CM, NSCLC, and BRCA are very similar to the center  $\hat{\beta}$ , whereas CRC and PDAC display significant differences from the center  $\hat{\beta}$ .

Tumor Type	$\ \hat{\alpha}_r - \hat{\alpha}\ /\ \hat{\alpha}\ $	$\ \hat{\beta}_r - \hat{\beta}\ /\ \hat{\beta}\ $
BRCA	0.224	0.175
CM	0.207	0.151
CRC	0.210	0.211
NSCLC	0.191	0.175
PDAC	0.183	0.195

Table 5: Relative distances for corresponding coefficients for 5 tumor types.

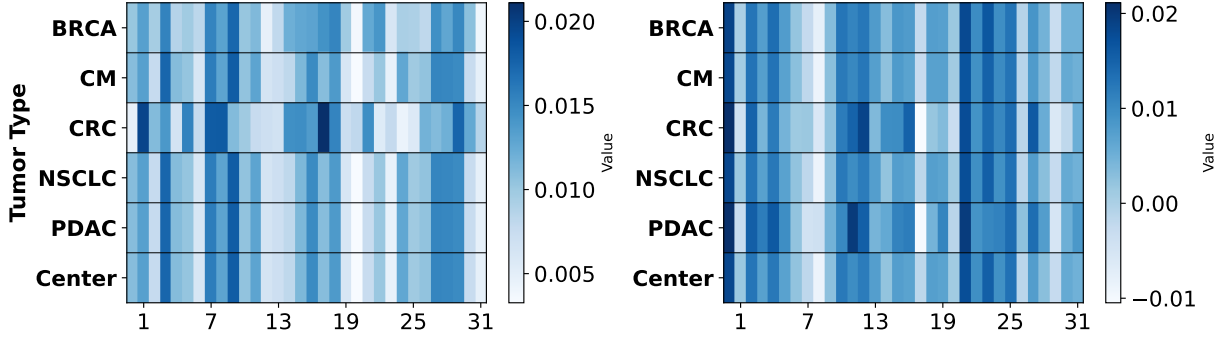


Figure 3: Left panel: the coefficients  $\{\hat{\alpha}_r\}_{r=1}^5$  corresponding to the task-specific latent factors and the center  $\hat{\alpha}$  for five tumor types, right panel: the coefficients  $\{\hat{\beta}_r\}_{r=1}^5$  corresponding to the task-shared latent factors and the center  $\hat{\beta}$  for five tumor types.

## 7 Discussion

In this paper, we introduced a unified framework for MTL that addresses both distribution and posterior heterogeneity, along with an alternating optimization algorithm. We investigated the excess risk bound of the proposed MTL framework and evaluated its empirical performance through various simulation studies and real data application on PDX data analysis. There are several promising directions for future research. First, the proposed method assumes a common latent factor component shared across all tasks, suggesting a relatively strong shared structure. However, in real-world scenarios with significant distribution heterogeneity, the datasets often follow a partially-shared structure (Gaynanova and Li, 2019). In such cases, an adaptive approach is needed to extract latent factors that reflect partially-shared structures among tasks while preserving the uniqueness of highly heterogeneous tasks. Current studies propose adaptive MTL methods that address posterior heterogeneity in simpler settings, such as linear cases (Duan and Wang, 2023; Tian et al., 2023). However, adaptive MTL which simultaneously addresses both distribution and posterior heterogeneity remains largely unexplored, making it a valuable area for future research. Second, extending our proposed method to more generalized implementations, such as specific network parameter sharing modes (Yang and Hospedales, 2016), merits further investigation. For example, assuming a structured-sharing pattern in soft-parameter sharing

could narrow the search to a smaller network space, and lead to enhancing computational efficiency.

## References

- Abdollahzadeh, M., Malekzadeh, T., and Cheung, N.-M. M. (2021). Revisit multimodal meta-learning through the lens of multi-task learning. *Advances in Neural Information Processing Systems*, 34:14632–14644.
- Bai, T., Xiao, Y., Wu, B., Yang, G., Yu, H., and Nie, J.-Y. (2022). A contrastive sharing model for multi-task recommendation. In *Proceedings of the ACM Web Conference 2022*, pages 3239–3247.
- Bartlett, P. L., Bousquet, O., and Mendelson, S. (2005). Local rademacher complexities. *Annals of Statistics*, pages 1497–1537.
- Bernal, J., Kushibar, K., Asfaw, D. S., Valverde, S., Oliver, A., Martí, R., and Lladó, X. (2019). Deep convolutional neural networks for brain image analysis on magnetic resonance imaging: a review. *Artificial intelligence in medicine*, 95:64–81.
- Bica, I. and van der Schaar, M. (2022). Transfer learning on heterogeneous feature spaces for treatment effects estimation. *Advances in Neural Information Processing Systems*, 35:37184–37198.
- Bing, X., Bunea, F., Ning, Y., and Wegkamp, M. (2020). Adaptive estimation in structured factor models with applications to overlapping clustering. *Annals of Statistics*, 48(4).
- Bousmalis, K., Trigeorgis, G., Silberman, N., Krishnan, D., and Erhan, D. (2016). Domain separation networks. *Advances in neural information processing systems*, 29.
- Boyd, S. and Vandenberghe, L. (2004). *Convex optimization*. Cambridge university press.
- Clark, K., Luong, M.-T., Khandelwal, U., Manning, C. D., and Le, Q. V. (2019). Bam! born-again multi-task networks for natural language understanding. *arXiv preprint arXiv:1907.04829*.
- Cohen Kalafut, N., Huang, X., and Wang, D. (2023). Joint variational autoencoders for multimodal imputation and embedding. *Nature Machine Intelligence*, 5(6):631–642.
- Crawshaw, M. (2020). Multi-task learning with deep neural networks: A survey. *arXiv preprint arXiv:2009.09796*.
- Devroye, L., Györfi, L., and Lugosi, G. (2013). *A probabilistic theory of pattern recognition*, volume 31. Springer Science & Business Media.

- Du, S. S., Hu, W., Kakade, S. M., Lee, J. D., and Lei, Q. (2020). Few-shot learning via learning the representation, provably. *arXiv preprint arXiv:2002.09434*.
- Du, Y., Czarnecki, W. M., Jayakumar, S. M., Farajtabar, M., Pascanu, R., and Lakshminarayanan, B. (2018). Adapting auxiliary losses using gradient similarity. *arXiv preprint arXiv:1812.02224*.
- Duan, Y. and Wang, K. (2023). Adaptive and robust multi-task learning. *The Annals of Statistics*, 51(5):2015–2039.
- Fagny, M., Paulson, J. N., Kuijjer, M. L., Sonawane, A. R., Chen, C.-Y., Lopes-Ramos, C. M., Glass, K., Quackenbush, J., and Platig, J. (2017). Exploring regulation in tissues with eqtl networks. *Proceedings of the National Academy of Sciences*, 114(37):E7841–E7850.
- Fan, J. and Gu, Y. (2023). Factor augmented sparse throughput deep relu neural networks for high dimensional regression. *Journal of the American Statistical Association*, pages 1–15.
- Gao, H., Korn, J. M., Ferretti, S., Monahan, J. E., Wang, Y., Singh, M., Zhang, C., Schnell, C., Yang, G., Zhang, Y., et al. (2015). High-throughput screening using patient-derived tumor xenografts to predict clinical trial drug response. *Nature medicine*, 21(11):1318–1325.
- Gao, Y., Ma, J., Zhao, M., Liu, W., and Yuille, A. L. (2019). Nddr-cnn: Layerwise feature fusing in multi-task cnns by neural discriminative dimensionality reduction. In *Proceedings of the IEEE/CVF conference on computer vision and pattern recognition*, pages 3205–3214.
- Gaynanova, I. and Li, G. (2019). Structural learning and integrative decomposition of multi-view data. *Biometrics*, 75(4):1121–1132.
- Golowich, N., Rakhlin, A., and Shamir, O. (2018). Size-independent sample complexity of neural networks. In *Conference On Learning Theory*, pages 297–299. PMLR.
- Györfi, L., Kohler, M., Krzyzak, A., Walk, H., et al. (2002). *A distribution-free theory of nonparametric regression*, volume 1. Springer.
- Han, Z., Gao, C., Liu, J., Zhang, S. Q., et al. (2024). Parameter-efficient fine-tuning for large models: A comprehensive survey. *arXiv preprint arXiv:2403.14608*.
- Hang, T., Gu, S., Li, C., Bao, J., Chen, D., Hu, H., Geng, X., and Guo, B. (2023). Efficient diffusion training via min-snr weighting strategy. In *Proceedings of the IEEE/CVF International Conference on Computer Vision*, pages 7441–7451.
- He, B., Liu, H., Zhang, X., and Huang, J. (2024). Representation transfer learning for semiparametric regression. *arXiv preprint arXiv:2406.13197*.

- Hidalgo, M., Amant, F., Biankin, A. V., Budinská, E., Byrne, A. T., Caldas, C., Clarke, R. B., de Jong, S., Jonkers, J., Mælandsmo, G. M., et al. (2014). Patient-derived xenograft models: an emerging platform for translational cancer research. *Cancer discovery*, 4(9):998–1013.
- Huang, J., Jiao, Y., Wang, W., Yan, X., and Zhu, L. (2023). Integrative analysis for high-dimensional stratified models. *Statistica Sinica*, 33.
- Jiao, Y., Shen, G., Lin, Y., and Huang, J. (2023). Deep nonparametric regression on approximate manifolds: Nonasymptotic error bounds with polynomial prefactors. *The Annals of Statistics*, 51(2):691–716.
- Jin, K. H., McCann, M. T., Froustey, E., and Unser, M. (2017). Deep convolutional neural network for inverse problems in imaging. *IEEE transactions on image processing*, 26(9):4509–4522.
- Kendall, A., Gal, Y., and Cipolla, R. (2018). Multi-task learning using uncertainty to weigh losses for scene geometry and semantics. In *Proceedings of the IEEE conference on computer vision and pattern recognition*, pages 7482–7491.
- Kingma, D. P. and Ba, J. (2014). Adam: A method for stochastic optimization. *arXiv preprint arXiv:1412.6980*.
- Li, S., Cai, T. T., and Li, H. (2022). Transfer learning for high-dimensional linear regression: Prediction, estimation and minimax optimality. *Journal of the Royal Statistical Society Series B: Statistical Methodology*, 84(1):149–173.
- Li, S., Zhang, L., Cai, T. T., and Li, H. (2024). Estimation and inference for high-dimensional generalized linear models with knowledge transfer. *Journal of the American Statistical Association*, 119(546):1274–1285.
- Litjens, G., Kooi, T., Bejnordi, B. E., Setio, A. A. A., Ciompi, F., Ghafoorian, M., Van Der Laak, J. A., Van Ginneken, B., and Sánchez, C. I. (2017). A survey on deep learning in medical image analysis. *Medical image analysis*, 42:60–88.
- Liu, S., Liang, Y., and Gitter, A. (2019a). Loss-balanced task weighting to reduce negative transfer in multi-task learning. In *Proceedings of the AAAI conference on artificial intelligence*, volume 33, pages 9977–9978.
- Liu, X., He, P., Chen, W., and Gao, J. (2019b). Improving multi-task deep neural networks via knowledge distillation for natural language understanding. *arXiv preprint arXiv:1904.09482*.
- Liu, X., He, P., Chen, W., and Gao, J. (2019c). Multi-task deep neural networks for natural language understanding. In *Proceedings of the 57th Annual Meeting of the Association*



- for *Computational Linguistics*, pages 4487–4496.
- Ma, C., Pathak, R., and Wainwright, M. J. (2023). Optimally tackling covariate shift in rkhs-based nonparametric regression. *The Annals of Statistics*, 51(2):738–761.
- Maity, S., Dutta, D., Terhorst, J., Sun, Y., and Banerjee, M. (2024). A linear adjustment-based approach to posterior drift in transfer learning. *Biometrika*, 111(1):31–50.
- Maity, S., Sun, Y., and Banerjee, M. (2022). Meta-analysis of heterogeneous data: integrative sparse regression in high-dimensions. *Journal of Machine Learning Research*, 23(198):1–50.
- Maninis, K.-K., Radosavovic, I., and Kokkinos, I. (2019). Attentive single-tasking of multiple tasks. In *Proceedings of the IEEE/CVF conference on computer vision and pattern recognition*, pages 1851–1860.
- Nair, N. G., Satpathy, P., Christopher, J., et al. (2019). Covariate shift: A review and analysis on classifiers. In *2019 Global Conference for Advancement in Technology (GCAT)*, pages 1–6. IEEE.
- Patterson, J. and Gibson, A. (2017). *Deep learning: A practitioner’s approach*. ” O’Reilly Media, Inc.”.
- Polyak, K. et al. (2011). Heterogeneity in breast cancer. *The Journal of clinical investigation*, 121(10):3786–3788.
- Qin, C., Xie, J., Li, T., and Bai, Y. (2024). An adaptive transfer learning framework for functional classification. *Journal of the American Statistical Association*, pages 1–13.
- Rashid, N. U., Luckett, D. J., Chen, J., Lawson, M. T., Wang, L., Zhang, Y., Laber, E. B., Liu, Y., Yeh, J. J., Zeng, D., et al. (2020). High-dimensional precision medicine from patient-derived xenografts. *Journal of the American Statistical Association*, 116(535):1140–1154.
- Sanh, V., Wolf, T., and Ruder, S. (2019). A hierarchical multi-task approach for learning embeddings from semantic tasks. In *Proceedings of the AAAI conference on artificial intelligence*, volume 33, pages 6949–6956.
- Shen, G. (2023). Exploring the complexity of deep neural networks through functional equivalence. *arXiv preprint arXiv:2305.11417*.
- Shimodaira, H. (2000). Improving predictive inference under covariate shift by weighting the log-likelihood function. *Journal of statistical planning and inference*, 90(2):227–244.
- Siolas, D. and Hannon, G. J. (2013). Patient-derived tumor xenografts: transforming clinical samples into mouse models. *Cancer research*, 73(17):5315–5319.
- Subramanian, S., Trischler, A., Bengio, Y., and Pal, C. J. (2018). Learning general purpose

- distributed sentence representations via large scale multi-task learning. In *International Conference on Learning Representations*.
- Tang, L. and Song, P. X. (2016). Fused lasso approach in regression coefficients clustering-learning parameter heterogeneity in data integration. *Journal of Machine Learning Research*, 17(113):1–23.
- Tang, X., Xue, F., and Qu, A. (2021). Individualized multidirectional variable selection. *Journal of the American Statistical Association*, 116(535):1280–1296.
- Teh, Y., Bapst, V., Czarnecki, W. M., Quan, J., Kirkpatrick, J., Hadsell, R., Heess, N., and Pascanu, R. (2017). Distal: Robust multitask reinforcement learning. *Advances in neural information processing systems*, 30.
- Tian, Y. and Feng, Y. (2023). Transfer learning under high-dimensional generalized linear models. *Journal of the American Statistical Association*, 118(544):2684–2697.
- Tian, Y., Gu, Y., and Feng, Y. (2023). Learning from similar linear representations: Adaptivity, minimaxity, and robustness. *arXiv preprint arXiv:2303.17765*.
- Tripuraneni, N., Jordan, M., and Jin, C. (2020). On the theory of transfer learning: The importance of task diversity. *Advances in neural information processing systems*, 33:7852–7862.
- Tu, X., Cao, Z.-J., Mostafavi, S., Gao, G., et al. (2022). Cross-linked unified embedding for cross-modality representation learning. *Advances in Neural Information Processing Systems*, 35:15942–15955.
- Van der Maaten, L. and Hinton, G. (2008). Visualizing data using t-sne. *Journal of machine learning research*, 9(11).
- Wainwright, M. J. (2019). *High-dimensional statistics: A non-asymptotic viewpoint*, volume 48. Cambridge university press.
- Wang, P., Li, Q., Shen, D., and Liu, Y. (2023). High-dimensional factor regression for heterogeneous subpopulations. *Statistica Sinica*, 33(1):27.
- Wang, P., Liu, Y., and Shen, D. (2018). Flexible locally weighted penalized regression with applications on prediction of alzheimer’s disease neuroimaging initiative’s clinical scores. *IEEE transactions on medical imaging*, 38(6):1398–1408.
- Wang, X., Zhang, Y., Ren, X., Zhang, Y., Zitnik, M., Shang, J., Langlotz, C., and Han, J. (2019). Cross-type biomedical named entity recognition with deep multi-task learning. *Bioinformatics*, 35(10):1745–1752.
- Wang, Z. and Tsvetkov, Y. (2021). Gradient vaccine: Investigating and improving multi-task optimization in massively multilingual models. In *Proceedings of the International*

- Watkins, A., Ullah, E., Nguyen-Tang, T., and Arora, R. (2024). Optimistic rates for multi-task representation learning. *Advances in Neural Information Processing Systems*, 36.
- Xu, G., Liu, Z., Li, X., and Loy, C. C. (2020). Knowledge distillation meets self-supervision. In *European conference on computer vision*, pages 588–604. Springer.
- Yang, Y. and Hospedales, T. M. (2016). Trace norm regularised deep multi-task learning. *arXiv preprint arXiv:1606.04038*.
- Yu, T., Kumar, S., Gupta, A., Levine, S., Hausman, K., and Finn, C. (2020). Gradient surgery for multi-task learning. *Advances in Neural Information Processing Systems*, 33:5824–5836.
- Yu, T. and Zhu, H. (2020). Hyper-parameter optimization: A review of algorithms and applications. *arXiv preprint arXiv:2003.05689*.
- Zhang, R., Zhang, Y., Qu, A., Zhu, Z., and Shen, J. (2024). Concert: Covariate-elaborated robust local information transfer with conditional spike-and-slab prior. *arXiv preprint arXiv:2404.03764*.
- Zhang, Y. and Yang, Q. (2018). An overview of multi-task learning. *National Science Review*, 5(1):30–43.
- Zhang, Y. and Yang, Q. (2021). A survey on multi-task learning. *IEEE transactions on knowledge and data engineering*, 34(12):5586–5609.
- Zhao, T., Cheng, G., and Liu, H. (2016). A partially linear framework for massive heterogeneous data. *Annals of statistics*, 44(4):1400.

# Supplementary Materials

In the Supplementary Material S.1, we further expand on the related works in detail.

In the Supplementary Material S.2, we provide additional simulation studies under linear setting.

In the Supplementary Material S.3, we present the detailed specification of hyper-parameter space in Section 4.

In the Supplementary Material S.4, we provide detailed descriptions of task-specific and task-shared encoders used in (1).

In the Supplementary Material S.5, we present a detailed discussion of the constraint minimization problem and the penalized minimization problem in Section 4, along with their relationships.

In the Supplementary Material S.6, we derive theoretical guarantees for a new but related task based on the results in Section 3.

In the Supplementary Material S.7, we offer an in-depth discussion of Assumption 4 in Supplementary Material S.6.

In the Supplementary Material S.8, we provide proofs of Theorems in Section 3 and Supplementary Material S.6.

In the Supplementary Material S.9, we offer lemmas used in the theorem proofs and their corresponding proofs.

## S.1 Related Literature

Our proposal intersects with a wide range of research fields, including econometrics, statistics, biometrics, and machine learning. Notably, integrating multiple datasets has been widely studied in both the statistics and machine learning communities, and we discuss related works from these two perspectives.

**Multi-group data integration.** Multi-group data, which includes the same set of input

features across separate groups of samples, is commonly encountered in practice. Multi-group data integration and MTL share the common goal of learning from multiple datasets or tasks simultaneously. The input features and response of a single task can be viewed as a separate group. In the statistical literature, several methods exist for multi-group data, which can be broadly classified into three categories:

1. The first category designs specialized regression models (Zhao et al., 2016; Wang et al., 2018; Huang et al., 2023) or factor regression models (Wang et al., 2023) to handle massive heterogeneous data and identify group-specific structures. For example, Huang et al. (2023) explored group and sparsity structures in high-dimensional and heterogeneous stratified models.
2. The second category employs parameter space constraints, such as fused penalties, to estimate regression coefficients that capture subgroup structures (Tang and Song, 2016; Tang et al., 2021; Duan and Wang, 2023). For instance, Tang and Song (2016) proposed a regularized fusion method to identify and merge inter-task homogeneous parameter clusters in regression analysis. Tang et al. (2021) constructed a separation penalty with multi-directional shrinkages, selecting different relevant variables for different individuals.
3. The third category involves transfer learning, where information is borrowed from source data to target data in the field of statistics (Li et al., 2022; Tian and Feng, 2023; Zhang et al., 2024). Transfer learning typically follows a two-step strategy: first, source and target data are aggregated to leverage the larger sample size of the source data for more accurate estimation, followed by de-biasing for the target data.

Most existing multi-group data integration methods only address one type of heterogeneity. For instance, transfer learning primarily focuses on posterior heterogeneity. Moreover, these approaches typically rely on structured model assumptions, such as linearity, which limits

their ability to capture complex relationships. However, many real-world datasets, including multi-modal single-cell data (Tu et al., 2022; Cohen Kalafut et al., 2023) and imaging data (Jin et al., 2017; Bernal et al., 2019), present complexities that further constrain the applicability of such methods.

**Multi-task learning (MTL).** There is a growing literature on learning multiple tasks simultaneously with a shared model; see Zhang and Yang (2018); Crawshaw (2020); Zhang and Yang (2021) for reviews. Here, we primarily focus on MTL with deep neural networks, as these networks can capture more complex relationships. These methods can be broadly classified into four categories:

1. The first category is balancing individual loss functions for different tasks, which is a common approach to ease multi-task optimization (Du et al., 2018; Liu et al., 2019a; Hang et al., 2023). However, these approaches can be sensitive to the choice of weighting strategy, potentially leading to instability or suboptimal performance if not well-tuned (Kendall et al., 2018).
2. The second category focuses on designing network architectures, particularly hard parameter sharing (Subramanian et al., 2018; Liu et al., 2019c; Bai et al., 2022), which shares main layers across tasks, and soft parameter sharing (Yang and Hospedales, 2016), which keeps task-specific parameters while enforcing similarity through regularization. However, these methods face limitations: hard parameter sharing struggles to capture task-specific details, forcing reliance on shared features (Han et al., 2024), while soft parameter sharing increases model complexity, leading to higher computational costs and potential overfitting with limited data.
3. The third category addresses the challenge of negative transfer, where explicit gradient modulation is used to alleviate conflicts in learning dynamics between tasks (Maninis et al., 2019; Yu et al., 2020; Abdollahzadeh et al., 2021). However, these methods can sometimes lead to unstable training due to the complexity of managing gradients

across diverse tasks (Wang and Tsvetkov, 2021).

4. The fourth category uses knowledge distillation to transfer knowledge from single-task networks to a multi-task student network (Teh et al., 2017; Liu et al., 2019b; Clark et al., 2019). One drawback of this category is that it can suffer from limited transferability when the tasks are too diverse, as the distilled knowledge may not generalize well across tasks (Xu et al., 2020).

Although the above approaches can integrate data from multiple tasks, it often incurs substantial computational costs and lacks interpretability. We aim to propose an interpretable and computationally efficient MTL framework to address different types of heterogeneity.

## S.2 Simulation Studies: Comparisons under Linear Setting

For a fair comparison, we generate simulated data under linear settings. The linear data-generating process (DGP) is similar to (7) and (8) in Section 5, but only involves linear relationships as follows:

$$\begin{aligned} X_r &= F_r B_r + E_r, \\ Y_r &= F_r^\top (\gamma_c + \gamma_r)/d + \varepsilon_r, \quad \forall r \in [R]. \end{aligned}$$

All other details of the DGP remain the same as those in Section 5, except that the relationship between  $F_r$  and  $Y_r$  is linear. We use the following parameter settings:  $n_r = 50$  for  $r \in [R]$ ,  $d = 40$ ,  $d_c = 20$ ,  $\sigma_e = 0.05$ ,  $\sigma_c = 10$ ,  $\sigma_r = 1$  for  $r \in [R]$ , and  $R = 3$ . We calculate the RMSEs on the testing data and summarize the prediction results in Table 6. From Table 6, it is clear that all four integration methods perform better than STL, as they can leverage shared information to enhance learning capacity. Among these integration methods, our proposed MTL method leads in prediction accuracy. Although Meta, FLARCC, and ARUML effectively address posterior heterogeneity, they still overlook

distribution heterogeneity.

Table 6: Comparison of prediction loss across different methods in linear setting.

Dataset	MTL	Meta	FLARCC	ARUML	STL
Dataset 1	<b>0.179 (0.035)</b>	0.197 (0.048)	0.181 (0.031)	0.184 (0.025)	0.213 (0.052)
Dataset 2	<b>0.176 (0.032)</b>	0.207 (0.048)	0.184 (0.032)	0.185 (0.023)	0.215 (0.055)
Dataset 3	<b>0.179 (0.034)</b>	0.217 (0.068)	0.181 (0.035)	0.192 (0.028)	0.218 (0.057)

### S.3 Hyper-parameter tuning

The search space for hyper-parameter tuning is outlined in Table 7. Note that the exact search space specification may vary depending on the specific problem, and we use the following search space in Table 7 throughout our numerical studies.

Table 7: Search space of hyper-parameter tuning.

Hyper-parameters	Search space
Task-specific encoders $\{S_r(\cdot)\}_{r=1}^R$ depth $D_S$	$\{3, 4, 5\}$
Task-specific encoders $\{S_r(\cdot)\}_{r=1}^R$ width $W_S$	$\{16, 32, 64, 128\}$
Task-specific encoders $\{S_r(\cdot)\}_{r=1}^R$ output dimension $q$	$\{8, 16, 32, 64\}$
Task-shared encoder $C(\cdot)$ depth $D_C$	$\{3, 4, 5\}$
Task-shared encoder $C(\cdot)$ width $W_C$	$\{16, 32, 64, 128\}$
Task-shared encoder $C(\cdot)$ output dimension $p$	$\{8, 16, 32, 64\}$
Regularization parameters for similarity structure $\{\lambda_r^s, \lambda_r^c\}_{r=1}^R$	$\{0.0001, 0.001, 0.01, 0.1, 1, 10, 100, 500, 1000, 5000\}$
Regularization parameter for discouraging redundancy $\lambda^o$	$\{0.001, 0.01\}$
Batch sizes $\{B_r\}_{r=1}^R$	$\{8, 16, 32\}$
learning rate $\eta$	$\{0.0001, 0.001\}$
Epochs $E$	$\{25000\}$



## S.4 Detailed Descriptions of Task-specific and Task-shared Encoders

We first declare that, for different tasks, the encoders  $\{S_r(\cdot)\}_{r=1}^R$  extracting task-specific latent factors can include different network architectures. However, to reduce computational costs and simplify theoretical analysis, we assume that  $\{S_r(\cdot)\}_{r=1}^R$  for all tasks comes from the same feed-forward neural network architecture defined as:

$$S_r(X_r) = V_{D_S} \sigma(V_{D_S-1} \sigma(\cdots \sigma(V_1 X_r + c_1) \cdots) + c_{D_S-1}) + c_{D_S},$$

where  $V_i \in \mathbb{R}^{p_{i+1,S} \times p_{i,S}}$  and  $c_i \in \mathbb{R}^{p_{i+1,S}}$  for  $i = 1, \dots, D_S$ ,  $p_{1,S} = d$  is the dimension of the input features  $X_r$ ,  $p_{D_S+1} = q$  is the dimension of the output layer, and  $\sigma(\cdot)$  is the activation function. The number  $W_S$  and  $D_S$  are the width and depth of the neural network, respectively. The weight matrices together with the bias vectors contains  $E_S = \sum_{i=1}^{D_S} p_{i+1,S}(p_{i,S} + 1)$  entries in total, the parameters are bounded by a constant  $B_S > 0$ . We denote the set of the neural network functions defined above by  $\mathcal{S} = \mathcal{NN}(W_S, D_S, B_S)$ . The prediction results in the numerical studies and real data analyses demonstrates that assuming an identical neural network architecture across different tasks is reasonable.

For the task-shared encoder  $C(\cdot)$ , we approximate it by feed-forward neural networks defined as:

$$C(X_r) = U_{D_C} \sigma(U_{D_C-1} \sigma(\cdots \sigma(U_1 X_r + b_1) \cdots) + b_{D_C-1}) + b_{D_C},$$

where  $U_i \in \mathbb{R}^{p_{i+1,C} \times p_{i,C}}$  and  $b_i \in \mathbb{R}^{p_{i+1,C}}$  for  $i = 1, \dots, D_C$ ,  $p_{1,C} = d$  is the dimension of the input features  $X_r$ ,  $p_{D_C+1} = p$  is the dimension of the output layer, and  $\sigma(\cdot)$  is the activation function. The number  $W_C$  and  $D_C$  are the width and depth of the neural network, respectively. The weight matrices together with the bias vectors contains  $E_C = \sum_{i=1}^{D_C} p_{i+1,C}(p_{i,C} + 1)$  entries in total, the parameters are bounded by a constant  $B_C > 0$ .

We denote the set of the neural network functions defined above by  $\mathcal{C} = \mathcal{NN}(W_C, D_C, B_C)$ .

## S.5 Discussions of Constraint Minimization and Penalized Minimization

In this subsection, we present a detailed discussion of the constraint minimization problem and the penalized minimization problem in Section 4, along with their relationships. For the constraint minimization problem,

$$\{\{\hat{\alpha}_r, \hat{\beta}_r, \hat{S}_r(\cdot)\}_{r=1}^R, \hat{\alpha}, \hat{\beta}, \hat{C}(\cdot)\} = \arg \min_{\{\{\alpha_r, \beta_r, S_r(\cdot)\}_{r=1}^R, \bar{\alpha}, \bar{\beta}, C(\cdot)\}} \frac{1}{R} \sum_{r=1}^R \frac{1}{n_r} \sum_{i=1}^{n_r} (Y_{ri} - \alpha_r^\top S_r(X_{ri}) - \beta_r^\top C(X_{ri}))^2, \quad (9)$$

where  $S_r(\cdot) \in \mathcal{S}$  for  $r \in [R]$ ,  $C(\cdot) \in \mathcal{C}$ , and  $\{\{\alpha_r, \beta_r\}_{r=1}^R, \bar{\alpha}, \bar{\beta}\}$  satisfy Assumption 1. Note that we drop the penalty term  $\|\bar{S}_r^\top \bar{C}_r\|_F^2$  in (9) for simplicity. We consider updating different components alternately through the following two steps:

Step 1: Given estimated  $\{\{\hat{\alpha}_r\}_{r=1}^R, \hat{\alpha}\}$  and  $\{\{\hat{\beta}_r\}_{r=1}^R, \hat{\beta}\}$ , we can estimate  $\{S_r(\cdot)\}_{r=1}^R$  and  $C(\cdot)$  through

$$\{\{\hat{S}_r(\cdot)\}_{r=1}^R, \hat{C}(\cdot)\} = \arg \min_{\{\{S_r(\cdot)\}_{r=1}^R, C(\cdot)\}} \frac{1}{R} \sum_{r=1}^R \frac{1}{n_r} \sum_{i=1}^{n_r} (Y_{ri} - \hat{\alpha}_r^\top S_r(X_{ri}) - \hat{\beta}_r^\top C(X_{ri}))^2, \quad (10)$$

where  $S_r(\cdot) \in \mathcal{S}$  for  $r \in [R]$ , and  $C(\cdot) \in \mathcal{C}$ .

Step 2: Given estimated  $\{\{\hat{S}_r(\cdot)\}_{r=1}^R, \hat{C}(\cdot)\}$  and  $\{\{\hat{\alpha}_r\}_{r=1}^R, \hat{\alpha}\}$ , we can estimate  $\{\{\alpha_r, \beta_r\}_{r=1}^R, \bar{\alpha}, \bar{\beta}\}$  through the following optimization:

$$\{\{\hat{\alpha}_r, \hat{\beta}_r\}_{r=1}^R, \hat{\alpha}, \hat{\beta}\} = \arg \min_{\{\{\alpha_r, \beta_r\}_{r=1}^R, \bar{\alpha}, \bar{\beta}\}} \frac{1}{R} \sum_{r=1}^R \frac{1}{n_r} \sum_{i=1}^{n_r} (Y_{ri} - \hat{\alpha}_r^\top \hat{S}_r(X_{ri}) - \beta_r^\top \hat{C}(X_{ri}))^2, \quad (11)$$

where  $\{\{\alpha_r, \beta_r\}_{r=1}^R, \bar{\alpha}, \bar{\beta}\}$  satisfy Assumption 1.

For the penalized minimization problem,

$$\begin{aligned}
& \{\{\hat{\alpha}_r, \hat{\beta}_r, \hat{S}_r(\cdot)\}_{r=1}^R, \hat{\alpha}, \hat{\beta}, \hat{C}(\cdot)\} \\
&= \arg \min_{\{\{\alpha_r, \beta_r, S_r(\cdot)\}_{r=1}^R, \bar{\alpha}, \bar{\beta}, C(\cdot)\}} \frac{1}{R} \sum_{r=1}^R \frac{1}{n_r} \sum_{i=1}^{n_r} (Y_{ri} - \alpha_r^\top S_r(X_{ri}) - \beta_r^\top C(X_{ri}))^2 + \sum_{r=1}^R (\lambda_r^s \|\alpha_r - \bar{\alpha}\| + \lambda_r^c \|\beta_r - \bar{\beta}\|), \quad (12)
\end{aligned}$$

where  $S_r(\cdot) \in \mathcal{S}$  for  $r \in [R]$ , and  $C(\cdot) \in \mathcal{C}$ . We consider alternately updating different components through the following two steps:

Step 1: Given estimated  $\{\{\hat{\alpha}_r\}_{r=1}^R, \hat{\alpha}\}$  and  $\{\{\hat{\beta}_r\}_{r=1}^R, \hat{\beta}\}$ , we can estimate  $\{S_r(\cdot)\}_{r=1}^R$  and  $C(\cdot)$  through

$$\{\{\hat{S}_r(\cdot)\}_{r=1}^R, \hat{C}(\cdot)\} = \arg \min_{\{\{S_r(\cdot)\}_{r=1}^R, C(\cdot)\}} \frac{1}{R} \sum_{r=1}^R \frac{1}{n_r} \sum_{i=1}^{n_r} (Y_{ri} - \hat{\alpha}_r^\top S_r(X_{ri}) - \hat{\beta}_r^\top C(X_{ri}))^2, \quad (13)$$

where  $S_r(\cdot) \in \mathcal{S}$  for  $r \in [R]$ , and  $C(\cdot) \in \mathcal{C}$ .

Step 2: Given estimated  $\{\hat{S}_r(\cdot)\}_{r=1}^R, \hat{C}(\cdot)$  and  $\{\hat{\alpha}_r\}_{r=1}^R$ , we can estimate  $\{\{\alpha_r, \beta_r\}_{r=1}^R, \bar{\alpha}, \bar{\beta}\}$  through the following optimization:

$$\begin{aligned}
& \{\{\hat{\alpha}_r, \hat{\beta}_r\}_{r=1}^R, \hat{\alpha}, \hat{\beta}\} \\
&= \arg \min_{\{\{\alpha_r, \beta_r\}_{r=1}^R, \bar{\alpha}, \bar{\beta}\}} \frac{1}{R} \sum_{r=1}^R \frac{1}{n_r} \sum_{i=1}^{n_r} (Y_{ri} - \alpha_r^\top \hat{S}_r(X_{ri}) - \beta_r^\top \hat{C}(X_{ri}))^2 + \sum_{r=1}^R (\lambda_r^s \|\alpha_r - \bar{\alpha}\| + \lambda_r^c \|\beta_r - \bar{\beta}\|). \quad (14)
\end{aligned}$$

In the penalized minimization problem (12), we omit the penalty term  $\lambda^o \|\bar{S}_r^\top \bar{C}_r\|_F^2$  from (3) for simplicity. By observing (10) and (13), it naturally holds that, given the same estimated  $\{\{\hat{\alpha}_r\}_{r=1}^R, \hat{\alpha}\}$  and  $\{\{\hat{\beta}_r\}_{r=1}^R, \hat{\beta}\}$ , the estimates  $\{\{\hat{S}_r(\cdot)\}_{r=1}^R, \hat{C}(\cdot)\}$  obtained from (10) and (13) are consistent. Subsequently, given the same estimated  $\{\{\hat{S}_r(\cdot)\}_{r=1}^R, \hat{C}(\cdot)\}$ , the estimates  $\{\{\hat{\alpha}_r, \hat{\beta}_r\}_{r=1}^R, \hat{\alpha}, \hat{\beta}\}$  obtained from (11) and (14) are also consistent. Since, given  $\{\{\hat{S}_r(\cdot)\}_{r=1}^R, \hat{C}(\cdot)\}$ , the loss function  $\frac{1}{R} \sum_{r=1}^R \frac{1}{n_r} \sum_{i=1}^{n_r} (Y_{ri} - \alpha_r^\top \hat{S}_r(X_{ri}) - \beta_r^\top \hat{C}(X_{ri}))^2$  is

convex with respect to  $\{\{\alpha_r, \beta_r\}_{r=1}^R, \bar{\alpha}, \bar{\beta}\}$ , the updates in Step 2 for  $\{\{\alpha_r, \beta_r\}_{r=1}^R, \bar{\alpha}, \bar{\beta}\}$  make the constraint optimization and penalized optimization equivalent (Boyd and Vandenberghe, 2004) when selecting appropriate  $\{B_r^s, B_r^c\}_{r=1}^R$  in (11) and  $\{\lambda_r^s, \lambda_r^c\}_{r=1}^R$  in (14).

In conclusion, from the perspective of the alternating update algorithm, the constraint minimization problem (9) and the penalized minimization problem (12) produce consistent estimates, as each individual step is equivalent.

## S.6 Supplementary Theoretical Results

Firstly, we introduce the following useful definitions, beginning with measures of complexity used in Section 3. Specifically, let  $u, R, \{n_r\}_{r=1}^R \in \mathbb{N}$ , an input space  $\mathcal{Z}$ , a class of vector-valued functions  $\mathcal{Q} : \mathcal{Z} \rightarrow \mathbb{R}^u$ , and a dataset  $Z = \{\{z_{ri}\}_{i \in [n_r]}\}_{r \in [R]}$  where  $z_{ri} \in \mathcal{Z}$ . Define the data-dependent Rademacher complexity,  $\widehat{\mathcal{R}}_Z(\cdot)$ , as

$$\widehat{\mathcal{R}}_Z(\mathcal{Q}^{\otimes R}) = \mathbb{E}_{\sigma_{rik}} \left[ \sup_{q \in \mathcal{Q}^{\otimes R}} \frac{1}{R} \sum_{r=1}^R \frac{1}{n_r} \sum_{i=1}^{n_r} \sum_{k=1}^u \sigma_{rik} (q_r(z_{ri}))_k \right],$$

where  $\sigma_{rik}$  are *i.i.d.* Rademacher random variables. Analogously, define the data-dependent Gaussian complexity,  $\widehat{\mathcal{G}}_Z(\cdot)$ , as

$$\widehat{\mathcal{G}}_Z(\mathcal{Q}^{\otimes R}) = \mathbb{E}_{g_{rik}} \left[ \sup_{q \in \mathcal{Q}^{\otimes R}} \frac{1}{R} \sum_{r=1}^R \frac{1}{n_r} \sum_{i=1}^{n_r} \sum_{k=1}^u g_{rik} (q_r(z_{ri}))_k \right],$$

where  $g_{rik}$  are *i.i.d.* Gaussian random variables. Next, we define local Rademacher complexity as  $\widehat{\mathcal{R}}_Z(\mathcal{Q}^{\otimes R}, r) = \widehat{\mathcal{R}}_Z(\{\tilde{q} \in \mathcal{Q}^{\otimes R} : V(\tilde{q}) \leq r\})$ , where  $V(\cdot) : \mathcal{Q}^{\otimes R} \rightarrow \mathbb{R}$ , which means that the local Rademacher complexity is simply the Rademacher complexity restricted by a functional. In our applications, we consider any  $V(\cdot)$  satisfying  $V(\tilde{q}) \leq \frac{b}{R} \sum_{r=1}^R \frac{1}{n_r} \sum_{i=1}^{n_r} \sum_{k=1}^u (q_r(z_{ri}))_k$ , as in (Watkins et al., 2024), where  $b$  is the uniform bound on the range of  $q$  in the  $\ell_2$  norm. Additionally, we consider sub-root function of  $r$ , a type of function we define below.

**Definition 1.** *Sub-root Function:* a function  $\psi : [0, \infty) \rightarrow [0, \infty)$  is sub-root if it is nonnegative, nondecreasing, and if  $r \rightarrow \psi(r)/\sqrt{r}$  is nonincreasing for  $r > 0$ . Sub-root functions have the desirable properties of always being continuous and having a unique fixed point, i.e.,  $r^* = \psi(r^*)$  is only satisfied by some  $r^*$ .

Based on theoretical results for the proposed MTL method in Section 3, we consider a new but related task  $(X_0, Y_0)$  given  $R$  existing tasks and explore the excess risk of this new task when sharing the same latent factor extractor  $C(\cdot)$ . Let  $(X_0, Y_0) \sim P_0$  represent this new task, and define its excess risk as:

$$R_0(\alpha_0, \beta_0, S_0, C) = \mathbb{E}_0 [(\alpha_0^\top S_0(X_0) + \beta_0^\top C(X_0) - Y_0)^2]$$

with the empirical risk minimization over  $n_0$  samples  $\{X_{0i}, Y_{0i}\}_{i \in [n_0]}$  given by:

$$\{\hat{\alpha}_0, \hat{\beta}_0, \hat{S}_0\} = \arg \min_{\{\alpha_0, \beta_0, S_0\}} \frac{1}{n_0} \sum_{i=1}^{n_0} (Y_{0i} - \alpha_0^\top S_0(X_{0i}) - \beta_0^\top \hat{C}(X_{0i}))^2, \quad (15)$$

where  $\alpha_r \in \mathcal{A}_0, S_0 \in \mathcal{S}, \beta_0 \in \mathcal{B}_0$ , and  $\hat{C}$  is the minimizer of Eqn. (2). Specifically,  $\mathcal{A}_0 = \{\alpha_0 \in \mathbb{R}^q : \|\alpha_0 - \bar{\alpha}\| \leq B_0^s\}$  and  $\mathcal{B}_0 = \{\beta_0 \in \mathbb{R}^p : \|\beta_0 - \bar{\beta}\| \leq B_0^c\}$ . We propose the following assumption to characterize the heterogeneity present in the new task relative to the existing  $R$  tasks:

**Assumption 4.** For  $\{\alpha_{*r}\}_{r=1}^R \in \mathcal{A}^{\otimes R}, \{S_{*r}\}_{r=1}^R \in \mathcal{S}^{\otimes R}, \{\beta_{*r}\}_{r=1}^R \in \mathcal{B}^{\otimes R}, \alpha_{*0} \in \mathcal{A}_0, S_{*0} \in \mathcal{S}, \beta_{*0} \in \mathcal{B}_0$  and  $C \in \mathcal{C}$ , we have that for any  $C' \in \mathcal{C}$ ,

$$\begin{aligned} & \inf_{\alpha' \in \mathcal{A}, S' \in \mathcal{S}, \beta' \in \mathcal{B}} R_0(\alpha', S', \beta', C') - R_0(\alpha_{*0}, S_{*0}, \beta_{*0}, C_*) \\ & \leq \frac{1}{v} \left( \inf_{\{\alpha'_r\}_{r=1}^R \in \mathcal{A}^{\otimes R}, \{S'_r\}_{r=1}^R \in \mathcal{S}^{\otimes R}, \{\beta'_r\}_{r=1}^R \in \mathcal{B}^{\otimes R}} R_{MTL}(\{\alpha'_r, S'_r, \beta'_r\}_{r=1}^R, C') - R_{MTL}(\{\alpha_{*r}, S_{*r}, \beta_{*r}\}_{r=1}^R, C_*) \right) + \varepsilon, \end{aligned}$$

where  $v$  and  $\varepsilon$  are two absolute constants.

Assumption 4 is grounded in the theory of task diversity (Tripuraneni et al., 2020;

Watkins et al., 2024). Provided there is useful information for the new task encoded in the existing datasets, learning a shared latent factor extractor  $C(\cdot)$  can offer benefits. To achieve this, we adopt the framework introduced by Tripuraneni et al. (2020), which quantifies task diversity. As discussed in their work, this framework replicates the task diversity assumption established by Du et al. (2020). The parameters  $v$  and  $\varepsilon$  measure the similarity between learning the new task and the existing tasks. For a detailed analysis of these parameters, see the Supplementary Material S.7. Given Assumption 4, we present the following local Rademacher complexity result for learning the new task conditional on the existing  $R$  tasks.

**Theorem 3.** *Let  $\widehat{C}$  and  $\{\widehat{\alpha}_0, \widehat{S}_0, \widehat{\beta}_0\}$  be the learned shared representation and new predictor in Eqns. (2) and (15). Let  $\psi_1(r) \geq b\mathbb{E}[\widehat{\mathcal{R}}_{X_0}(\ell_2 \circ (\mathcal{A}(\mathcal{S}) + \mathcal{B}(\widehat{C})), r)]$  and  $\psi_2(r) \geq b\mathbb{E}[\widehat{\mathcal{R}}_X(\ell_2 \circ (\mathcal{A}(\mathcal{S})^{\otimes R} + \mathcal{B}^{\otimes R}(\mathcal{C})), r)]$  with  $r_1^*$  and  $r_2^*$  being the fixed point of  $\psi_1(r)$  and  $\psi_2(r)$ , respectively. Then, under Assumptions 2 and 4, with probability at least  $1 - 4\delta$ ,*

$$\begin{aligned} & R_0(\widehat{\alpha}_0, \widehat{S}_0, \widehat{\beta}_0, \widehat{C}) - R_0(\alpha_{*0}, S_{*0}, \beta_{*0}, C_*) \\ & \leq c_1 \left( \sqrt{R_0(\alpha_{*0}, S_{*0}, \beta_{*0}, C_*)} \left( \sqrt{\frac{b\delta}{n_0}} + \sqrt{\frac{r_1^*}{b}} \right) + \frac{b\delta}{n_0} + \frac{r_1^*}{b} \right) \\ & \quad + \frac{1}{v} \left( c_2 \left( \sqrt{R_{MTL}(\{\alpha_{*r}, \beta_{*r}, S_{*r}\}_{r=1}^R, C_*)} \left( \sqrt{\frac{b\delta}{N}} + \sqrt{\frac{r_2^*}{b}} \right) + \frac{b\delta}{N} + \frac{r_2^*}{b} \right) \right) + \varepsilon, \end{aligned} \quad (16)$$

where  $c_1$  and  $c_2$  are two constants.

In Theorem 3, the inequality (16) establishes a relationship between the excess risk for the new task in terms of the heterogeneity parameters  $v$  and  $\varepsilon$ , along with local Rademacher complexity parameters and fixed points  $r_1^*$  and  $r_2^*$ . As highlighted by Du et al. (2020); Watkins et al. (2024), certain conditions make the heterogeneity parameters  $v$  and  $\varepsilon$  favorable, specifically when  $\varepsilon = 0$  and  $v = O(1)$ . The bound is considered optimistic as it interpolates between  $\sqrt{r_1^*} + \sqrt{r_2^*}$  and  $r_1^* + r_2^*$ . Assuming that  $\mathcal{C}$  is complex while  $\mathcal{S}$  is simple, learning the new task directly would typically require the complexity of  $\mathcal{A}(\mathcal{S}) + \mathcal{B}(\mathcal{C})$  across  $n_0$  samples. In contrast, our bound only considers the complexity of  $\mathcal{A}(\mathcal{S})$  and  $\mathcal{B}$

for  $n_0$  samples and  $\mathcal{C}$  for  $N$  samples. We can effectively leverage shared information to facilitate learning the new task. For instance, when  $N \gg n_0$  with  $R_0(\alpha_{*0}, S_{*0}, \beta_{*0}, C_*) > 0$  and  $R_{MTL}(\{\alpha_{*r}, \beta_{*r}, S_{*r}\}_{r=1}^R, C_*) = 0$ , we obtain a bound of  $\sqrt{r_1^*} + r_2^*$ . This demonstrates that data-rich environments which enable the learning of task-shared encoders  $C(\cdot)$  will perform well on a new but related task even with limited samples.

The fixed point  $r_1^*$  depends on the complexity of  $\mathcal{A}(\mathcal{S}) + \mathcal{B}(\widehat{C})$ , measured with respect to the sample size  $n_0$  of the new task along with other specific parameters. Similarly,  $r_2^*$  is defined in terms of  $\mathcal{A}(\mathcal{S})^{\otimes R} + \mathcal{B}^{\otimes R}(\mathcal{C})$ . The upper bounds for the fixed points  $r_1^*$  and  $r_2^*$  are provided in Theorem 4.

**Theorem 4.** *Under the setting of Theorem 3 and Assumption 3, with probability at least  $1 - 6e^{-\delta}$ , it holds that*

$$\begin{aligned} r_1^* &\leq c_3 b \left( \left( \widehat{\mathcal{F}}_{X_0}(\mathcal{A}(\mathcal{S}) + \mathcal{B}(\widehat{C})) \right)^2 (\log \sqrt{n_0})^4 + \frac{b}{n_0} + \frac{b\delta}{n_0} \right), \\ r_2^* &\leq c_4 b \left( \left( \widehat{\mathcal{F}}_X(\mathcal{A}(\mathcal{S})^{\otimes R} + \mathcal{B}^{\otimes R}(\mathcal{C})) \right)^2 (\log \sqrt{N})^4 + \frac{b}{N} + \frac{D_X^2 (\log \sqrt{N})^2}{N} + \frac{b\delta}{N} \right), \end{aligned}$$

where

$$\widehat{\mathcal{F}}_{X_0}(\mathcal{A}(\mathcal{S}) + \mathcal{B}(\widehat{C})) = c_1 \left( (B_\alpha + B_0^s) L_{sq} \sqrt{\frac{\log n_0}{n_0}} + (B_\alpha + B_0^s) \sqrt{\frac{q}{n_0}} + (B_\beta + B_0^c) \sqrt{\frac{p}{n_0}} \right),$$

and  $\widehat{\mathcal{F}}_X(\mathcal{A}(\mathcal{S})^{\otimes R} + \mathcal{B}^{\otimes R}(\mathcal{C}))$  and  $D_X$  are discussed in Theorem 2.

In Theorem 4, we observe that the terms on the right side are consistently fast, so the decay rate depends critically on  $\widehat{\mathcal{F}}_{X_0}(\mathcal{A}(\mathcal{S}) + \mathcal{B}(\widehat{C}))$  and  $\widehat{\mathcal{F}}_X(\mathcal{A}(\mathcal{S})^{\otimes R} + \mathcal{B}^{\otimes R}(\mathcal{C}))$ . Based on the discussions following Theorem 3,  $r_1^*$  and  $r_2^*$  govern the rate order. Consequently, Theorem 3 interpolates between a rate of  $1/\sqrt{n_0} + 1/\sqrt{N}$  and  $1/n_0 + 1/N$ . The impact of various parameters in  $\widehat{\mathcal{F}}_X(\mathcal{A}(\mathcal{S})^{\otimes R} + \mathcal{B}^{\otimes R}(\mathcal{C}))$ , including sample sizes, similarity structure parameters, and network architecture parameters, on the excess risk bound is consistent

with the analysis following Theorem 3 and will be omitted here. We primarily focus on analyzing the influence of different parameters in  $\widehat{\mathcal{F}}_{X_0}(\mathcal{A}(\mathcal{S}) + \mathcal{B}(\widehat{C}))$  on the excess risk bound. In particular, a larger sample size  $n_0$  of the new task and smaller dimensions  $d$ ,  $q$ , and  $p$  contribute to a faster rate. Additionally, the similarity structure parameters  $B_0^s$  and  $B_0^c$  also influence the rate order. When the values of  $B_0^s$  and  $B_0^c$  are too large, it indicates that  $\alpha_0$  and  $\bar{\alpha}$ , as well as  $\beta_0$  and  $\bar{\beta}$ , are too far apart, suggesting strong heterogeneity. In such cases, even with information from existing tasks, the learning capability for the new task will remain limited. Furthermore, the network architecture parameters of the task-specific encoder  $S_0(\cdot)$ , such as the network depth  $D_S$ , may also lead to a less tight upper bound on the generalization error.

## S.7 Discussions of Assumption 4

Following Tripuraneni et al. (2020); Watkins et al. (2024), we define two definitions that are used to relate the average performance of all  $R$  tasks to a new task performance, including the average difference of all  $R$  tasks with respect to  $C', C \in \mathcal{C}$  and the worst-case difference with respect to  $C', C \in \mathcal{C}$ .

**Definition 2** (The average difference of all  $R$  tasks with respect to  $C', C \in \mathcal{C}$ ).

$$\begin{aligned} \bar{d}_{\{\alpha_r, S_r, \beta_r\}_{r=1}^R}(C'; C) &= \frac{1}{R} \sum_{r=1}^R \inf_{\alpha'_r \in \mathcal{A}, S'_r \in \mathcal{S}, \beta'_r \in \mathcal{B}} \mathbb{E}_r[(\alpha'_r{}^\top S'_r(X_r) + \beta'_r{}^\top C'(X_r) - Y_r)^2 \\ &\quad - (\alpha_r{}^\top S_r(X_r) + \beta_r{}^\top C(X_r) - Y_r)^2]. \end{aligned}$$

**Definition 3** (The worst-case difference with respect to  $C', C \in \mathcal{C}$ ).

$$\begin{aligned} d(C'; C) &= \sup_{\alpha_0 \in \mathcal{A}, S_0 \in \mathcal{S}, \beta_0 \in \mathcal{B}} \inf_{\alpha' \in \mathcal{A}, S' \in \mathcal{S}, \beta' \in \mathcal{B}} \mathbb{E}[(\alpha'{}^\top S'(X_0) + \beta'{}^\top C'(X_0) - Y_0)^2 \\ &\quad - (\alpha_0{}^\top S_0(X_0) + \beta_0{}^\top C(X_0) - Y_0)^2]. \end{aligned}$$



We will examine these two quantities, as they offer significant simplifications within our framework. To start, observe that

$$\bar{d}_{\{\alpha_r, S_r, \beta_r\}_{r=1}^R}(C'; C) = \inf_{\{\alpha'_r, S'_r, \beta'_r\}_{r=1}^R} (R_{MTL}(\{\alpha'_r, S'_r, \beta'_r\}_{r=1}^R, C') - R_{MTL}(\{\alpha_r, S_r, \beta_r\}_{r=1}^R, C))$$

and

$$d(C'; C) = \sup_{\alpha_0 \in \mathcal{A}, S_0 \in \mathcal{S}, \beta_0 \in \mathcal{B}} \inf_{\alpha' \in \mathcal{A}, S' \in \mathcal{S}, \beta' \in \mathcal{B}} (R_0(\alpha', S', \beta', C') - R_0(\alpha_0, S_0, \beta_0, C)).$$

Now, for  $\hat{C}, C_* \in \mathcal{C}$  and  $\{\alpha_{*r}\}_{r=1}^R \in \mathcal{A}^{\otimes R}, \{S_{*r}\}_{r=1}^R \in \mathcal{S}^{\otimes R}, \{\beta_{*r}\}_{r=1}^R \in \mathcal{B}^{\otimes R}$ , consider the following ratio

$$\begin{aligned} \frac{d(\hat{C}; C_*)}{\bar{d}_{\{\alpha_{*r}, S_{*r}, \beta_{*r}\}_{r=1}^R}(\hat{C}; C_*)} &= \frac{\sup_{\alpha_0 \in \mathcal{A}, S_0 \in \mathcal{S}, \beta_0 \in \mathcal{B}} \inf_{\alpha' \in \mathcal{A}, S' \in \mathcal{S}, \beta' \in \mathcal{B}} (R_0(\alpha', S', \beta', \hat{C}) - R_0(\alpha_0, S_0, \beta_0, C_*))}{\inf_{\{\alpha'_r, S'_r, \beta'_r\}_{r=1}^R} (R_{MTL}(\{\alpha'_r, S'_r, \beta'_r\}_{r=1}^R, \hat{C}) - R_{MTL}(\{\alpha_{*r}, S_{*r}, \beta_{*r}\}_{r=1}^R, C_*))} \\ &= \frac{\inf_{\alpha' \in \mathcal{A}, S' \in \mathcal{S}, \beta' \in \mathcal{B}} R_0(\alpha', S', \beta', \hat{C}) - \inf_{\alpha_0 \in \mathcal{A}, S_0 \in \mathcal{S}, \beta_0 \in \mathcal{B}} R_0(\alpha_0, S_0, \beta_0, C_*)}{\inf_{\{\alpha'_r, S'_r, \beta'_r\}_{r=1}^R} (R_{MTL}(\{\alpha'_r, S'_r, \beta'_r\}_{r=1}^R, \hat{C}) - R_{MTL}(\{\alpha_{*r}, S_{*r}, \beta_{*r}\}_{r=1}^R, C_*))} \\ &= \frac{\inf_{\alpha' \in \mathcal{A}, S' \in \mathcal{S}, \beta' \in \mathcal{B}} R_0(\alpha', S', \beta', \hat{C}) - R_0(\alpha_{*0}, S_{*0}, \beta_{*0}, C_*)}{\inf_{\{\alpha'_r, S'_r, \beta'_r\}_{r=1}^R} (R_{MTL}(\{\alpha'_r, S'_r, \beta'_r\}_{r=1}^R, \hat{C}) - R_{MTL}(\{\alpha_{*r}, S_{*r}, \beta_{*r}\}_{r=1}^R, C_*))} \end{aligned}$$

This ratio measures the similarity in performance we can expect when applying the task-shared encoder  $\hat{C}(\cdot)$  learned from existing tasks to a new task. Specifically, if we aim to control this quantity, our focus is not necessarily on achieving small risks or high accuracy relative to the ground truth, but rather on how comparable our performance is between existing tasks and the new one. We seek to control this ratio with some  $v$

$$\frac{\inf_{\alpha' \in \mathcal{A}, S' \in \mathcal{S}, \beta' \in \mathcal{B}} R_0(\alpha', S', \beta', \hat{C}) - R_0(\alpha_{*0}, S_{*0}, \beta_{*0}, C_*)}{\inf_{\{\alpha'_r, S'_r, \beta'_r\}_{r=1}^R} (R_{MTL}(\{\alpha'_r, S'_r, \beta'_r\}_{r=1}^R, \hat{C}) - R_{MTL}(\{\alpha_{*r}, S_{*r}, \beta_{*r}\}_{r=1}^R, C_*))} \leq \frac{1}{v}.$$

If the risk on the existing tasks and the new task is similar with respect to the ground truth for all tasks, then  $v \approx 1$ . In other words, a low (or high) average risk on the existing tasks

results in a correspondingly low (or high) risk on the new task. This is especially evident in the realizable setting.

$$\frac{\inf_{\alpha' \in \mathcal{A}, S' \in \mathcal{S}, \beta' \in \mathcal{B}} R_0(\alpha', S', \beta', \widehat{C})}{\inf_{\{\alpha'_r, S'_r, \beta'_r\}_{r=1}^R} \left( R_{MTL}(\{\alpha'_r, S'_r, \beta'_r\}_{r=1}^R, \widehat{C}) \right)} \leq \frac{1}{v}.$$

Consider a setting in which there are multiple tasks, and we achieve good performance on all but a few of the existing tasks.

$$\frac{\inf_{\alpha' \in \mathcal{A}, S' \in \mathcal{S}, \beta' \in \mathcal{B}} R_0(\alpha', S', \beta', \widehat{C})}{\inf_{\{\alpha'_r, S'_r, \beta'_r\}_{r=1}^R} \left( R_{MTL}(\{\alpha'_r, S'_r, \beta'_r\}_{r=1}^R, \widehat{C}) \right)} \leq \frac{\text{relatively small}}{\text{relatively big}}.$$

Then  $1/v$  will be small, which is acceptable if we are not concerned with performance across all  $R$  tasks, as long as the new task performs well. Alternatively, if the new task performs poorly, this could result in a large  $1/v$ , which is not desirable.

$$\frac{\inf_{\alpha' \in \mathcal{A}, S' \in \mathcal{S}, \beta' \in \mathcal{B}} R_0(\alpha', S', \beta', \widehat{C})}{\inf_{\{\alpha'_r, S'_r, \beta'_r\}_{r=1}^R} \left( R_{MTL}(\{\alpha'_r, S'_r, \beta'_r\}_{r=1}^R, \widehat{C}) \right)} \leq \frac{\text{relatively big}}{\text{relatively small}}.$$

Therefore, we introduce an additive term  $\varepsilon$  to account for situations where the risk on the existing tasks is very small, but we are willing to accept relatively lower performance on the new task. We then make the following assumption for any  $C' \in \mathcal{C}$ :

$$\begin{aligned} & \inf_{\alpha' \in \mathcal{A}, S' \in \mathcal{S}, \beta' \in \mathcal{B}} R_0(\alpha', S', \beta', \widehat{C}) - R_0(\alpha_{*0}, S_{*0}, \beta_{*0}, C_*) \\ & \leq \frac{1}{v} \left( \inf_{\{\alpha'_r\} \in \mathcal{A}^{\otimes R}, \{S'_r\} \in \mathcal{S}^{\otimes R}, \{\beta'_r\} \in \mathcal{B}^{\otimes R}} R_{MTL}(\{\alpha'_r, S'_r, \beta'_r\}_{r=1}^R, \widehat{C}) - R_{MTL}(\{\alpha_{*r}, S_{*r}, \beta_{*r}\}_{r=1}^R, C_*) \right) + \varepsilon, \end{aligned}$$

where  $\varepsilon$  represents the level of tolerance we have for the difference in performance between the existing tasks and the new task.

## S.8 Proof of Theorems

In this subsection, we present the proofs of the theorems in Section 3. To start, we define  $\theta = \{\{\alpha_r, S_r, \beta_r\}_{r=1}^R, C\}$ ,  $\theta_r = \{\alpha_r, S_r, \beta_r, C\}$ , and  $\Theta = \mathcal{A}(\mathcal{S})^{\otimes R} + \mathcal{B}^{\otimes R}(\mathcal{C})$ . For  $\theta = (\theta_1, \dots, \theta_R)$ , we define

$$P\ell_{2,\theta} := \frac{1}{R} \sum_{r=1}^R P_r \ell_2(\theta_r) = \frac{1}{R} \sum_{r=1}^R \mathbb{E}_r[\ell_2(\theta_r(X_r))],$$

$$\widehat{P}\ell_{2,\theta} := \frac{1}{R} \sum_{r=1}^R \widehat{P}_r \ell_2(\theta_r) = \frac{1}{R} \sum_{r=1}^R \frac{1}{n_r} \sum_{i=1}^{n_r} \ell_2(\theta_r(X_{ri})),$$

where  $\ell_{2,\theta} = \{\ell_{2,\theta} : \theta \in \Theta\} = \{(X, Y) \mapsto (\theta(X) - Y)^2 : \theta \in \Theta\}$  with  $\ell_2$  representing the square loss and  $\Theta$  being the function class.

*Proof of Theorem 1.* To simplify the notation within the proof, let

$$R_{MTL}(\theta_*) = R_{MTL}(\{\alpha_{*,r}, \beta_{*,r}, S_{*,r}\}_{r=1}^R, C_*) = \frac{1}{R} \sum_{r=1}^R \mathbb{E}_r [Y_r - \alpha_{*,r}^\top S_{*,r}(X_r) - \beta_{*,r}^\top C_*(X_r)]^2$$

Assume that  $\{\alpha_{*,r}, S_{*,r}, \beta_{*,r}, C_*\} = \theta_{*,r} = \arg \min_{\theta_r} P_r \ell_{2,\theta_r}$  exists (For simplicity, assume that the minimum exists; if it does not, the proof is easily extended by considering the limit of a sequence of functions with expected loss approaching the infimum as mentioned in Bartlett et al. (2005)). Note that  $\{\{\ell_{2,\theta_{*,r}}(X_{ri}, Y_{ri})\}_{i \in [n_r]}\}_{r \in [R]} = \{\{(\alpha_{*,r}^\top S_{*,r}(X_{ri}) + \beta_{*,r}^\top C_*(X_{ri}) - Y_{ri})^2\}_{i \in [n_r]}\}_{r \in [R]}$  are  $N = \sum_{r=1}^R n_r$  independent random variables. Under Assumption 2, it holds that

$$\begin{aligned} \frac{1}{R} \sum_{r=1}^R \frac{1}{n_r} \sum_{i=1}^{n_r} \text{Var}[\ell_{2,\theta_{*,r}}(X_{ri}, Y_{ri})] &\leq \frac{1}{R} \sum_{r=1}^R \frac{1}{n_r} \sum_{i=1}^{n_r} \mathbb{E}_r[\ell_{2,\theta_{*,r}}(X_{ri}, Y_{ri})]^2 \\ &\leq \frac{b}{R} \sum_{r=1}^R \frac{1}{n_r} \sum_{i=1}^{n_r} \mathbb{E}_r[\ell_{2,\theta_{*,r}}(X_{ri}, Y_{ri})] = b R_{MTL}(\theta_*). \end{aligned}$$

We can apply Bernstein inequality (see, e.g., Devroye et al. (2013), Theorem 8.2) to show

that with probability at least  $1 - e^{-\delta}$ ,

$$\widehat{P}\ell_{2,\widehat{\theta}} \leq \widehat{P}\ell_{2,\theta_*} \leq R_{MTL}(\theta_*) + \sqrt{\frac{2R_{MTL}(\theta_*)b\delta}{N}} + \frac{2b\delta}{3N}. \quad (17)$$

Combining (17) with Theorem 11 in Watkins et al. (2024) gives that with probability at least  $1 - 2e^{-\delta}$ ,

$$\begin{aligned} P\ell_{2,\widehat{\theta}} &\leq \frac{K}{K-1} \widehat{P}\ell_{2,\widehat{\theta}} + \frac{1789bK\delta}{882N} + \frac{68b\delta}{3N} + \frac{144Kr^*}{b} \\ &\leq \frac{K}{K-1} \left( R_{MTL}(\theta_*) + \sqrt{\frac{2R_{MTL}(\theta_*)b\delta}{N}} + \frac{2b\delta}{3N} \right) + \frac{1789bK\delta}{882N} + \frac{68b\delta}{3N} + \frac{144Kr^*}{b} \\ &\stackrel{(i)}{\leq} R_{MTL}(\theta_*) + \sqrt{R_{MTL}(\theta_*)} \left( 6\sqrt{\frac{b\delta}{N}} + 146\sqrt{\frac{r^*}{b}} \right) + \frac{102b\delta}{N} + \frac{217r^*}{b}, \end{aligned}$$

where the last inequality (i) follows from the step-by-step derivation in Theorem 12 of Watkins et al. (2024) that eliminates the influence of the constant  $K > 1$ . The details are omitted here. Noting that  $P\ell_{2,\widehat{\theta}} = R_{MTL}(\widehat{\theta}) = R_{MTL}(\{\widehat{\alpha}_r, \widehat{\beta}_r, \widehat{S}_r\}_{r=1}^R, \widehat{C})$ , where  $(\{\widehat{\alpha}_r, \widehat{\beta}_r, \widehat{S}_r\}_{r=1}^R, \widehat{C})$  is defined in Theorem 1, gives the result (4) in Theorem 1.  $\square$

*Proof of Theorem 2.* In Theorem 2, we derive an upper-bound for the fixed point  $r^*$  of the sub-root function  $\psi(r)$ , which satisfies that  $\psi(r) \geq b\mathbb{E}[\widehat{\mathcal{R}}_X(\ell_2 \circ (\mathcal{A}(\mathcal{S})^{\otimes R} + \mathcal{B}^{\otimes R}(\mathcal{C}), r))]$ . In  $\mathbb{E}[\widehat{\mathcal{R}}_X(\ell_2 \circ (\mathcal{A}(\mathcal{S})^{\otimes R} + \mathcal{B}^{\otimes R}(\mathcal{C}), r))]$ , the expectation is taken over the combination of all samples  $X = \{\{X_{ri}\}_{i \in [n_r]}\}_{r \in [R]}$ . Following Lemma 19 in Watkins et al. (2024), we have that, for any  $\delta > 0$ , with probability at least  $1 - e^{-\delta}$ ,

$$\widehat{\mathcal{R}}_X \left( \ell_2 \circ \Theta \left| P\ell_{2,\theta} \leq \frac{r}{b} \right. \right) \leq \widehat{\mathcal{R}}_X \left( \ell_2 \circ \Theta \left| \widehat{P}\ell_{2,\theta} \leq \frac{2r}{b} \right. \right).$$

We can apply the concentration of Rademacher complexity (Lemma A.4 in Bartlett et al. (2005)) to bound the expected value of the left-hand side as follows. With probability at

least  $1 - e^{-\delta}$ ,

$$\mathbb{E} \left[ \widehat{\mathcal{R}}_X \left( \ell_2 \circ \Theta \left| P\ell_{2,\theta} \leq \frac{r}{b} \right. \right) \right] \leq 2\widehat{\mathcal{R}}_X \left( \ell_2 \circ \Theta \left| P\ell_{2,\theta} \leq \frac{r}{b} \right. \right) + \frac{b^2\delta}{N}.$$

Hence, with probability at least  $1 - 2e^{-\delta}$ , it holds that

$$\mathbb{E} \left[ \widehat{\mathcal{R}}_X \left( \ell_2 \circ \Theta \left| P\ell_{2,\theta} \leq \frac{r}{b} \right. \right) \right] \leq 2\widehat{\mathcal{R}}_X \left( \ell_2 \circ \Theta \left| \widehat{P}\ell_{2,\theta} \leq \frac{2r}{b} \right. \right) + \frac{b^2\delta}{N}.$$

From Eqn. (32) in Lemma 20 of Watkins et al. (2024), we deduce that for any  $\delta > 0$  and  $\kappa > 0$ , with probability at least  $1 - 3e^{-\delta}$ , it holds that

$$\begin{aligned} b\mathbb{E}[\widehat{\mathcal{R}}_X(\ell_2 \circ (\mathcal{A}(\mathcal{S})^{\otimes R} + \mathcal{B}^{\otimes R}(\mathcal{C}), r))] &= b\mathbb{E} \left[ \widehat{\mathcal{R}}_X \left( \ell_2 \circ \Theta \left| P\ell_{2,\theta} \leq \frac{r}{b} \right. \right) \right] \\ &\leq 8(1 + \kappa)\mathbb{E} \left[ \widehat{\mathcal{R}}_X \left( b\ell_2 \circ \Theta \left| \widehat{P}\ell_{2,\theta} \leq \frac{2r}{b} \right. \right) \right] + \frac{b^2\delta}{N} \left( \frac{8}{3} + 4(1 + \kappa) + \frac{2}{\kappa} \right). \end{aligned}$$

Now bounding the local Rademacher complexity with the result in Lemma 3, we have

$$b\mathbb{E}[\widehat{\mathcal{R}}_X(\ell_2 \circ (\mathcal{A}(\mathcal{S})^{\otimes R} + \mathcal{B}^{\otimes R}(\mathcal{C}), r))] \leq 8(1 + \kappa)\sqrt{2br}B + \frac{b^2\delta}{N} \left( \frac{8}{3} + 4(1 + \kappa) + \frac{2}{\kappa} \right),$$

where

$$B = 10240\sqrt{6}\widehat{\mathcal{F}}_X(\mathcal{A}(\mathcal{S})^{\otimes R} + \mathcal{B}^{\otimes R}(\mathcal{C}))(\log \sqrt{N})^2 + \frac{4\sqrt{b} + 160\sqrt{6}D_X(\log \sqrt{N})}{\sqrt{N}}.$$

Note that  $b\mathbb{E}[\widehat{\mathcal{R}}_X(\ell_2 \circ (\mathcal{A}(\mathcal{S})^{\otimes R} + \mathcal{B}^{\otimes R}(\mathcal{C}), r))]$  can be viewed as being bounded by a function of  $\sqrt{r}$ , i.e.  $b\mathbb{E}[\widehat{\mathcal{R}}_X(\ell_2 \circ (\mathcal{A}(\mathcal{S})^{\otimes R} + \mathcal{B}^{\otimes R}(\mathcal{C}), r))] \leq E\sqrt{r} + F$  where  $E = 8(1 + \kappa)\sqrt{2b}B$  and  $F = b^2\delta/N (8/3 + 4(1 + \kappa) + 2/\kappa)$ . We solve for a fixed point  $r^*$  of this expression

$E\sqrt{r^*} + F = r^*$ . Thus, with  $\kappa = 1/8$  we can conclude thta the fixed point  $r^*$  is bounded as:

$$\begin{aligned} r^* &\leq E^2 + 2F \\ &\leq 162bB^2 + \frac{139b^2\delta}{3N} \\ &\stackrel{(i)}{\leq} cb \left( \left( \widehat{\mathcal{F}}_X(\mathcal{A}(\mathcal{S})^{\otimes R} + \mathcal{B}^{\otimes R}(\mathcal{C})) \right)^2 (\log \sqrt{N})^4 + \frac{b}{N} + \frac{D_X^2 (\log \sqrt{N})^2}{N} + \frac{b\delta}{N} \right), \end{aligned}$$

where  $c$  is a constant satisfying  $c \leq 1.02 \times 10^{12}$ . Note that (i) is based on AM-GM inequality and the definition of  $\widehat{\mathcal{F}}_X(\mathcal{A}(\mathcal{S})^{\otimes R} + \mathcal{B}^{\otimes R}(\mathcal{C}))$  is in Lemma 2.  $\square$

*Proof of Theorem 3.* Let  $X_0$  denote the sample set  $\{X_{0i}\}_{i \in [n_0]}$  of the new task. We begin with the discussions of Assumption 4 in the Supplementary Material S.7. For  $\bar{d}_{\{\alpha_{*r}, S_{*r}, \beta_{*r}\}_{r=1}^R}(\widehat{C}; C_*)$ , it holds that with probability at least  $1 - e^\delta$ ,

$$\begin{aligned} \bar{d}_{\{\alpha_{*r}, S_{*r}, \beta_{*r}\}_{r=1}^R}(\widehat{C}; C_*) &= \inf_{\{\alpha'_r, S'_r, \beta'_r\}_{r=1}^R} \left( R_{MTL}(\{\alpha'_r, S'_r, \beta'_r\}_{r=1}^R, \widehat{C}) - R_{MTL}(\{\alpha_{*r}, S_{*r}, \beta_{*r}\}_{r=1}^R, C_*) \right) \\ &\leq R_{MTL}(\{\widehat{\alpha}_r, \widehat{S}_r, \widehat{\beta}_r\}_{r=1}^R, \widehat{C}) - R_{MTL}(\{\alpha_{*r}, S_{*r}, \beta_{*r}\}_{r=1}^R, C_*) \\ &\leq \sqrt{R_{MTL}(\{\alpha_{*r}, S_{*r}, \beta_{*r}\}_{r=1}^R, C_*)} \left( 6\sqrt{\frac{b\delta}{N}} + 146\sqrt{\frac{r^*}{b}} \right) + \frac{102b\delta}{N} + \frac{217r^*}{b}, \end{aligned}$$

where the last inequality is from the proof of Theorem 1.

Let  $\{\widehat{\alpha}_0, \widehat{S}_0, \widehat{\beta}_0\}$  be the empirical minimizer of  $R_0(\cdot, \widehat{C})$  for any  $\widehat{C}$ . Let  $\psi(r) \geq b\mathbb{E}[\widehat{\mathcal{R}}_{X_0}(\ell_2 \circ (\mathcal{A}(\mathcal{S}) + \mathcal{B}(\cdot))), r]$  with  $r^*$  being the fixed point of  $\psi(r)$ . Next, we give the upper bound for  $R_0(\widehat{\alpha}_0, \widehat{S}_0, \widehat{\beta}_0, \widehat{C})$ . Let  $\{\tilde{\alpha}_0, \tilde{S}_0, \tilde{\beta}_0\} = \arg \min R_0(\alpha, S, \beta, \widehat{C})$ , by applying Theorem 1, we have with probability at least  $1 - 2e^\delta$ ,

$$\begin{aligned} R_0(\widehat{\alpha}_0, \widehat{S}_0, \widehat{\beta}_0, \widehat{C}) &= R_0(\widehat{\alpha}_0, \widehat{S}_0, \widehat{\beta}_0, \widehat{C}) - d(\widehat{C}; C_*) + d(\widehat{C}; C_*) \\ &= R_0(\widehat{\alpha}_0, \widehat{S}_0, \widehat{\beta}_0, \widehat{C}) - \left( R_0(\tilde{\alpha}_0, \tilde{S}_0, \tilde{\beta}_0, \widehat{C}) - R_0(\alpha_{*0}, S_{*0}, \beta_{*0}, C_*) \right) + d(\widehat{C}; C_*) \\ &\leq \sqrt{R_0(\tilde{\alpha}_0, \tilde{S}_0, \tilde{\beta}_0, \widehat{C})E_0 + F_0} + R_0(\alpha_{*0}, S_{*0}, \beta_{*0}, C_*) + d(\widehat{C}; C_*), \end{aligned}$$

where  $E_0 = 6\sqrt{b\delta/n_0} + 146\sqrt{r^*/b}$  and  $F_0 = 102b\delta/n_0 + 217r^*/b$ . Note that  $R_0(\tilde{\alpha}_0, \tilde{S}_0, \tilde{\beta}_0, \hat{C}) = R_0(\alpha_{*0}, S_{*0}, \beta_{*0}, C_*) + \bar{d}_{\{\alpha_{*0}, S_{*0}, \beta_{*0}\}}(\hat{C}, C_*)$ . Then

$$\begin{aligned}
R_0(\hat{\alpha}_0, \hat{S}_0, \hat{\beta}_0, \hat{C}) &\leq \sqrt{R_0(\alpha_{*0}, S_{*0}, \beta_{*0}, C_*) + \bar{d}_{\{\alpha_{*0}, S_{*0}, \beta_{*0}\}}(\hat{C}, C_*)} E_0 + F_0 + R_0(\alpha_{*0}, S_{*0}, \beta_{*0}, C_*) \\
&\quad + d(\hat{C}; C_*) \\
&\leq \sqrt{R_0(\alpha_{*0}, S_{*0}, \beta_{*0}, C_*)} E_0 + \sqrt{\bar{d}_{\{\alpha_{*0}, S_{*0}, \beta_{*0}\}}(\hat{C}, C_*)} E_0 + F_0 \\
&\quad + R_0(\alpha_{*0}, S_{*0}, \beta_{*0}, C_*) + d(\hat{C}; C_*) \\
&\leq \sqrt{R_0(\alpha_{*0}, S_{*0}, \beta_{*0}, C_*)} E_0 + \frac{\bar{d}_{\{\alpha_{*0}, S_{*0}, \beta_{*0}\}}(\hat{C}, C_*)}{2} + \frac{E_0^2}{2} + F_0 \\
&\quad + R_0(\alpha_{*0}, S_{*0}, \beta_{*0}, C_*) + d(\hat{C}; C_*) \\
&\leq \sqrt{R_0(\alpha_{*0}, S_{*0}, \beta_{*0}, C_*)} E_0 + \frac{\sqrt{R_0(\alpha_{*0}, S_{*0}, \beta_{*0}, C_*)} E_0 + F_0}{2} + \frac{E_0^2}{2} + F_0 \\
&\quad + R_0(\alpha_{*0}, S_{*0}, \beta_{*0}, C_*) + d(\hat{C}; C_*) \\
&\leq \frac{3}{2} \sqrt{R_0(\alpha_{*0}, S_{*0}, \beta_{*0}, C_*)} E_0 + \frac{E_0^2}{2} + \frac{3}{2} F_0 + R_0(\alpha_{*0}, S_{*0}, \beta_{*0}, C_*) + d(\hat{C}; C_*) \\
&\leq \sqrt{R_0(\alpha_{*0}, S_{*0}, \beta_{*0}, C_*)} \left( 9\sqrt{\frac{b\delta}{n_0}} + 219\sqrt{\frac{r^*}{b}} \right) + \frac{171b\delta}{n_0} + \frac{21967r^*}{2b} \\
&\quad + R_0(\alpha_{*0}, S_{*0}, \beta_{*0}, C_*) + d(\hat{C}; C_*).
\end{aligned} \tag{18}$$

Under Assumption 4, we have that

$$d(\hat{C}; C_*) \leq \frac{1}{v} \left( \sqrt{R_{MTL}(\theta_*)} \left( 6\sqrt{\frac{b\delta}{N}} + 146\sqrt{\frac{r_2^*}{b}} \right) + \frac{102b\delta}{N} + \frac{217r_2^*}{b} \right) + \varepsilon. \tag{19}$$

Combining (18) and (19), we verify Theorem 3.  $\square$

*Proof of Theorem 4.* For  $r_1^*$ , by following the proof of Lemma 3 and Lemma 2, we obtain that

$$r_1^* \leq cb \left( \left( \hat{\mathcal{F}}_{X_0}(\mathcal{A}(\mathcal{S}) + \mathcal{B}(\hat{C})) \right)^2 (\log \sqrt{n_0})^4 + \frac{b}{n_0} + \frac{b\delta}{n_0} \right),$$

where

$$\widehat{\mathcal{F}}_{X_0}(\mathcal{A}(\mathcal{S}) + \mathcal{B}(\widehat{C})) = c_1 \left( (B_\alpha + B_0^s) L_S q \sqrt{\frac{\log n_0}{n_0}} + \sqrt{\frac{q}{n_0}} (B_\alpha + B_0^s) + \sqrt{\frac{p}{n_0}} (B_\beta + B_0^c) \right),$$

with  $L_S = B_X(B_S)^{D_S} \sqrt{D_S + 1 + \log d}$ . For  $r_2^*$ , apply the fixed point bound from Lemma 3, which always holds, and substitute it into Theorem 3.  $\square$

## S.9 Technical Lemmas

In this subsection, we provide several useful lemmas, including bounds on Gaussian complexity and local Rademacher complexity for  $\mathcal{A}(\mathcal{S})^{\otimes R} + \mathcal{B}^{\otimes R}(\mathcal{C})$ . First, we introduce a detailed discussion of  $D_X$  in Theorem 1.

**Lemma 1.** *Under the setting of Theorem 1, let  $X = \{\{X_{ri}\}_{i \in [n_r]}\}_{r \in [R]}$  where  $X_{ri} \in \mathcal{X}$  denote the combination of  $R$  datasets with a total of  $N = \sum_{r=1}^R n_r$  samples. We define*

$$D_X = \sup_{\{\{\alpha_r, S_r, \beta_r\}_{r=1}^R, C\}, \{\{\alpha'_r, S'_r, \beta'_r\}_{r=1}^R, C'\}} \frac{1}{R} \sum_{r=1}^R \frac{1}{n_r} \sum_{i=1}^{n_r} f_{ri}(\alpha_r, S_r, \beta_r, C; \alpha'_r, S'_r, \beta'_r, C'),$$

where  $f_{ri}(\alpha_r, S_r, \beta_r, C; \alpha'_r, S'_r, \beta'_r, C') = (\alpha_r^\top S_r(X_{ri}) + \beta_r^\top C(X_{ri}) - \alpha'_r{}^\top S'_r(X_{ri}) - \beta'_r{}^\top C'(X_{ri}))^2$ .

Suppose that Assumptions 1 and 3 hold,  $\bar{n} = \max_r n_r$ ,  $\underline{n} = \min_r n_r$ , we have

$$\begin{aligned} D_X \leq & O((B_\alpha + B_{max}^s)^2) + O((B_\alpha + B_{max}^s) \underline{n}^{1/2}) + O\left((B_\alpha + B_{max}^s) \sqrt{\frac{p \log((B_\alpha + B_{max}^s) \bar{n})}{\underline{n}}}\right) \\ & + O\left((B_\alpha + B_{max}^s) \sqrt{\frac{E_S \log((B_\alpha + B_{max}^s)^2 Q_S \bar{n})}{\underline{n}}}\right) \\ & + O((B_\beta + B_{max}^c)^2) + O((B_\beta + B_{max}^c) \underline{n}^{-1/2}) + O\left((B_\beta + B_{max}^c) \sqrt{\frac{p \log((B_\beta + B_{max}^c) \bar{n})}{\underline{n}}}\right) \\ & + O\left((B_\beta + B_{max}^c) \sqrt{\frac{E_C \log((B_\beta + B_{max}^c)^2 Q_C \bar{n})}{\underline{n}}}\right), \end{aligned}$$

with  $Q_S = D_S(2B_S)^{D_S+1}(\prod_{j=1}^{D_S} p_{j,S})(\prod_{j=2}^{D_S} p_{j,S!})^{-1/E_S}$ ,  $Q_C = D_C(2B_C)^{D_C+1}(\prod_{j=1}^{D_C} p_{j,C})(\prod_{j=2}^{D_C} p_{j,C!})^{-1/E_C}$ .



*Proof of Lemma 1.* First, we divide  $f_{ri}(\alpha_r, S_r, \beta_r, C; \alpha'_r, S'_r, \beta'_r, C')$  into two parts as follows,

$$\begin{aligned}
& (\alpha_r^\top S_r(X_{ri}) + \beta_r^\top C(X_{ri}) - \alpha_r'^\top S'_r(X_{ri}) - \beta_r'^\top C'(X_{ri}))^2 \\
& \leq 2(\alpha_r^\top S_r(X_{ri}) - \alpha_r'^\top S'_r(X_{ri}))^2 + 2(\beta_r^\top C(X_{ri}) - \beta_r'^\top C'(X_{ri}))^2 \\
& = 2f_{ri}(\alpha_r, S_r; \alpha'_r, S'_r) + 2f_{ri}(\beta_r, C; \beta'_r, C').
\end{aligned}$$

Then, we can simplify the task of finding the upper bound of  $D_X$  by individually determining the upper bounds of  $\sup_{\{\{\alpha_r, S_r\}_{r=1}^R\}, \{\{\alpha'_r, S'_r\}_{r=1}^R\}} \frac{1}{R} \sum_{r=1}^R \frac{1}{n_r} \sum_{i=1}^{n_r} f_{ri}(\alpha_r, S_r; \alpha'_r, S'_r)$  and  $\sup_{\{\{\beta_r, C\}_{r=1}^R\}, \{\{\beta'_r, C'\}_{r=1}^R\}} \frac{1}{R} \sum_{r=1}^R \frac{1}{n_r} \sum_{i=1}^{n_r} f_{ri}(\beta_r, C; \beta'_r, C')$ . The processes for deriving their upper bounds are similar; here, we will detail the derivation of the upper bound for  $\sup_{\{\{\beta_r, C\}_{r=1}^R\}, \{\{\beta'_r, C'\}_{r=1}^R\}} \frac{1}{R} \sum_{r=1}^R \frac{1}{n_r} \sum_{i=1}^{n_r} f_{ri}(\beta_r, C; \beta'_r, C')$ . By Lemma 9.1 of Györfi et al. (2002), it holds that, for any  $\tau > 0$ ,

$$\begin{aligned}
& P \left( \sup_{\{\{\beta_r, C\}_{r=1}^R\}, \{\{\beta'_r, C'\}_{r=1}^R\}} \left| \frac{1}{n_r} \sum_{i=1}^{n_r} f_{ir}(\beta_r, C; \beta'_r, C') - \mathbb{E}[f_r(\beta_r, C; \beta'_r, C')] \right| > \tau \right) \\
& \leq 2\mathcal{N}(\tau/3; d_\infty, f_r(\mathcal{B}(C) - \mathcal{B}(C))) \exp \left( -\frac{n_r \tau^2}{18B_{fc}^2} \right),
\end{aligned}$$

where  $\mathcal{N}(\tau/3; d_\infty, f_r(\mathcal{B}(C) - \mathcal{B}(C)))$  is the  $\tau/3$ -covering number of  $f_r(\mathcal{B}(C) - \mathcal{B}(C))$  w.r.t. the infinity norm and  $B_{fc} = (B_\beta + B_{max}^c)B_c$ . By Theorem 2 in Shen (2023) and Lemma 1 in He et al. (2024),

$$\begin{aligned}
& \mathcal{N}(\tau/3; d_\infty, f_r(\mathcal{B}(C) - \mathcal{B}(C))) \\
& \leq \left( \frac{48B_c^2(B_\beta + B_{max}^c)}{\tau} \right)^{2p} \left( \frac{\left( 192(B_\beta + B_{max}^c)^2 B_c D_C (B_X + 1) (2B_C)^{D_C+1} (\prod_{j=1}^{D_C} p_{j,C}) \right)^{2E_C}}{\tau^{2E_C} \left( \prod_{j=2}^{D_C} p_{j,C}! \right)^2} \right).
\end{aligned}$$

Denote  $a = 1/(18B_{fc}^2)$  and  $A = 2\mathcal{N}(1/(3n_r); d_\infty, f_r(\mathcal{B}(C) - \mathcal{B}(C)))$ . Note that  $\log A/(an_r) \geq$

$1/n_r$ . Then,

$$\begin{aligned}
& \mathbb{E} \left[ \sup_{\{\beta_r, C\}, \{\beta'_r, C'\}} \left\{ \frac{1}{n_r} \sum_{i=1}^{n_r} f_{ir}(\beta_r, C; \beta'_r, C') - \mathbb{E}[f_r(\beta_r, C; \beta'_r, C')] \right\} \right] \\
& \leq \sqrt{\mathbb{E} \left[ \left( \sup_{\{\beta_r, C\}, \{\beta'_r, C'\}} \left\{ \frac{1}{n_r} \sum_{i=1}^{n_r} f_{ir}(\beta_r, C; \beta'_r, C') - \mathbb{E}[f_r(\beta_r, C; \beta'_r, C')] \right\} \right)^2 \right]} \\
& \leq \sqrt{\int_0^\infty P \left\{ \left( \sup_{\{\beta_r, C\}, \{\beta'_r, C'\}} \left\{ \frac{1}{n_r} \sum_{i=1}^{n_r} f_{ir}(\beta_r, C; \beta'_r, C') - \mathbb{E}[f_r(\beta_r, C; \beta'_r, C')] \right\} \right)^2 > \tau \right\} d\tau} \\
& \leq \sqrt{\frac{\log A}{an_r} + \int_{\frac{\log A}{an_r}}^\infty 2\mathcal{N}(\tau/3; d_\infty, f_r(\mathcal{B}(\mathcal{C}) - \mathcal{B}(\mathcal{C}))) \exp \left\{ -\frac{n_r \tau}{18B_{fc}^2} \right\} d\tau} \\
& \leq \sqrt{\frac{\log A}{an_r} + \int_{\frac{\log A}{an_r}}^\infty 2\mathcal{N}(1/(3n_r); d_\infty, f_r(\mathcal{B}(\mathcal{C}) - \mathcal{B}(\mathcal{C}))) \exp \left\{ -\frac{n_r \tau}{18B_{fc}^2} \right\} d\tau} \\
& = \sqrt{\frac{18B_{fc}^2 (1 + \log 2 + \log \{\mathcal{N}(1/(3n_r); d_\infty, f_r(\mathcal{B}(\mathcal{C}) - \mathcal{B}(\mathcal{C})))\})}{n_r}}.
\end{aligned} \tag{20}$$

Based on (20) and Assumption 3, it follows that

$$\begin{aligned}
& \mathbb{E} \left[ \sup_{\{\beta_r, C\}, \{\beta'_r, C'\}} \frac{1}{n_r} \sum_{i=1}^{n_r} f_{ir}(\beta_r, C; \beta'_r, C') \right] \\
& \leq 4B_{fc}^2 + \sqrt{\frac{18B_{fc}^2 (1 + \log 2)}{n_r}} + \sqrt{\frac{36pB_{fc}^2}{n_r} \log (48n_r B_c^2 (B_\beta + B_{max}^c))} \\
& \quad + \sqrt{\frac{36E_c B_{fc}^2}{n_r} \log \left( \frac{192n_r B_c (B_\beta + B_{max}^c)^2 D_C (B_X + 1) (2B_C)^{D_C+1} (\prod_{j=1}^{D_C} p_{j,C})}{(\prod_{j=2}^{D_C} p_{j,C}!)^{1/E_C}} \right)}.
\end{aligned} \tag{21}$$

Finally, we conclude that  $\sup_{\{\{\beta_r\}_{r=1}^R, C\}, \{\{\beta'_r\}_{r=1}^R, C'\}} \frac{1}{R} \sum_{r=1}^R \frac{1}{n_r} \sum_{i=1}^{n_r} f_{ri}(\beta_r, C; \beta'_r, C')$  is upper-

bounded by

$$4B_{fc}^2 + \sqrt{\frac{18B_{fc}^2(1 + \log 2)}{\underline{n}}} + \sqrt{\frac{36pB_{fc}^2}{\underline{n}} \log(48\bar{n}B_c^2(B_\beta + B_{max}^c))}$$

$$+ \sqrt{\frac{36E_cB_{fc}^2}{\underline{n}} \log \left( \frac{192\bar{n}B_c(B_\beta + B_{max}^c)^2 D_C(B_X + 1)(2B_C)^{D_C+1} (\prod_{j=1}^{D_C} p_{j,C})}{(\prod_{j=2}^{D_C} p_{j,C}!)^{1/E_C}} \right)}$$

Using the same type of argument, we have that  $\sup_{\{\{\alpha_r, S_r\}_{r=1}^R\}, \{\{\alpha'_r, S'_r\}_{r=1}^R\}} \frac{1}{R} \sum_{r=1}^R \frac{1}{n_r} \sum_{i=1}^{n_r} f_{ri}(\alpha_r, S_r; \alpha'_r, S'_r)$  is upper bounded by

$$4B_{fs}^2 + \sqrt{\frac{18B_{fs}^2(1 + \log 2)}{\underline{n}}} + \sqrt{\frac{36qB_{fs}^2}{\underline{n}} \log(48\bar{n}B_s^2(B_\alpha + B_{max}^s))}$$

$$+ \sqrt{\frac{36E_sB_{fs}^2}{\underline{n}} \log \left( \frac{192\bar{n}B_s(B_\alpha + B_{max}^s)^2 D_S(B_X + 1)(2B_S)^{D_S+1} (\prod_{j=1}^{D_S} p_{j,S})}{(\prod_{j=2}^{D_S} p_{j,S}!)^{1/E_S}} \right)},$$

where  $B_{fs} = (B_\alpha + B_{max}^s)B_s$ . Thus, under Assumption, we verify Lemma 1 as follows,

$$D_X \leq O((B_\beta + B_{max}^c)^2) + O((B_\beta + B_{max}^c)\underline{n}^{-1/2}) + O((B_\beta + B_{max}^c)(p \log((B_\beta + B_{max}^c)\bar{n}))^{1/2}\underline{n}^{-1/2})$$

$$+ O \left( (B_\beta + B_{max}^c)\underline{n}^{-1/2} \left( E_C \log \left( (B_\beta + B_{max}^c)^2 \bar{n} D_C (2B_C)^{D_C+1} \left( \prod_{j=1}^{D_C} p_{j,C} \right) \left( \prod_{j=2}^{D_C} p_{j,C}! \right)^{-1/E_C} \right) \right)^{1/2} \right)$$

$$+ O((B_\alpha + B_{max}^s)^2) + O((B_\alpha + B_{max}^s)\underline{n}^{-1/2}) + O((B_\alpha + B_{max}^s)(p \log((B_\alpha + B_{max}^s)\bar{n}))^{1/2}\underline{n}^{-1/2})$$

$$+ O \left( (B_\alpha + B_{max}^s)\underline{n}^{-1/2} \left( E_S \log \left( (B_\alpha + B_{max}^s)^2 \bar{n} D_S (2B_S)^{D_S+1} \left( \prod_{j=1}^{D_S} p_{j,S} \right) \left( \prod_{j=2}^{D_S} p_{j,S}! \right)^{-1/E_S} \right) \right)^{1/2} \right).$$

□

Next, we derive Gaussian complexity bound for  $\mathcal{A}(\mathcal{S})^{\otimes R} + \mathcal{B}^{\otimes R}(\mathcal{C})$  in the following Lemma 2.

**Lemma 2** (Gaussian complexity bound). *Let  $X = \{\{X_{ri}\}_{i \in [n_r]}\}_{r \in [R]}$  where  $X_{ri} \in \mathcal{X}$  denote*

the combination of  $R$  datasets with a total of  $N = \sum_{r=1}^R n_r$  samples. The empirical Gaussian complexity of the function class satisfies,

$$\widehat{\mathcal{G}}_X(\mathcal{A}(\mathcal{S})^{\otimes R} + \mathcal{B}^{\otimes R}(\mathcal{C})) \leq \inf_{D_X \geq \delta > 0} \left\{ 4\delta + 256 \widehat{\mathcal{F}}_X(\mathcal{A}(\mathcal{S})^{\otimes R} + \mathcal{B}^{\otimes R}(\mathcal{C})) \log \left( \frac{D_X}{\delta} \right) \right\},$$

where  $D_X$  is defined in Lemma 1 and

$$\begin{aligned} \widehat{\mathcal{F}}_X(\mathcal{A}(\mathcal{S})^{\otimes R} + \mathcal{B}^{\otimes R}(\mathcal{C})) &= \left( 4(B_\alpha + \max_r B_r^s) L_S q \sqrt{\frac{R \log \bar{n}}{N}} + \sqrt{\frac{R}{N}} (B_\alpha + \max_r B_r^s) O(\sqrt{q}) \right. \\ &\quad \left. + 4(B_\beta + B_{max}^c) L_C p \sqrt{\frac{\log N}{N}} + \sqrt{\frac{R}{N}} (B_\beta + B_{max}^c) O(\sqrt{p}) \right), \end{aligned} \quad (22)$$

with  $L_S = B_S(B_S)^{D_S} \sqrt{D_S + 1 + \log d}$  and  $L_C = B_X(B_C)^{D_C} \sqrt{D_C + 1 + \log d}$ .

*Proof of Lemma 2.* We follow steps similar to the proof of Theorem 7 within Tripuraneni et al. (2020). For ease of notation we define  $\theta = \{\{\alpha_r, S_r, \beta_r\}_{r=1}^R, C\}$ ,  $\theta_r = \{\alpha_r, S_r, \beta_r, C\}$  and  $\Theta = \mathcal{A}(\mathcal{S})^{\otimes R} + \mathcal{B}^{\otimes R}(\mathcal{C})$  in the following. We rewrite the Gaussian complexity of the function class  $\Theta = \mathcal{A}(\mathcal{S})^{\otimes R} + \mathcal{B}^{\otimes R}(\mathcal{C})$  as,

$$\widehat{\mathcal{G}}_X(\mathcal{A}(\mathcal{S})^{\otimes R} + \mathcal{B}^{\otimes R}(\mathcal{C})) = \mathbb{E} \left[ \sup_{\theta \in \Theta} \frac{1}{R} \sum_{r=1}^R \frac{1}{n_r} \sum_{i=1}^{n_r} \iota_{ri} (\alpha_r^\top S_r(X_{ri}) + \beta_r^\top C(X_{ri})) \right] = \mathbb{E} \left[ \frac{1}{\sqrt{N}} \sup_{\theta \in \Theta} Z_\theta \right],$$

where we define the mean-zero stochastic process  $Z_\theta = \frac{\sqrt{N}}{R} \sum_{r=1}^R \frac{1}{n_r} \sum_{i=1}^{n_r} \iota_{ri} (\alpha_r^\top S_r(X_{ri}) + \beta_r^\top C(X_{ri}))$  for a fixed sequence of samples  $\{\{X_{ri}\}_{i \in [n_r]}\}_{r \in [R]}$ , indexed by elements  $\{\theta \in \Theta\}$ , and for a sequence of independent Gaussian random variables  $\{\{\iota_{ri}\}_{i \in [n_r]}\}_{r \in [R]}$ . Note that the process  $Z_\theta$  has sub-Gaussian increments, meaning that  $Z_\theta - Z_{\theta'}$  is a sub-Gaussian

random variable with parameter

$$\begin{aligned} d_{2,X}^2(\theta; \theta') &= d_{2,X}^2(\{\alpha_r, S_r, \beta_r\}_{r=1}^R, C; \{\alpha'_r, S'_r, \beta'_r\}_{r=1}^R, C') \\ &= \frac{1}{N} \sum_{r=1}^R \sum_{i=1}^n (\alpha_r^\top S_r(X_{ri}) + \beta_r^\top C(X_{ri}) - \alpha'_r{}^\top S'_r(X_{ri}) + \beta'_r{}^\top C'(X_{ri}))^2. \end{aligned}$$

Since  $Z_\theta$  is a mean-zero stochastic process, we have

$$\mathbb{E} \left[ \sup_{\theta \in \Theta} Z_\theta \right] = \mathbb{E} \left[ \sup_{\theta \in \Theta} Z_\theta - Z_{\theta'} \right] \leq \mathbb{E} \left[ \sup_{\theta, \theta' \in \Theta} Z_\theta - Z_{\theta'} \right].$$

Now, using the Dudley entropy integral bound from Wainwright (2019), we obtain

$$\mathbb{E} \left[ \sup_{\theta, \theta' \in \Theta} Z_\theta - Z_{\theta'} \right] \leq 4\mathbb{E} \left[ \sup_{d_{2,X}(\theta, \theta') \leq \delta} Z_\theta - Z_{\theta'} \right] + 32 \int_\delta^D \sqrt{\log \mathcal{N}_X(u; d_{2,X}, \Theta)} du. \quad (23)$$

For the first part in (23), we parameterize the sequence of *i.i.d.* Gaussian random variables  $\{\{\iota_{ri}\}_{i \in [n_r]}\}_{r \in [R]}$ , as  $\bar{\iota}$ . It follows that  $\sup_{d_{2,X}(\theta, \theta') \leq \delta} Z_\theta - Z_{\theta'} \leq \sup_{\nu: \|\nu\| \leq \delta} \bar{\iota}^\top \nu \leq \sup_{\nu: \|\nu\| \leq \delta} \|\bar{\iota}\| \|\nu\| = \delta \|\bar{\iota}\|$ . Then, by Jensen's inequality, we have  $\mathbb{E} \left[ \sup_{d_{2,X}(\theta, \theta') \leq \delta} Z_\theta - Z_{\theta'} \right] \leq \mathbb{E}[\delta \|\bar{\iota}\|] \leq \delta \sqrt{N}$ . For the second part in (23), applying the triangle inequality, we can decompose the distance over the function class  $\Theta = \mathcal{A}(\mathcal{S})^{\otimes R} + \mathcal{B}^{\otimes R}(\mathcal{C})$  into separate distances

over  $\mathcal{A}^{\otimes R}$ ,  $\mathcal{S}^{\otimes R}$ ,  $\mathcal{B}^{\otimes R}$ , and  $\mathcal{C}$  as follows,

$$\begin{aligned}
& d_{2,X}(\{\alpha_r, S_r, \beta_r\}_{r=1}^R, C; \{\alpha'_r, S'_r, \beta'_r\}_{r=1}^R, C') \\
& \leq d_{2,X}(\{\alpha'_r, S_r, \beta'_r\}_{r=1}^R, C'; \{\alpha'_r, S'_r, \beta'_r\}_{r=1}^R, C') \\
& \quad + d_{2,X}(\{\alpha_r, S_r, \beta'_r\}_{r=1}^R, C'; \{\alpha'_r, S_r, \beta'_r\}_{r=1}^R, C') \\
& \quad + d_{2,X}(\{\alpha_r, S_r, \beta_r\}_{r=1}^R, C'; \{\alpha_r, S_r, \beta'_r\}_{r=1}^R, C') \\
& \quad + d_{2,X}(\{\alpha_r, S_r, \beta_r\}_{r=1}^R, C; \{\alpha_r, S_r, \beta_r\}_{r=1}^R, C') \\
& \leq \max_r \|\alpha_r\| d_{2,X}(\{S_r\}_{r=1}^R; \{S'_r\}_{r=1}^R) + d_{2,X}(\{\alpha_r\}_{r=1}^R; \{\alpha'_r\}_{r=1}^R) \\
& \quad + d_{2,X}(\{\beta_r\}_{r=1}^R; \{\beta'_r\}_{r=1}^R) + \max_r \|\beta_r\| d_{2,X}(C; C').
\end{aligned}$$

We then use a covering argument on each of the spaces  $\mathcal{A}^{\otimes R}$ ,  $\mathcal{S}^{\otimes R}$ ,  $\mathcal{B}^{\otimes R}$  and  $\mathcal{C}$  to witness a covering of the composed spaces  $\Theta = \mathcal{A}(\mathcal{S})^{\otimes R} + \mathcal{B}^{\otimes R}(\mathcal{C})$ . First, let  $C_{\mathcal{S}^{\otimes R}}$  be a  $\tau_0$ -covering for the function class  $\mathcal{S}^{\otimes R}$  of the empirical  $\ell_2$  norm. Then for each  $\{S_r\}_{r=1}^R \in \mathcal{S}^{\otimes R}$ , construct a  $\tau_1$ -covering  $C_{\mathcal{A}^{\otimes R}}$  for the function class  $\mathcal{A}^{\otimes R}$ . Next, for each  $\{S_r\}_{r=1}^R \in \mathcal{S}^{\otimes R}$  and  $\{\alpha_r\}_{r=1}^R \in \mathcal{A}^{\otimes R}$ , construct a  $\tau_2$ -covering  $C_{\mathcal{C}}$  for the function class  $\mathcal{C}$ . Last, for each  $\{S_r\}_{r=1}^R \in \mathcal{S}^{\otimes R}$ ,  $\{\alpha_r\}_{r=1}^R \in \mathcal{A}^{\otimes R}$  and  $C \in \mathcal{C}$ , we build a  $\tau_3$ -covering  $C_{\mathcal{B}^{\otimes R}}$ . Using the decomposition of distance, we have

$$C_{\mathcal{A}(\mathcal{S})^{\otimes R}} \cdot C_{\mathcal{B}^{\otimes R}(\mathcal{C})} = \cup_{\{S_r\}_{r=1}^R \in C_{\mathcal{S}^{\otimes R}}} \left( \cup_{\{\alpha_r\}_{r=1}^R \in C_{\mathcal{A}^{\otimes R}}} \left( \cup_{C \in C_{\mathcal{C}}} (C_{\mathcal{B}^{\otimes R}}) \right) \right)$$

is a  $(\max_r \|\alpha_r\| \tau_0 + \tau_1 + \max_r \|\beta_r\| \tau_2 + \tau_3)$ -covering for  $\Theta$  in the empirical  $\ell_2$  norm. To see this, let  $\{S_r\}_{r=1}^R \in \mathcal{S}^{\otimes R}$ ,  $\{\alpha_r\}_{r=1}^R \in \mathcal{A}^{\otimes R}$ ,  $\{\beta_r\}_{r=1}^R \in \mathcal{B}^{\otimes R}$ ,  $C \in \mathcal{C}$  be arbitrary. Let  $\{S'_r\}_{r=1}^R \in C_{\mathcal{S}^{\otimes R}}$  be  $\tau_0$  close to  $\{S_r\}_{r=1}^R$ , given this  $\{S'_r\}_{r=1}^R$ , there exists  $\{\alpha'_r\}_{r=1}^R \in C_{\mathcal{A}^{\otimes R}}$  such that  $\{\alpha'_r\}_{r=1}^R$  is  $\tau_1$  close to  $\{\alpha_r\}_{r=1}^R$ . Given  $\{S'_r\}_{r=1}^R$  and  $\{\alpha'_r\}_{r=1}^R$ , there exists  $C' \in C_{\mathcal{C}}$  such that  $C'$  is  $\tau_2$  close to  $C$ . Last, given  $\{S'_r\}_{r=1}^R$ ,  $\{\alpha'_r\}_{r=1}^R$  and  $C'$ , there exists  $\{\beta'_r\}_{r=1}^R \in C_{\mathcal{B}^{\otimes R}}$  such that

$\{\beta'_r\}_{r=1}^R$  is  $\tau_3$  close to  $\{\beta_r\}_{r=1}^R$ . By the process of constructing  $\{\{\alpha'_r, S'_r, \beta'_r\}_{r=1}^R, C'\}$ , we have

$$d_{2,X}(\{\alpha_r, S_r, \beta_r\}_{r=1}^R, C; \{\alpha'_r, S'_r, \beta'_r\}_{r=1}^R, C') \leq \max_r \|\alpha_r\| \tau_0 + \tau_1 + \max_r \|\beta_r\| \tau_2 + \tau_3.$$

We now bound the cardinality of the covering  $C_{\mathcal{A}(S)^{\otimes R}} \cdot C_{\mathcal{B}^{\otimes R}(\mathcal{C})}$ ,

$$C_{\mathcal{A}(S)^{\otimes R}} \cdot C_{\mathcal{B}^{\otimes R}(\mathcal{C})} \leq |C_{S^{\otimes R}}| \max_{\{S_r\}_{r=1}^R \in S^{\otimes R}} \left| C_{\mathcal{A}_{\{S_r\}_{r=1}^R}^{\otimes R}} \right| |C_{\mathcal{C}}| \max_{C \in \mathcal{C}} \left| C_{\mathcal{A}_C^{\otimes R}} \right|.$$

First, to control  $\max_{\{S_r\}_{r=1}^R \in S^{\otimes R}} \left| C_{\mathcal{A}_{\{S_r\}_{r=1}^R}^{\otimes R}} \right|$ , note an  $\tau$ -cover of  $\mathcal{A}_{\{S_r\}_{r=1}^R}^{\otimes R}$  in the empirical  $\ell_2$  norm can be obtained from the cover  $C_{\mathcal{A}_S} \times \cdots \times C_{\mathcal{A}_S}$ . Hence,

$$\max_{\{S_r\}_{r=1}^R \in S^{\otimes R}} \left| C_{\mathcal{A}_{\{S_r\}_{r=1}^R}^{\otimes R}} \right| \leq \left| \max_{S \in \mathcal{S}} C_{\mathcal{A}_S} \right|^R.$$

Similarly, it holds that  $\max_{C \in \mathcal{C}} \left| C_{\mathcal{B}_C^{\otimes R}} \right| \leq |\max_{C \in \mathcal{C}} C_{\mathcal{B}_C}|^R$ . Then we have

$$C_{\mathcal{A}(S)^{\otimes R}} \cdot C_{\mathcal{B}^{\otimes R}(\mathcal{C})} \leq |C_S|^R \left| \max_{S \in \mathcal{S}} C_{\mathcal{A}_S} \right|^R |C_{\mathcal{C}}| \left| \max_{C \in \mathcal{C}} C_{\mathcal{B}_C} \right|^R.$$

It follows that the metric entropy can be bounded by

$$\begin{aligned} & \log \mathcal{N}_{2,X}(\max_r \|\alpha_r\| \tau_0 + \tau_1 + \max_r \|\beta_r\| \tau_2 + \tau_3; d_{2,X}, \Theta) \\ & \leq R \log \mathcal{N}_{2,X}(\tau_0; d_{2,X}, \mathcal{S}) + R \max_S \log \mathcal{N}_{2,S}(\tau_1; d_{2,S}, \mathcal{A}) \\ & \quad + \log \mathcal{N}_{2,X}(\tau_2; d_{2,X}, \mathcal{C}) + R \max_C \log \mathcal{N}_{2,C}(\tau_3; d_{2,C}, \mathcal{B}), \end{aligned}$$

where we use  $S$  to denote  $S = \{\{S_r(X_{ri})\}_{i \in [n_r]}\}_{r \in [R]}$  and  $C$  to denote  $C = \{\{C(X_{ri})\}_{i \in [n_r]}\}_{r \in [R]}$  in the covering number notations  $\mathcal{N}_{2,S}(\cdot)$  and  $\mathcal{N}_{2,C}(\cdot)$ , respectively. Applying the covering number upper bound with  $\tau_0 = \tau/(4 \max_r \|\alpha_r\|)$ ,  $\tau_1 = \tau/4$ ,  $\tau_2 = \tau/(4 \max_r \|\beta_r\|)$ , and  $\tau_3 = \tau/4$ , along with the sub-additivity of the  $\sqrt{\cdot}$  function, then provides a bound on the

entropy integral of

$$\begin{aligned}
& \int_{\delta}^D \sqrt{\log \mathcal{N}_{2,X}(\tau; d_{2,X}, \Theta)} d\tau \\
& \leq \sqrt{R} \int_{\delta}^D \sqrt{\log \mathcal{N}_{2,X} \left( \frac{\tau}{4 \max_r \|\alpha_r\|}; d_{2,X}, \mathcal{S} \right)} d\tau + \sqrt{R} \int_{\delta}^D \max_S \sqrt{\mathcal{N}_{2,S} \left( \frac{\tau}{4}; d_{2,S}, \mathcal{A} \right)} d\tau \\
& \quad + \int_{\delta}^D \sqrt{\log \mathcal{N}_{2,X} \left( \frac{\tau}{4 \max_r \|\beta_r\|}; d_{2,X}, \mathcal{C} \right)} d\tau + \sqrt{R} \int_{\delta}^D \max_C \sqrt{\mathcal{N}_{2,C} \left( \frac{\tau}{4}; d_{2,C}, \mathcal{B} \right)} d\tau.
\end{aligned}$$

Using the Sudakov minoration theorem in (Wainwright, 2019) for Gaussian process, along with the fact that packing numbers at scale  $\tau$  provide an upper bound for covering numbers at the same scale, we find

$$\begin{aligned}
\log \mathcal{N}_{2,X}(\tau; d_{2,X}, \mathcal{S}) & \leq 4 \left( \frac{\sqrt{n} \widehat{\mathcal{G}}_{n,X}(\mathcal{S})}{\tau} \right)^2, & \log \mathcal{N}_{2,S}(\tau; d_{2,S}, \mathcal{A}) & \leq 4 \left( \frac{\sqrt{n} \widehat{\mathcal{G}}_{n,S}(\mathcal{A})}{\tau} \right)^2, \\
\log \mathcal{N}_{2,X}(\tau; d_{2,X}, \mathcal{C}) & \leq 4 \left( \frac{\sqrt{N} \widehat{\mathcal{G}}_{N,X}(\mathcal{C})}{\tau} \right)^2, & \log \mathcal{N}_{2,C}(\tau; d_{2,C}, \mathcal{B}) & \leq 4 \left( \frac{\sqrt{n} \widehat{\mathcal{G}}_{n,C}(\mathcal{B})}{\tau} \right)^2.
\end{aligned} \tag{24}$$

In the following proof of Lemma 2, we use the sample size and individual samples as subscripts for Gaussian complexity and Rademacher complexity to more clearly indicate these complexities over different sample combinations. Under Assumptions 1 and 3, and by



the definition of empirical Gaussian complexity, we have

$$\begin{aligned}
\max_{r \in [R]} \widehat{\mathcal{G}}_{n_r, \{X_{ri}\}_{i \in [n_r]}}(\mathcal{B}) &= \max_{r \in [R]} \mathbb{E}_\ell \left[ \sup_{\beta_r \in \mathcal{B}} \frac{1}{n_r} \sum_{i=1}^{n_r} \ell_{ir} C(X_{ri}) \beta_r \right] \\
&\leq \max_{r \in [R]} \frac{B_\beta + B_{max}^c}{n_r} \sqrt{\mathbb{E}_\ell \left[ \sum_{i=1}^{n_r} \|\ell_{ir} C(X_{ri})\|^2 \right]} \\
&\leq \max_{r \in [R]} \frac{B_\beta + B_{max}^c}{n_r} \sqrt{\sum_{i=1}^{n_r} \|C(X_{ri})\|^2} \\
&= \max_{r \in [R]} \frac{B_\beta + B_{max}^c}{\sqrt{n_r}} \sqrt{\text{tr}(\Sigma_{C(X_r)})} \\
&= \max_{r \in [R]} \frac{B_\beta + B_{max}^c}{\sqrt{n_r}} \sqrt{\sum_{j=1}^p \sigma_j(\Sigma_{C(X_r)})},
\end{aligned} \tag{25}$$

where  $\sigma_j(\Sigma_{C(X_r)})$  is the  $j$ -th largest eigenvalue of  $\sum_{i=1}^{n_r} C(X_{ri})C^\top(X_{ri})/n_r$ . Similarly, we can demonstrate that

$$\max_{r \in [R]} \widehat{\mathcal{G}}_{n_r, \{X_{ri}\}_{i \in [n_r]}}(\mathcal{A}) \leq \max_{r \in [R]} \frac{B_\alpha + B_{max}^s}{\sqrt{n_r}} \sqrt{\sum_{j=1}^q \sigma_j(\Sigma_{S_r(X_r)})}, \tag{26}$$

where  $\sigma_j(\Sigma_{S_r(X_r)})$  is the  $j$ -th largest eigenvalue of  $\sum_{i=1}^{n_r} S_r(X_{ri})S_r^\top(X_{ri})/n_r$ . For  $\widehat{\mathcal{G}}_{N,X}(\mathcal{C})$ , we obtain that

$$\begin{aligned}
\widehat{\mathcal{G}}_{N,X}(\mathcal{C}) &= \frac{1}{N} \mathbb{E}_\ell \left[ \sup_{C \in \mathcal{C}} \sum_{j=1}^p \sum_{r=1}^R \sum_{i=1}^{n_r} \ell_{jir} C_j(X_{ri}) \right] \\
&\leq \sum_{j=1}^p \widehat{\mathcal{G}}_{N,X}(C_j) \leq 2\sqrt{\log N} \sum_{j=1}^p \widehat{\mathcal{R}}_{N,X}(C_j).
\end{aligned} \tag{27}$$

Recall that  $\mathcal{C} = \mathcal{NN}(W_C, D_C, B_C)$ . By Theorem 2 of (Golowich et al., 2018),

$$\widehat{\mathcal{R}}_{N,X}(C_j) \leq \frac{2B_X(B_C)^{D_C} \sqrt{D_C + 1 + \log d}}{\sqrt{N}}. \tag{28}$$

Combining (27) and (28) gives that

$$\widehat{\mathcal{G}}_{N,X}(\mathcal{C}) \leq 4B_X(B_C)^{D_C} \sqrt{D_C + 1 + \log dp} \sqrt{\frac{\log N}{N}}. \quad (29)$$

Similarly, we can obtain that

$$\widehat{\mathcal{G}}_{n_r, (X_{ri})_{i \in [n_r]}}(\mathcal{S}) \leq 4B_S(B_S)^{D_S} \sqrt{D_S + 1 + \log dq} \sqrt{\frac{\log n_r}{n_r}}. \quad (30)$$

Combining (24), (25), (26), (29) and (30) gives the bound of  $\widehat{\mathcal{G}}_X(\mathcal{A}(\mathcal{S})^{\otimes R} + \mathcal{B}^{\otimes R}(\mathcal{C}))$  as follows,

$$\begin{aligned} & \widehat{\mathcal{G}}_X(\mathcal{A}(\mathcal{S})^{\otimes R} + \mathcal{B}^{\otimes R}(\mathcal{C})) \\ & \leq \frac{1}{\sqrt{N}} \left( 4\sqrt{N}\delta + 256 \left( \sqrt{R}(\max_r \|\alpha_r\|) \max_r (\sqrt{n_r} \widehat{\mathcal{G}}_{n_r, (X_{ri})_{i \in [n_r]}}(\mathcal{S})) + \sqrt{R} \max_r (\sqrt{n_r} \widehat{\mathcal{G}}_{n_r, (X_{ri})_{i \in [n_r]}}(\mathcal{A})) \right. \right. \\ & \quad \left. \left. + \sqrt{N} \max_r \|\beta_r\| \widehat{\mathcal{G}}_{N,X}(\mathcal{C}) + \sqrt{R} \max_r (\sqrt{n_r} \widehat{\mathcal{G}}_{n_r, (X_{ri})_{i \in [n_r]}}(\mathcal{B})) \right) \int_{\delta}^{D_X} \frac{1}{\tau} d\tau \right) \\ & \stackrel{(i)}{\leq} \frac{1}{\sqrt{N}} \left( 4\sqrt{N}\delta + 256 \left( 4\sqrt{R}(B_{\alpha} + B_{max}^s) L_S q \sqrt{\log \bar{n}} + \sqrt{R}(B_{\alpha} + B_{max}^s) O(\sqrt{q}) \right. \right. \\ & \quad \left. \left. + 4(B_{\beta} + B_{max}^c) L_C p \sqrt{\log N} + \sqrt{R}(B_{\beta} + B_{max}^c) O(\sqrt{p}) \right) \int_{\delta}^{D_X} \frac{1}{\tau} d\tau \right) \\ & \leq 4\delta + 256 \left( 4(B_{\alpha} + B_{max}^s) L_S q \sqrt{\frac{R \log \bar{n}}{N}} + \sqrt{\frac{R}{N}} (B_{\alpha} + B_{max}^s) O(\sqrt{q}) \right. \\ & \quad \left. + 4(B_{\beta} + B_{max}^c) L_C p \sqrt{\frac{\log N}{N}} + \frac{R}{N} (B_{\beta} + B_{max}^c) O(\sqrt{p}) \right) \log \left( \frac{D_X}{\delta} \right) \\ & = 4\delta + 256 \widehat{\mathcal{F}}_X(\mathcal{A}(\mathcal{S})^{\otimes R} + \mathcal{B}^{\otimes R}(\mathcal{C})) \log \left( \frac{D_X}{\delta} \right), \end{aligned}$$

where

$$\begin{aligned} \widehat{\mathcal{F}}_X(\mathcal{A}(\mathcal{S})^{\otimes R} + \mathcal{B}^{\otimes R}(\mathcal{C})) & = \left( 4(B_{\alpha} + B_{max}^s) L_S q \sqrt{\frac{R \log \bar{n}}{N}} + \sqrt{\frac{R}{N}} (B_{\alpha} + B_{max}^s) O(\sqrt{q}) \right. \\ & \quad \left. + 4(B_{\beta} + B_{max}^c) L_C p \sqrt{\frac{\log N}{N}} + \sqrt{\frac{R}{N}} (B_{\beta} + B_{max}^c) O(\sqrt{p}) \right), \end{aligned}$$

where  $L_S = B_S(B_S)^{D_S} \sqrt{D_S + 1 + \log d}$  and  $L_C = B_X(B_C)^{D_C} \sqrt{D_C + 1 + \log d}$  for ease of notation. Note that (i) follows from the fact that  $\sqrt{\sum_{j=1}^p \sigma_j(\Sigma_{C(X_r)})} \leq O(\sqrt{p})$  and  $\sqrt{\sum_{j=1}^p \sigma_j(\Sigma_{S_r(X_r)})} \leq O(\sqrt{q})$  by Lemma 4 in Tripuraneni et al. (2020) and the concavity of the  $\sqrt{\cdot}$  function.  $\square$

Based on Lemma 2, we provide local Rademacher complexity bound for  $\mathcal{A}(\mathcal{S})^{\otimes R} + \mathcal{B}^{\otimes R}(\mathcal{C})$  in Lemma 3.

**Lemma 3** (Local Rademacher complexity bound). *Under the setting of Theorem 2, we have*

$$\begin{aligned} & \widehat{\mathcal{R}}_X(\ell_2 \circ (\mathcal{A}(\mathcal{S})^{\otimes R} + \mathcal{B}^{\otimes R}(\mathcal{C})), r) \\ & \leq 10240\sqrt{6r}\widehat{\mathcal{F}}_X(\mathcal{A}(\mathcal{S})^{\otimes R} + \mathcal{B}^{\otimes R}(\mathcal{C}))(\log \sqrt{N})^2 + \frac{4\sqrt{br} + 160\sqrt{6}D_X\sqrt{r}(\log \sqrt{N})}{\sqrt{N}}, \end{aligned}$$

where  $\widehat{\mathcal{F}}_X(\mathcal{A}(\mathcal{S})^{\otimes R} + \mathcal{B}^{\otimes R}(\mathcal{C}))$  is defined in Lemma 2.

*Proof of Lemma 3.* For ease of notation, we denote

$$\sup_{\{\{\alpha_r, S_r, \beta_r\}_{r=1}^R, C\} \in \mathcal{A}(\mathcal{S})^{\otimes R} + \mathcal{B}^{\otimes R}(\mathcal{C})} \sup_X \|(\{\alpha_r, S_r, \beta_r\}_{r=1}^R, C)\|_{L^2(X)} = \sup_{\theta \in \Theta} \sup_X \|\theta\|_{L^2(X)}.$$

We first compute  $\sup_{\theta \in \Theta} \sup_X \|\theta\|_{L^2(X)}$ . By the definition of  $b$  and  $r$  in Section 3, we obtain that

$$\begin{aligned} \sup_{\theta \in \Theta} \sup_X \|\theta\|_{L^2(X)} & \leq \sup_{\theta \in \Theta} \frac{1}{R} \sum_{r=1}^R \frac{1}{n_r} \sum_{i=1}^{n_r} (\alpha_r^\top S_r(X_{ri}) + \beta_r^\top C(X_{ri}) - Y_{ri})^4 \\ & \leq \sup_{\theta \in \Theta} b \frac{1}{R} \sum_{r=1}^R \frac{1}{n_r} \sum_{i=1}^{n_r} (\alpha_r^\top S_r(X_{ri}) + \beta_r^\top C(X_{ri}) - Y_{ri})^2 \leq br. \end{aligned}$$

Therefore, applying Dubley entropy integral bound within Wainwright (2019) gives that

$$\begin{aligned}
& \widehat{\mathcal{R}}_X(\ell_2 \circ (\mathcal{A}(\mathcal{S})^{\otimes R} + \mathcal{B}^{\otimes R}(\mathcal{C})), r) \\
& \stackrel{(i)}{\leq} \inf_{\sqrt{br} \geq \alpha \geq 0} \left\{ 4\alpha + 10 \int_{\alpha}^{\sqrt{br}} \sqrt{\frac{\log \mathcal{N}(\frac{\tau}{24Nr}; d_{2,X}, (\mathcal{A}(\mathcal{S})^{\otimes R} + \mathcal{B}^{\otimes R}(\mathcal{C})))}{N}} d\tau \right\} \\
& \stackrel{(ii)}{\leq} \inf_{\sqrt{br} \geq \alpha \geq 0} \left\{ 4\alpha + 20 \int_{\alpha}^{\sqrt{br}} \frac{\sqrt{24Nr} \widehat{\mathcal{G}}_X(\mathcal{A}(\mathcal{S})^{\otimes R} + \mathcal{B}^{\otimes R}(\mathcal{C}))}{\sqrt{N}\tau} d\tau \right\} \\
& \leq \inf_{\sqrt{br} \geq \alpha \geq 0} \left\{ 4\alpha + 40\sqrt{6r} \widehat{\mathcal{G}}_X(\mathcal{A}(\mathcal{S})^{\otimes R} + \mathcal{B}^{\otimes R}(\mathcal{C})) \log \left( \frac{\sqrt{br}}{\alpha} \right) \right\},
\end{aligned} \tag{31}$$

where (i) is based on the Lemma 18 in Watkins et al. (2024), with the  $H$ -smoothness parameter of the square loss being  $H = 2$ , and (ii) follows from the Sudakov minoration theorem in Wainwright (2019). By Lemma 2, it holds that

$$\begin{aligned}
& \widehat{\mathcal{R}}_X(\ell_2 \circ (\mathcal{A}(\mathcal{S})^{\otimes R} + \mathcal{B}^{\otimes R}(\mathcal{C})), r) \\
& \leq \inf_{\sqrt{br} \geq \alpha \geq 0} \left\{ 4\alpha + 40\sqrt{6r} \inf_{D \geq \alpha \geq 0} \left\{ 4\delta + 256\widehat{\mathcal{F}}_X(\mathcal{A}(\mathcal{S})^{\otimes R} + \mathcal{B}^{\otimes R}(\mathcal{C})) \log \left( \frac{D_X}{\delta} \right) \right\} \log \left( \frac{\sqrt{br}}{\alpha} \right) \right\}.
\end{aligned}$$

Setting  $\alpha = \sqrt{\frac{br}{N}}$  and  $\delta = \frac{D}{\sqrt{N}}$ , we can always obtain the upper bound of  $\widehat{\mathcal{R}}_X(\ell_2 \circ (\mathcal{A}(\mathcal{S})^{\otimes R} + \mathcal{B}^{\otimes R}(\mathcal{C})), r)$  as follows,

$$\begin{aligned}
& \widehat{\mathcal{R}}_X(\ell_2 \circ (\mathcal{A}(\mathcal{S})^{\otimes R} + \mathcal{B}^{\otimes R}(\mathcal{C})), r) \\
& \leq 10240\sqrt{6r}\widehat{\mathcal{F}}_X(\mathcal{A}(\mathcal{S})^{\otimes R} + \mathcal{B}^{\otimes R}(\mathcal{C}))(\log \sqrt{N})^2 + \frac{4\sqrt{br} + 160\sqrt{6}D_X\sqrt{r}(\log \sqrt{N})}{\sqrt{N}},
\end{aligned}$$

where  $\widehat{\mathcal{F}}_X(\mathcal{A}(\mathcal{S})^{\otimes R} + \mathcal{B}^{\otimes R}(\mathcal{C}))$  is defined in Lemma 2. □

**Remark 1** (Standard single task learning setting). *Everything in the proof of Lemma 3 up to Eqn. (31) holds for a general model and where  $R = 1$  which corresponds to the standard single task learning setting. In this context, let  $\mathcal{Q} : \mathcal{X} \rightarrow \mathbb{R}$  be a hypothesis function class and suppose that we have  $n$  i.i.d. samples  $X = \{X_i\}_{i \in [n]}$ . Similarly, we set  $\alpha = \sqrt{br}/\sqrt{n}$  as*

in Lemma 3 to obtain the upper bound of local Rademacher complexity as follows,

$$\widehat{\mathcal{R}}_X(\ell_2 \circ \mathcal{Q}, r) \leq 4\sqrt{\frac{br}{n}} + 40\sqrt{6r}\widehat{\mathcal{R}}_X(\mathcal{Q})\log \sqrt{n},$$

where  $\widehat{\mathcal{R}}_X(\mathcal{Q})$  is the empirical complexity of the function class  $\mathcal{Q}$ . If  $\mathcal{Q}$  is also a neural network class, we can easily use a similar derivation as in Lemma 2 to obtain an upper bound for  $\widehat{\mathcal{R}}_X(\mathcal{Q})$ . The details are omitted here.